TENMAK BOREN BOR ARAŞTIRMA ENSTİTÜSÜ
TENMAK BOREN BORON RESEARCH INSTITUTE

ISSN: 2149-9020
e-ISSN: 2667-8438

BOR DERGİSİ
JOURNAL OF BORON

CİLT/VOL 10 SAYI/ISSUE 01 YIL/YEAR 2025

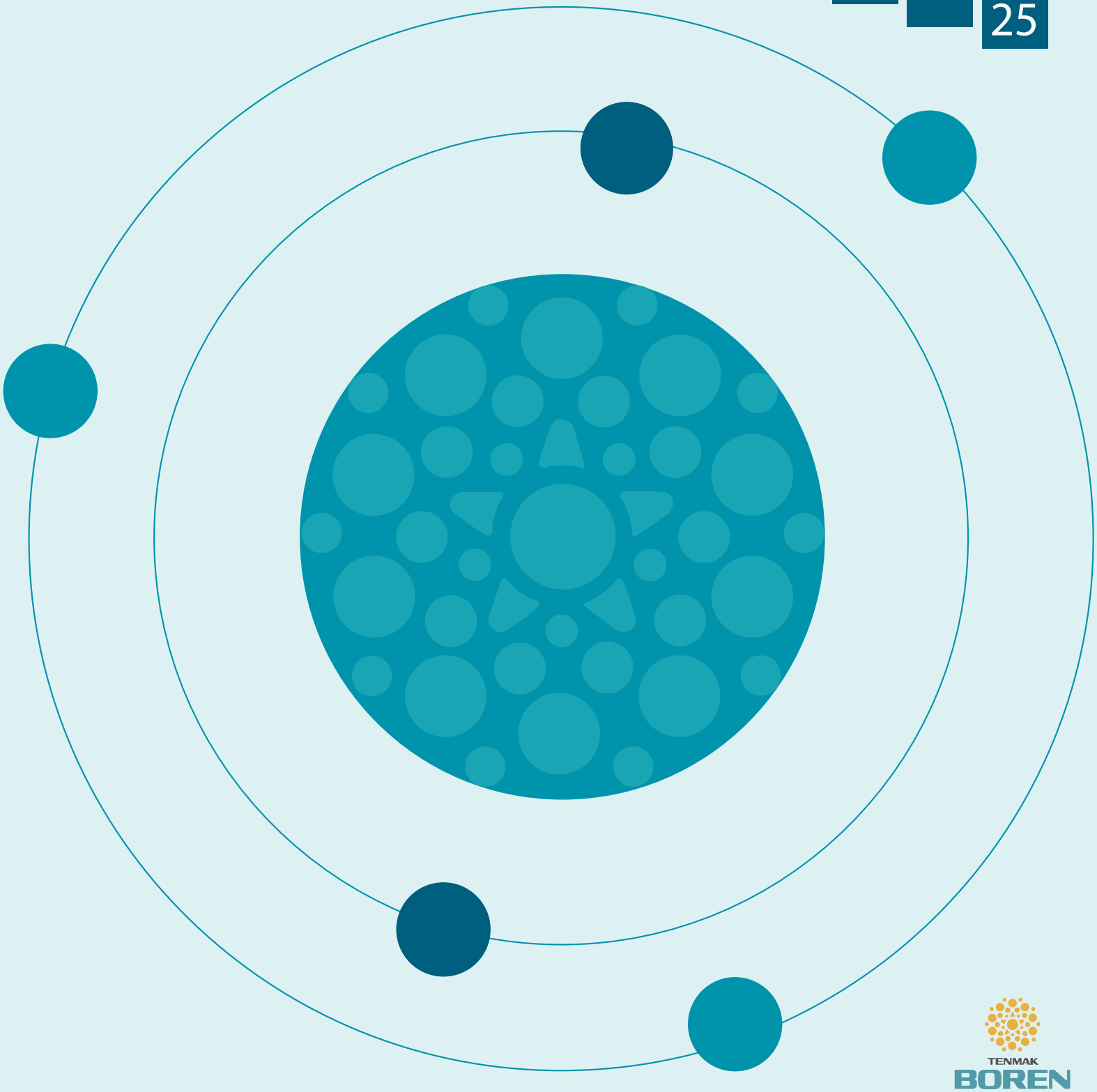

TENMAK BOREN

ISSN: 2149-9020
e-ISSN: 2667-8438

BOR DERGİSİ
JOURNAL OF BORON

CİLT VOL **10** **SAYI** ISSUE **01** **YIL** YEAR **2025**

Yayıncı/Publisher
Türkiye Enerji Nükleer Maden Araştırma Kurumu (TENMAK)
Yayın İdare Adresi/Adress of Publication Manager
Mustafa Kemal Mahallesi, Dumlupınar Blv. No:192, Ankara, 06530, Türkiye
Tel: (0312) 212 62 30
E-posta: journalofboron@tenmak.gov.tr
Web: https://dergipark.org.tr/tr/pub/boron

Yayın Türü/Type of Publication: Yaygın süreli yayın
Yayın Aralığı/Range of Publication: 3 Aylık
Yayın Tarihi/Publication Date: 31/03/2025

ANKARA
MART 2025 / MARCH 2025

TENMAK BOREN BOR ARAŞTIRMA ENSTİTÜSÜ

BOR DERGİSİ
JOURNAL OF BORON
https://dergipark.org.tr/boron

İÇİNDEKİLER/CONTENTS

TENMAK BOREN BOR ARAŞTIRMA ENSTİTÜSÜ

BOR DERGİSİ
JOURNAL OF BORON
https://dergipark.org.tr/boron

Borik asidin C6 glioma hücrelerinde glutamat eksitotoksisitesine karşı koruyucu etkinliğinde oksidatif stresin rolü

Ayşegül Öztürk [1,*], Ahmet Şevki Taşkıran [2], Emin Gündoğdu [3]

[1]*Sivas Cumhuriyet Üniversitesi, Sağlık Hizmetleri Meslek Yüksekokulu, Terapi ve Rehabilitasyon Bölümü, Sivas, 58140, Türkiye*
[2]*Sivas Cumhuriyet Üniversitesi Tıp Fakültesi, Fizyoloji Anabilim Dalı, Sivas, 58140, Türkiye*
[3]*Sivas Cumhuriyet Üniversitesi Tıp Fakültesi, Tıbbi Genetik Anabilim Dalı, Sivas, 58140, Türkiye*

MAKALE BİLGİSİ

Makale Geçmişi:
İlk gönderi 19 Temmuz 2024
Kabul 2 Ocak 2025
Online 31 Mart 2025

Araştırma Makalesi

DOI: 10.30728/boron.1519354

Anahtar kelimeler:
Borik asit
C6 hücreleri
Glutamat eksitotoksisitesi
Oksidatif stres

ÖZET

Bu çalışma, borik asidin (BA) glutamat ile indüklenen eksitotoksisiteye karşı glial hücrelerde meydana gelen oksidan/antioksidan sistem değişikliklerini biyokimyasal olarak incelemek amacıyla tasarlanmıştır. Bu çalışmada C6 glial hücreleri kullanılmıştır. Hücreler kontrol, glutamat (10mM), glutamat+BA(0,23; 0,46; 0,93; 1,87 ve 3,75 µg/mL) ve BA (0,23; 0,46; 0,93; 1,87 ve 3,75 µg/ml) olmak üzere 4 gruba ayrılmıştır. Kontrol grubuna herhangi bir tedavi yapılmamıştır. Glutamat grubundaki hücreler 24 saat boyunca 10 mM glutamat ile muamele edilmiştir. BA ise glutamat eklenmeden 1 saat önce verildi ve 24 saat boyunca inkübe edilmiştir. Hücre canlılığı XTT testi ile ölçülmüştür. Biyokimyasal analizler için ticari kitler kullanılmıştır. Anlamlılık 0.05'ten küçük olarak kabul edilmiştir. Biyokimyasal analiz ile glutamat grubunda malondialdehit (MDA), nitrik oksit (NO), indüklenmiş nitrik oksit sentaz (iNOS), nöronal nitrik oksit sentaz (nNOS) ve toplam oksidant (TOS) seviyelerinin kontrol grubuna göre arttığı ($p<0,05$), BA ön tedavisi ile glutamat grubuna göre istatistiksel olarak azaldığı tespit edilmiştir ($p<0,05$). SOD ve TAS seviyesi glutamat grubunda azalırken BA ön tedavisi ile artmıştır ($p<0,05$). BA, glial hücreler üzerinde glutamat maruziyetine karşı koruyucu etkiler göstermiştir. Bu nöroprotektif etkiyi antioksidan savunma mekanizmasını artırarak, oksidatif ve nitrozatif stresi azaltarak oluşturmuştur.

The role of oxidative stress in the protective effect of boric acid against glutamate excitotoxicity in C6 glioma cells

ARTICLE INFO

Article History:
Received July 19, 2024
Accepted January 2, 2025
Available online March 31, 2025

Research Article

DOI: 10.30728/boron.1519354

Keywords:
Boric acid
C6 cells
Glutamate excitotoxicity
Oxidative stress

ABSTRACT

This study designed to investigate the biochemical changes in glial cells' oxidant/antioxidant systems in response to glutamate-induced excitotoxicity of boric acid (BA). The present study employed C6 glial cells. For the study, cells were separated into 4 groups as control, glutamate (10mM), glutamate+BA (0,23; 0,46; 0,93; 1,87 and 3,75 µg/mL), and BA (0,23; 0,46; 0,93; 1,87 and 3,75 µg/mL). The control group was not treated. The cells in the glutamate group were treated with 10 mM glutamate for 24 hours. BA was administered one hour prior to the addition of glutamate and incubated for 24 hours. The viability of the cells was evaluated using an XTT assay. Commercial kits were used for biochemical analyses. Significance was set at less than 0.05. The biochemical analysis revealed that the levels of malondialdehyde (MDA), nitric oxide (NO), inducible nitric oxide snythase (iNOS), neuronal nitric oxide synthase (nNOS), and total oxidant status (TOS) were elevated in the glutamate group compared to the control group ($p<0.05$). It was detemined that BA treatment resulted in a statistically significant reduction in these levels compared to the glutamate group. ($p<0.05$). The levels of SOD and TAS were found to decrease in the glutamate group and to increase with BA pretreatment ($p<0.05$). The results demonstrated that BA exhibited protective effects on glial cells against glutamate exposure. Furthermore, BA was observed to exert its neuroprotective effect by increasing the antioxidant defense mechanism and reducing oxidative and nitrosative stress.

1. Giriş (Introduction)

Glutamat merkezi sinir sisteminde uyarıcı etkiye sahip bir nörotransmitterdir. Glutamat, iyonotropik ve/veya metabotropik glutamat reseptörlerini aktive ederek nöral fizyolojik süreçlerde anahtar rol oynar. Buna karşın glutamatın aşırı miktarı eksitotoksisite denen toksik bir sürece neden olur [1]. Eksitotoksisite, ekstrasellüler alanda yüksek konsantrasyonda bulunan glutamatın, glutamat reseptörleri aracılığıyla Ca^{2+}'nın hücre

*Corresponding author: aysegulozturk@cumhuriyet.edu.tr

dışından hücre içine büyük bir akışı olarak tanımlanır. Bunu hücre içi depolardan Ca^{2+} salınımı takip eder ve sonuçta sitozolik serbest Ca^{2+} konsantrasyonu fazla miktarda artar [2]. Bu durum reaktif oksijen türlerinin (ROS) oluşmasına ve mitokondriyal hasara neden olarak nöronal ölüm süreçlerini başlatır [1,3].

Glutamat eksitotoksisitesi nöronal, oligodendroglial, astroglial ve retinal ganglion hücreleri dahil olmak üzere çeşitli hücre hatlarında gösterilmiştir [4,5]. Astrositler, özellikle amino asit alım metabolizmasına katılarak yapısal, metabolik, trofik ve antioksidan savunma sağlayarak nöronlarla etkileşime girerler [6]. Astroglial hücreler ayrıca beynin ana antioksidanı olan glutatyon (GSH) seviyelerini korumak için de gereklidir [7,8]. Bu nedenle C6 hücre hattı, hücresel fonksiyonları ve hücre sinyalleşmesini incelemek için astroglial bir model olarak kullanılmaktadır [9,10].

Oksidatif stres (OS), reaktif oksijen ve/veya nitrojen türlerinin (RNS) aşırı üretiminin bir sonucudur; bu da protein ve DNA oksidasyonu ve/veya nitrasyonuna aynı zamanda lipid peroksidasyonuna yol açmaktadır [11,12]. Lipid peroksidasyonu ve serbest oksijen radikallerinin oluşumunu, lipid peroksidasyon ürünü olan nitrik oksit (NO) ve malondialdehit (MDA) konsantrasyonunun artmasına neden olur [13]. ROS'un aşırı üretimi nedeniyle membran ve enzim fonksiyonu zarar görebilir. Glutatyon peroksidaz (GPx), katalaz (CAT) ve süperoksit dismutaz (SOD) gibi antioksidanlar ROS'u detoksifiye eder [14]. OS'in artması ise GSH, CAT ve SOD gibi antioksidan enzimlerin tükenmesine neden olur [15]. Bu sonuçlarla birlikte OS'in nörodejeneratif hastalıklar ve merkezi sinir sistemi (MSS) bozukluklarında önemli bir risk faktörü olduğu gösterilmiştir [16,17].

Bor, memelilerde düşük toksisiteye sahip eser bir elementtir [18]. Bu nedenle borun fizyolojik ve biyokimyasal rolü geniş çapta araştırılmaktadır. Uygun miktardaki borun hücrelerde farklılaşma ve çoğalması gibi koruyucu ve tedavi edici etkileri bulunmaktadır [19]. Yapılan *in vitro* ve *in vivo* çalışmalarının çoğunda bor kaynağının borik asit veya boraks olduğu tespit edilmiştir [20]. Zayıf bir Lewis asidi olan borik asit (BA), suda çözünürlüğü nedeniyle biyolojik sistemlerde en fazla bulunan bor türevidir [21]. BA, oksidatif ve inflamatuar süreçlerin yanı sıra mitokondriyal membran potansiyelini düzenleyerek apoptotik süreçlerde koruyucu bir ajan olarak görev yapar [22]. İnce ve ark. tarafından yapılan bir araştırma diyete eklenen bor takviyesi (100 mg/kg) ile lipit peroksidasyonunun azaldığını, antioksidan savunma mekanizmasının arttırdığını göstermişlerdir [23]. Ancak mevcut çalışmalarda BA'nın nörodejeneratif hastalıklar üzerindeki nöroprotektif etkilerini değerlendiren çok az sayıda araştırma bulunmaktadır. Bu çalışma oksidatif ve nitrozatif strese karşı koruyucu özelliklere sahip olan BA'nın *in vitro* model sistem olan astroglial hücrelerde glutamat ile indüklenen nörodejeneratif hasara karşı olası nöroprotektif etkilerini belirlemeyi amaçlamıştır.

2. Malzemeler ve Yöntemler (Materials and Methods)

2.1. Hücre Kültürü (Cell Culture)

C6 Glioma (CRL107) hücre hattı glutamat kaynaklı sitotoksisiteye sahip olduğu için bu araştırmada kullanıldı [4]. C6 hücreleri Amerikan Tipi Kültür Koleksiyonundan (ATCC, ABD) satın alındı. Hücreler %10 fetal sığır serumu (FBS), %1 L-glutamin ve %1 penisilin/streptomisin içeren DMEM'de (Thermo Fisher Scientific, ABD) kültive edildi. FBS, L-glutamin ve penisilin/streptomisin Sigma-Aldrich firmasından (ABD) temin edildi. Hücreler %5 CO_2 içeren nemli ortamda 37°C'de inkübe edildi

2.2. İlaç Uygulaması (Drug Administration)

Tedavi öncesinde BA ve glutamat DMEM içerisinde çözülerek stok çözeltiler hazırlandı. Borik asit (%99.5) ve glutamat Sigma-Aldrich (ABD) firmasından temin edildi.

2.3. Glutamat Eksitotoksisitesi (Glutamate Excitotoxicity)

Borik asitin glutamat kaynaklı sitotoksisite üzerindeki etkisini incelemek için dört hücre grubu oluşturuldu. Kontrol grubuna herhangi bir tedavi uygulanmadı. Glutamat grubunun hücrelerine 24 saat boyunca 10 mM glutamat verildi. Literatüre göre glial hücrelerin %50'sinin ölümüne neden olan glutamat konsantrasyonu (10 mM) seçildi [24]. Bu çalışma yapılmadan önce bir pilot deney gerçekleştirildi. Buna göre borik asit konsantrasyonları seçildi. Borik asit grubundaki hücrelere 24 saat boyunca çeşitli konsantrasyonlarda (0,23; 0,46; 0,93; 1,87 ve 3,75 µg/mL) borik asit verildi. Borik asit + glutamat grubunun hücreleri, 24 saat boyunca 10 mM glutamata maruz bırakılmadan önce 1 saat boyunca çeşitli konsantrasyonlarda borik asit (0,23; 0,46; 0,93; 1,87 ve 3,75 µg/mL) ile ön işleme tabi tutuldu.

2.4. Hücre Canlılığı (Cell Viability)

Hücre canlılığını belirlemek için XTT tahlil kiti kullanıldı (Roche Diagnostic, ABD). 100 µL DMEM'de, C6 Glioma hücreleri, 96 kuyulu plakalara oyuk başına $1x10^4$ hücre yoğunluğunda ekildi ve borik asit ile işleme tabi tutulmadan önce gece boyunca inkübatörde bekletildi. Glutamatın neden olduğu sitotoksisite prosedürü daha önceki çalışmalar referans alınarak gerçekleştirildi [25,26]. 24 saatlik inkübasyonun ardından besi yeri uzaklaştırıldı ve tüm kuyucuklar, fosfat tamponlu salin (PBS) ile iki kez yıkandı. Son aşamada her kuyucuğa 100 µL fenol kırmızısı içermeyen DMEM ve 50 µL XTT karışım solüsyonu eklenerek plakalar 37°C'de 4 saat bekletildi. Plakalar ELISA mikroplaka okuyucusu (Thermo Fisher Scientific, ABD) kullanılarak 450 nm'de ölçüldü. Testlerin tümü üç kez tekrarlandı ve hücre canlılığı, kontrole göre canlı hücrelerin yüzdesi olarak hesaplandı.

2.5. Hücre Homojenatlarının Hazırlanması (Preparation of Cell Homogenates)

Her grubun hücreleri steril tüplerde toplandı. Hücreler 10 dakika boyunca 2000 rpm'de santrifüjlendi ve sonrasında süpernatanlar çıkarıldı. Tüplerdeki hücreler, hücre süspansiyonunun PBS (pH: 7.4) ile yaklaşık 1 milyon/ml'lik bir hücre yoğunluğuna kadar seyreltilmesiyle süspanse edildi. İç bileşenlerin dışarı çıkmasını sağlamak için hücreler tekrarlanan donma-çözülme döngüleriyle patlatıldı. Ardından 4°C sıcaklıkta 4000 rpm'de 10 dakika santrifüj işlemi yapıldı. Daha sonra süpernatanlar toplandı ve biyokimyasal analize tabi tutuldu. Numunelerdeki toplam protein seviyeleri Bradford protein tahlil kiti (Merck Millipore, Almanya) kullanılarak belirlendi [27].

2.6. Hücrelerdeki iNOS, NO, nNOS, MDA, SOD ve CAT Seviyeleri Ölçümü (Measurement of iNOS, NO, nNOS, MDA, SOD and CAT Levels in Cells)

Her grup için hücrelerin süpernatanlarındaki iNOS(kat. no: SL0365Ra), NO (kat. no: QS0531Ra), nNOS (kat. no: SL1065Ra), MDA (kat. no: SL0475Ra), SOD (kat. no: SL0664Ra) ve CAT (kat. no: SL1084Ra) seviyeleri, ELISA ticari kitleri (Sunlong Biotech, Çin) kullanılarak ölçüldü. Uygulama prosedürleri için üreticinin yönergeleri takip edildi. Kısaca, standart ve hücre numuneleri plakalara yerleştirildi ve 37°C'de 60 dakika inkübe edildi. Hücreler yıkandı ve ardından boyama solüsyonları eklenerek 37°C'de 15 dakika bekletildi. Absorbans, durdurma solüsyonu eklendikten sonra bir ELISA mikroplaka okuyucusu kullanılarak 450 nm'de ölçüldü. Numunelerin değerini belirlemek için standart eğriler çizildi. Plakaların içinde ve arasındaki varyasyon katsayıları %10'dan azdı.

2.7. TAS ve TOS Seviyelerinin Değerlendirilmesi (Assessment of TAS and TOS Levels)

Hücre süpernatantlarındaki TAS ve TOS seviyeleri, Erel tarafından tasarlanan otomatik bir test yöntemi kullanılarak belirlendi [28]. Ölçüm hidrojen peroksit ile kalibre edilir ve sonuçlar μmol H_2O_2 eşd/mg protein olarak ifade edilir. Numunelerdeki toplam protein seviyeleri, bir Bradford protein tahlil kiti (Merck Millipore, Almanya) kullanılarak belirlendi [29,30]. TAS seviyesi, hidrojen peroksit varlığında 2,2-azino-bis(3-etilbenzotiyazolin-6-sülfonik asit (ABTS) molekülünün $ABTS^+$ molekülüne okside olmasından kaynaklanmaktadır. Antioksidan varlığına göre ABTS radikali yeşil ve mavi rengini kaybeder. Mevcut renk değişimi, 660 nm dalga boyunda ölçülerek değerlendirilebilmektedir. Örneklerdeki antioksidan konsantrasyonlarıyla orantılı olarak renk açılımı hızlanmaktadır. Sonuçlar μmol Trolox Eşdeğeri/mg protein cinsinden ifade edilir. TOS seviyesi tayini, örneklerdeki oksitleyici maddeler tarafından Fe^{2+}-o-dianisidin kompleksinin Fe^{3+} iyonuna oksidasyonuna dayanmaktadır. Asidik bir ortamda, Fe^{3+} iyonu ksilanol ile renkli bir kompleks oluşturur. Renk değişimi örneklerdeki oksitleyici moleküllerin konsantrasyonuna orantılıdır ve spektrofotometrik olarak ölçülebilir. Renk değişimi, 530 nm dalga boyunda ölçülerek değerlendirilir.

2.8. İstatistiksel Analiz (Statistical Analysis)

Çalışma sonucunda elde edilen verilerin değerlendirilmesinde IBM SPSS 23.0 for Windows (IBM, Armonk, NY, USA) paket programı kullanıldı. Veriler ortalama ± SH olarak sunuldu ve tek yönlü bir varyans analizi (tek yönlü ANOVA) kullanılarak analiz edildi. Anlamlı farklılıklar elde edildiğinde post-hoc Tukey testi kullanılarak karşılaştırmalar yapıldı. Sonuçlardan $p<0,05$ olan değerler anlamlı kabul edildi.

3. Bulgular (Results)

3.1. Borik Asidin C6 Hücre Hattında Glutamat Toksisitesi Üzerine Etkisi (Effect of Boric Acid on Glutamate Toxicity in C6 Cell Line)

XTT kiti, C6 hücrelerinde glutamat tarafından indüklenen toksisiteye karşı borik asidin nöroprotektif özelliklerini değerlendirmek için kullanıldı. Bu araştırmada, ilacın hem kontrol hem de glutamatla tedavi edilen C6 hücrelerinde hücre canlılığı üzerindeki etkisini test etmek için farklı konsantrasyonlarda (0,23-3,75 μg/mL) uygulandı. Hücreler ilk önce 1 saat boyunca çeşitli konsantrasyonlarda borik asit (0,23-3,75 μg/mL) ile muamele edildi, ardından 24 saat daha 10 mM glutamat ile ya da glutamatsız inkübe edildi. C6 hücrelerinin 24 saat boyunca glutamat uygulanması, tedavi edilmemiş kontrol hücreleriyle karşılaştırıldığında hücre hayatta sağ kalımını önemli ölçüde azalttı ($p<0,001$; Şekil 1). Öte yandan 0,23; 0,46; 0,93 ve 1,87 μg/mL konsantrasyonlardaki borik asit, glutamatla muamele edilen hücrelerle karşılaştırıldığında C6 hücrelerinde hücre canlılığını arttırdı ($p<0,05$; Şekil 1).

Ayrıca tedavi edilmemiş kontrol hücreleriyle karşılaştırıldığında borik asitin tek başına herhangi

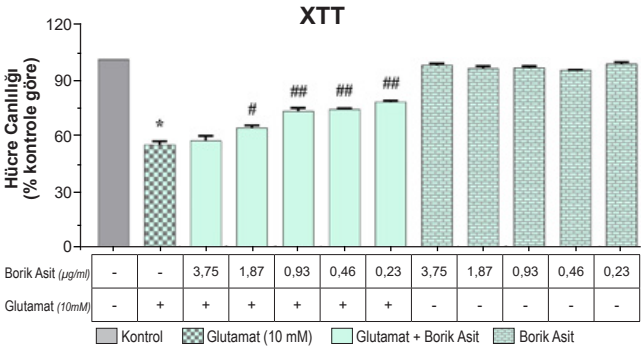

Şekil 1. BA'nın, glutamatın neden olduğu sitotoksisiteden sonra C6 hücrelerinde, hücre sağ kalımı üzerindeki etkisi. Veriler, ortalama ± standart hata ortalaması olarak ifade edilmiştir. *p<0,05 tedavi edilmemiş kontrol grubu ile karşılaştırıldığında; #p<0,05; ## p<0,01 glutamat ile tedavi edilene kıyasla (Effect of BA on cell viability in C6 cells after glutamate-induced cytotoxicity. Data are expressed as mean ± standard error of the mean. *p<0.05 compared with untreated control group; #p<0.05; ## p<0.01 compared with glutamate-treated).

bir konsantrasyonda C6 hücrelerinin canlılığı üzerine hiçbir etkisi bulunmadı (p>0,05; Şekil 1).

3.2. Borik Asitin C6 Hücre Hattında Glutamatın Toksisitesi Sonrası TAS ve TOS Düzeylerine Etkisi (Effect of Boric Acid on TAS and TOS Levels After Glutamate Toxicity in C6 Cell Line)

Hücreler 1 saat boyunca etkin konsatrasyon olarak belirlenen 0,23 µg/mL borik asit ile muamele edildi, sonrasında hücreler 10 mM glutamat ile ya da glutamatsız inkübe edildi ve ticari kitler kullanılarak TAS-TOS düzeyleri saptandı.

Sadece glutamat uygulanan C6 hücreleri, kontrol grubuna kıyasla TAS düzeyleri önemli ölçüde azaldı (p<0,05; Şekil 2a). Öte yandan hücreler 0,23 µg/mL konsantrasyondaki borik asit ile 1 saat önceden muamele edilmesi hücrelerdeki TAS seviyesini glutamat grubu hücrelerine göre artırdı (p<0,05; Şekil 2a).

C6 hücrelerini glutamat ile 24 saat boyunca önceden inkübe edildiğinde kontrol grubuna kıyasla TOS seviyelerini önemli ölçüde artırdı (p<0,05; Şekil 2b). Buna karşın 0,23 µg/mL konsantrasyondaki borik asit ile ön uygulama, glutamatla tedavi edilen hücrelere kıyasla C6 hücrelerinde TOS seviyelerini önemli ölçüde düşürdü (p<0,05; Şekil 2b). Tek başına 0,23 µg/mL konsantrasyonundaki borik asit, kontrole kıyasla C6 hücrelerinde TAS ve TOS düzeylerinde önemli bir değişikliğe neden olmadı (p>0.05; Şekil 2a ve b).

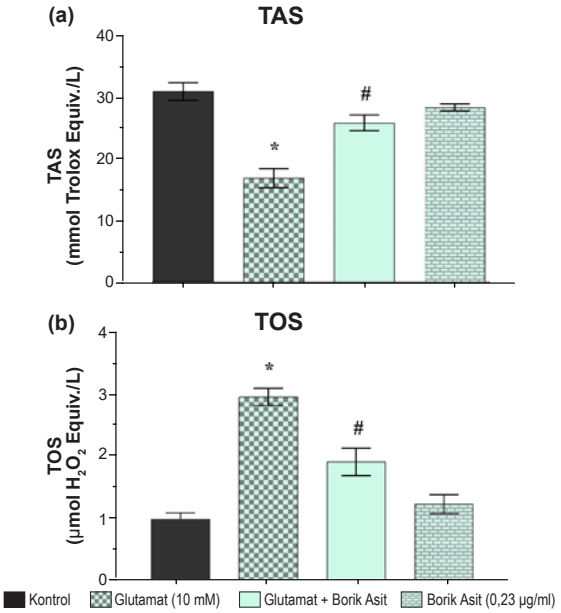

Şekil 2. C6 hücrelerinde glutamatın neden olduğu sitotoksisiteden sonra 0,23 µg/ml BA'nın TAS (a) ve TOS (b) seviyeleri üzerindeki etkisi. Veriler, ortalama ± standart hata ortalaması olarak ifade edilmiştir *p<0,05 tedavi edilmemiş kontrol grubu ile karşılaştırıldığında; #p<0,05; ## p<0,01 glutamat ile tedavi edilene kıyasla. (Effect of 0.23 µg/ml BA on TAS (a) and TOS (b) levels after glutamate-induced cytotoxicity in C6 cells. Data are expressed as mean ± standard error of the mean. *p<0.05 compared with untreated control group; #p<0.05; ## p<0.01 compared with glutamate-treated).

3.3. Borik Asitin C6 Hücre Hattında Glutamatın Toksisitesi Sonrası MDA, SOD ve CAT Düzeylerine Etkisi (Effect of Boric Acid on MDA, SOD and CAT Levels After Glutamate Toxicity in C6 Cell Line)

C6 hücrelerine BA eklendi ve 1 saat sonra 10 mM glutamat ile ya da glutamatsız olarak hücreler 24 saat boyunca inkübe edildi. MDA, SOD ve CAT düzeyleri ELISA kiti ile belirlendi.

Tek başına glutamat uygulanan hücrelerde MDA düzeyi kontrol grubu hücrelerine göre anlamlı bir artış gösterdi (p<0,05; Şekil 3a). Borik asit ile ön muamele edilen hücrelerde ise MDA seviyesi glutamat grubuna göre azaldı (p<0,05; Şekil 3a).

C6 hücrelerine 24 saat süresince glutamat uygulanması, hücrelerin SOD seviyesinde anlamlı derecede azalmaya neden olmuştur (p<0,05; Şekil 3b). Ancak hücrelere 1 saat önce BA uygulanması SOD seviyesini glutamat gruba göre artırmıştır (p<0,05; Şekil 3b).

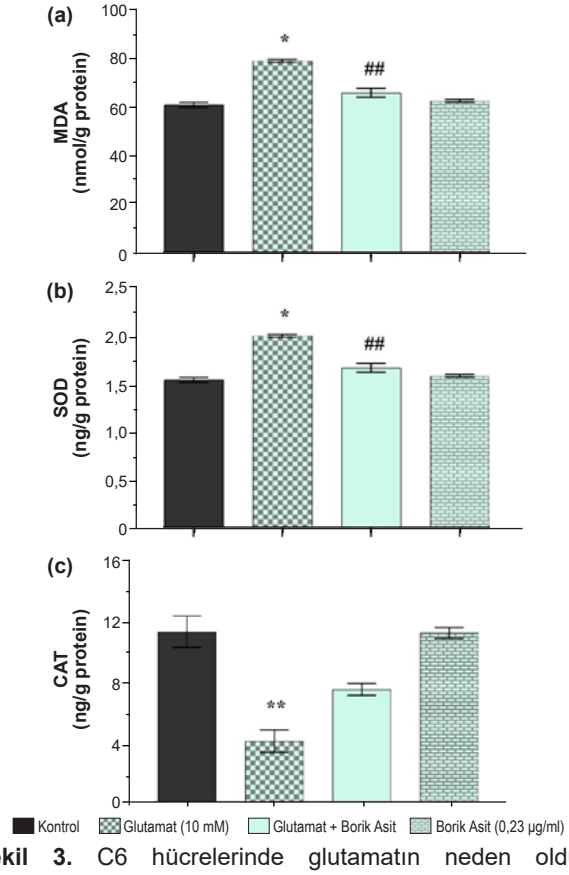

Şekil 3. C6 hücrelerinde glutamatın neden olduğu sitotoksisiteden sonra 0,23 µg/ml BA'nın MDA (a), SOD (b) ve CAT (c) seviyeleri üzerindeki etkisi. Veriler, ortalama ± standart hata ortalaması olarak ifade edilmiştir. *p<0,05; **p<0,01 tedavi edilmemiş kontrol grubu ile karşılaştırıldığında; #p<0,05; ## p<0,01 glutamat ile tedavi edilene kıyasla (Effect of 0.23 µg/ml BA on MDA (a), SOD (b) and CAT (c) levels after glutamate-induced cytotoxicity in C6 cells. Data are expressed as mean ± standard error of the mean. *p<0.05; **p<0.01 compared with untreated control group; #p<0.05; ## p<0.01 compared with glutamate-treated).

Tek başına BA uygulaması ile SOD seviyesinde kontrol grubuna göre herhangi bir değişiklik oluşturmamıştır (p>0,05; Şekil 3b).

Glutamat ile muamele edilen hücrelerin CAT seviyeleri kontrol grubuna göre azaldığı saptanmıştır (p<0,05; Şekil 3c). Bununla birlikte 0,23 µg/mL BA ile ön işleme tabi tutulan hücrelerde glutamat grubuna kıyasla CAT seviyesindeki artış istatistiksel olarak anlamlı bulunmamıştır (p>0,05; Şekil 3c).

3.4. Borik Asitin C6 Hücre Hattında Glutamatın Toksisitesi Sonrası NO, iNOS ve nNOS Düzeylerine Etkisi (Effect of Boric Acid on NO, iNOS and nNOS Levels After Glutamate Toxicity in C6 Cell Line)

BA uygulanan hücrelerin glutamatlı ya da glutamatsız NO, iNOS ve nNOS seviyelerini biyokimyasal olarak analiz etmek amacıyla ELISA testi kullanıldı.

ELISA testi sonuçlarına göre C6 hücrelerinde sadece glutamata maruz kalan hücrelerin NO seviyesi kontrol grubuna göre istatistiksel açıdan anlamlı olarak artış gösterirken hücrelerin 1 saat önce BA muamele edilmesi NO seviyesini azaltmıştır (p<0.05; Şekil 4a). Ancak sadece BA uygulanan hücrelerin NO seviyesi kontrol grubuna göre değişiklik göstermemiştir (p>0,05; Şekil 4c).

Hücrelerin glutamat ile 24 saat boyunca önceden inkübe edilmesi kontrol grubuna kıyasla iNOS seviyesini önemli ölçüde artırmıştır (p<0.05; Şekil 4b). BA ile 1 saat ön muamele edilen C6 hücrelerinde ise iNOS düzeyi glutamat grubuna göre arttığı saptanmıştır (p<0,05; Şekil 4b).

nNOS seviyesi tek başına glutamat uygulanan grupta kontrole kıyasla anlamlı derecede artmıştır (p<0,05; Şekil 4c). Buna karşın 0,23 µg/mL BA ile ön işleme tabi tutulan hücrelerde nNOS seviyesi glutamat grubuna kıyasla istatistiksel olarak anlamlı düzeyde azalmıştır (p>0,05; Şekil 4c).

4. Tartışma (Discussion)

Bu çalışma, BA ön uygulamasının, C6 astroglial hücrelerinde glutamatın neden olduğu sitotoksisiteye karşı antioksidan etkiler gösterdiğini ortaya koyan ilk çalışmadır. C6 hücre hattında, BA ön uygulaması ile glutamat kaynaklı sitotoksisitede hücre sağ kalımı artmıştır. Veriler, BA'nın glial hücrelerin glutamat kaynaklı sitotoksisite sonrası hücre ölümünü ve oksidatif ve nitrozatif stresi azalttığını göstermiştir. Çalışmanın sonucunda borik asit ön uygulaması iNOS, nNOS, NO, MDA ve TOS düzeylerini düşürmüş, TAS, CAT ve SOD düzeylerini ise artırmıştır. Böylelikle glutamatın neden olduğu sitotoksisiteye karşı BA'nın antioksidan özellikler gösterdiği tespit edilmiştir.

Bor içeren bileşikler, nöronal süreçlerin düzenlenmesinde nöroprotektif etkilere sahiptir. Bunlar arasında nöronal ateşleme, nörotrofik faktörlerin

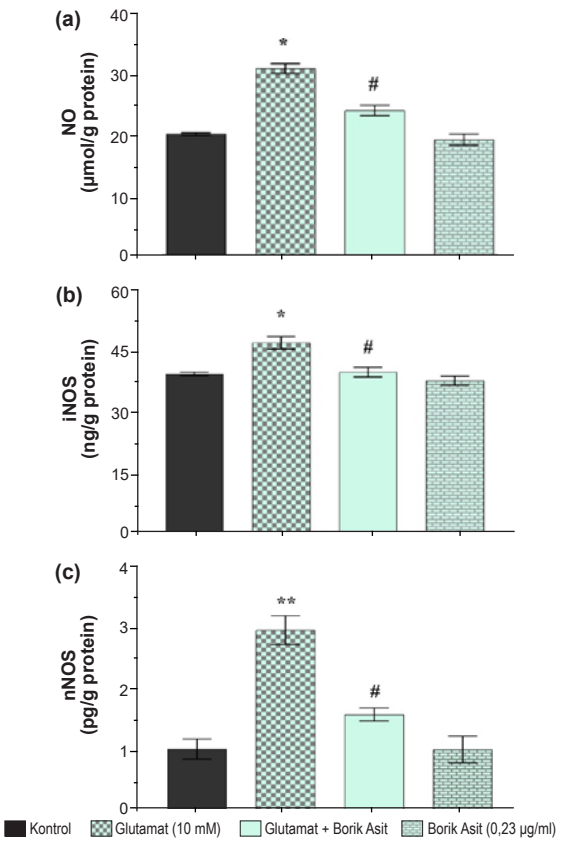

Şekil 4. C6 hücrelerinde glutamatın neden olduğu sitotoksisiteden sonra 0,23 µg/ml BA'nın NO (a), iNOS (b) ve nNOS (c) seviyeleri üzerindeki etkisi. Veriler, ortalama ± standart hata ortalaması olarak ifade edilmiştir. *p<0,05; **p<0,01 tedavi edilmemiş kontrol grubu ile karşılaştırıldığında; #p<0,05; ## p<0,01 glutamat ile tedavi edilene kıyasla (Effect of 0.23 µg/ml BA on NO (a), iNOS (b), nNOS (c) and levels after glutamate-induced cytotoxicity in C6 cells. Data are expressed as mean ± standard error of the mean. *p<0.05; **p<0.01 compared with untreated control group; #p<0.05; ## p<0.01 compared with glutamate-treated).

üretimi, oksidatif belirteçlerin kontrolü ve davranışsal kontrol mekanizmaları bulunur. Bor bu etkilerini, iyon kanalları, G-proteinine bağlı reseptörler veya nöronal davranış üzerinde değişiklik yapan diğer reseptörler aracılığıyla gerçekleştirmektedir [31-33]. Ayrıca, inflamasyon veya oksidatif süreçlerin modülasyonunda da etkilidir [20].

BA'nın nöroprotektif etkileri üzerine yapılan bir çalışmada, sıçanlarda alüminyum klorid enjeksiyonu ile hasar oluşturulan beyin dokusunun değişen seviyelerde BA konsantrasyonlarına nasıl tepki verdiği araştırılmıştır. Deney sonucunda, düşük dozdaki BA'nın (3,25 mg/kg) nöronlarda koruyucu etkisinin olduğu, yüksek dozların (36 ve 58,5 mg/kg) ise beyin dokusunda daha fazla hasara yol açtığı gösterilmiştir [34]. BA ve C6 glioblastoma hücrelerinin etkileşimine dair yapılan bir çalışmada BA'in yüksek konsantrasyonlarda (0,39-25 mM) ferroptoz, apoptoz ve semaforin sinyal yolunu düzenleyerek tümör ilerlemesini önlediğine dair kanıt sağlamıştır [35]. Kızılay ve ark. ise yaptıkları araştırmada, siyatik sinir yaralanmasını takiben sıçanlara 100 mg/kg dozunda

borik asit verilmesinin miyelin ve aksonlardaki hasarı önemli ölçüde azalttığını ve yaralanan sinirin elektriksel fonksiyonunu iyileştirdiğini göstermiştir. Oksidatif parametrelerden biri olan NF-κB seviyesinin siyatik sinir yaralanması sonucu arttığı buna karşın BA uygulaması ile azaldığı immunohistokimyasal boyama yöntemi ile belirlenmiştir. Bu iyileşme muhtemelen oksidatif stres reaksiyonlarının azalmasından kaynaklanmaktadır [36].

Nörodejeneratif hastalıklar, psikiyatrik bozukluklar ve sinir dokusu yaralanmalarında gözlemlenen yaygın bir bulgu, ROS ve serbest radikallerin neden olduğu oksidatif strestir. Enzimler, kofaktörler ve peptitler gibi hücre antioksidan mekanizmalarındaki değişiklikler, ROS ve serbest radikallerin stabilize edilmesini oldukça zor hale getirir. Nöronlar ve glial hücreler içindeki artan olumsuz süreç, proteinler, lipitler ve nükleik asitlerle etkileşime girmeye başladıkça oksidanların miktarında daha fazla bir artışa yol açar ve bu durum hücrelerde fonksiyon bozukluğu ve ölümle sonuçlanır. Bu bağlamda, antioksidan etki gösterebilecek bir mekanizmaya sahip bor içeren bir bileşik olmasa da, besin maddesi olarak borun çeşitli hücre tiplerinde sistemik oksidatif stresi iyileştirdiğine dair kanıtlar mevcuttur [37-39]. Özellikle BA'nın lipid peroksidasyonu, oksidatif stres ve bu oksidatif süreçlerle ilgili inflamatuar yanıta karşı etkili olduğu kanıtlanmıştır [40,41]. Ataizi ve ark. kapalı kafa travması geçiren sıçanların beyin dokularındaki CAT ve MDA aktivitesindeki değişiklikleri ve ayrıca bu sıçanlarda BA'in potansiyel nöroprotektif etkisini incelemişlerdir. Çalışmanın sonucunda travmalı sıçanların beyin dokusunda CAT düzeyi azalırken BA uygulaması ile arttığı, MDA düzeyi artarken BA arttığı tespit edilmiştir [42]. Yavuz ve ark., Wistar-albino sıçanlarda yaptıkları Parkinson modelinde BA ve kuersetinin oksidatif stres belirteçleri ve davranış testleri üzerine olan etkilerini araştırmışlardır. Bu çalışmada beyin doku örneklerinde glutatyon, MDA ve aynı zamanda TAS seviyelerini incelenmiştir. Çalışmanın sonuçları BA ve kuersetin kombine olarak uygulandığında lipid peroksidasyon seviyelerinin azaldığı ileri sürülmüştür. Bu sonuç BA'nın gıda takviyesi olarak kullanılabileceğini anlamlı kılmaktadır [43]. Benzer şekilde nöronal hücrelerin uzun süreli glutamata maruz kalması ile oksidatif stresin arttığı bildirilmiştir [44]. Literatürle uyumlu olarak çalışmamızda, glutamat uygulanan grupta MDA seviyesinin arttığı, CAT ve SOD seviyesinin azaldığı, BA ön uygulaması ile artan MDA seviyesinin azaldığı, CAT ve SOD seviyesinin ise arttığı bulunmuştur. Bu sonuçlar bozulan antioksidan mekanizmanın BA uygulaması ile düzelebileceğini göstermektedir.

ROS oluşumu ve lipit peroksidasyonu (LP), uyarıcı glutamat ve aspartatın salınmasına, hücreye kalsiyum akışına yol açar. Bu durum hücre zarı geçirgenliğini bozar ve ikincil hücre hasarına neden olur. Çeşitli çalışmalar oksijensiz radikallerin ikincil hasarlarda anahtar rol oynadığını ve nörotoksisiteye yol açtığını göstermiştir [26,45-47]. İkincil beyin hasarının önemli bir kısmı, antioksidan mekanizmalar, ROS seviyeleri ve RNS arasındaki dengenin bozulması ve bunun sonucunda LP'nin ortaya çıkmasından kaynaklanmaktadır. Antioksidanların MSS üzerinde olumlu etkisi daha önce gösterilmiştir[48,49]. Şahin ve ark. bir besin takviyesi olarak BA'in, oksidatif strese karşı ana hücre mekanizmalarından biri olan Nrf2 yolunu aktive ettiğini ileri sürmüşlerdir. Bu yolun aktivasyonu antioksidan özelliklere sahip proteinlerin ekspresyonuna yol açmaktadır [50]. Hazman ve ark. sıçanlarda sisplatin toksikasyonu sonrası artan oksidatif stres, inflamasyon ve apoptozun farklı dozlarda BA ve boraks tedavileri ile azaltılabileceği bildirmişlerdir [51]. Benzer olarak bizim çalışmamızda glutamat sonrası artan TOS seviyesinin BA ön uygulaması ile azaldığı, azalan TAS seviyesinin ise BA uygulaması sonrası arttığı bulunmuştur. Hacıoğlu ve ark. nöronal iletim ve nörodejeneratif süreçlerin araştırılmasında ex vivo model sistem olan sinaptozomlar üzerinde Aβ1-42 kaynaklı nörodejeneratif hasara karşı BA ve kurkuminin koruyucu etkilerini incelemişlerdir. Deney verilerinde BA tedavisinin LP, MDA ve NO düzeylerini azalttığını tespit etmişlerdir [52]. Çalışmamızın sonuçları BA uygulaması ile glutamat kaynaklı nitrozatif stresi inhibe ederek iNOS, nNOS ve NO seviyelerini azalttığını gösteren önceki çalışmalarla tutarlıdır.

5. Sonuçlar (Conclusions)

BA'nın oksidatif ve nitrozatif süreçlerde etkili olan proteinler üzerinde çok yönlü etkisi olduğu bulunmuştur. Bu bakımdan BA takviyesi nörodejeneratif hastalıklar üzerinde önleyici bir role sahip olabilir. Ayrıca, bor atomunun rolü, özellikleri ve kimyasal yapısal çekirdeklerin tanımlanması, nörodejenerasyona karşı yenilikçi bor içeren aktif ilaçlar için potansiyel farmakoforlar olarak seçilebilir ve önerilebilir.

6. Teşekkürler (Acknowledgements)

Bu çalışma TUBİTAK 2209-A (Proje no: 1919B012004287) projesi kapsamında yapılmıştır. Çalışmada gerekli olanakları sağladığı için Sivas Cumhuriyet Üniversitesi Tıp Fakültesi Araştırma Merkezi'ne (CÜTFAM) teşekkür ederiz.

7. Yazar Katkısı Beyanı (Author Contribution Statement)

Ayşegül Öztürk: Kavramsallaştırma, metadoloji, veri analizi, yazım analizi, orijinal taslak yazma.

Ahmet Şevki Taşkıran: Proje yönetimi, yazım analizi, denetim, grafiksel tasarım.

Emin Gündoğdu: Metadoloji, grafiksel tasarım.

Kaynaklar (References)

[1] Wang, Y., & Qin, Z. (2010). Molecular and cellular mechanisms of excitotoxic neuronal death. *Apoptosis*, *15*(11), 1382-1402. https://doi.org/10.1007/s10495-010-0481-0

[2] Daniele, S. G., Trummer, G., Hossmann, K. A., Vrselja, Z., Benk, C., Gobeske, K. T., … & Sestan, N. (2021).

Brain vulnerability and viability after ischaemia. *Nature Reviews Neuroscience*, *22*(9), 553-572. https://doi.org/10.1038/s41583-021-00488-y

[3] Dong, X., Wang, Y., & Qin, Z. (2009). Molecular mechanisms of excitotoxicity and their relevance to pathogenesis of neurodegenerative diseases. *Acta Pharmacologica Sinica*, *30*(4), 379-387. https://doi.org/10.1038/aps.2009.24

[4] Kritis, A. A., Stamoula, E. G., Paniskaki, K. A., & Vavilis, T. D. (2015). Researching glutamate-induced cytotoxicity in different cell lines: A comparative/collective analysis/study. *Frontiers in Cellular Neuroscience*, *9*. https://doi.org/10.3389/fncel.2015.00091

[5] Felek, H., Çatal, T., Yulak, F., Filiz, A. K., & Karabulut, S. (2024). The effect of myostatin on glutamate excitotoxicity induced in SH-SY5Y cell line. *Health Sciences Student Journal*, *4*(1), 1-6. Erişim Adresi: https://ojs.healthssj.com/index.php/panel/article/view/15

[6] Barbeito, L. H., Pehar, M., Cassina, P., Vargas, M. R., Peluffo, H., Viera, L., … & Beckman, J. S. (2004). A role for astrocytes in motor neuron loss in amyotrophic lateral sclerosis. *Brain Research Reviews*, *47*(1-3), 263-274. https://doi.org/10.1016/j.brainresrev.2004.05.003

[7] Hertz, L. (2006). Glutamate, a neurotransmitter-and so much more. *Neurochemistry International*, *48*(6-7), 416-425. https://doi.org/10.1016/j.neuint.2005.12.021

[8] Pope, S. A., Milton, R., & Heales, S. J. (2008). Astrocytes protect against copper-catalysed loss of extracellular glutathione. *Neurochemical Research*, *33*(7), 1410-1418. https://doi.org/10.1007/s11064-008-9602-3

[9] Quincozes-Santos, A., & Gottfried, C. (2011). Resveratrol modulates astroglial functions: Neuroprotective hypothesis. *Annals of the New York Academy of Sciences*, *1215*(1), 72-78. https://doi.org/10.1111/j.1749-6632.2010.05857.x

[10] Benda, P., Lightbody, J., Sato, G., Levine, L., & Sweet, W. (1968). Differentiated rat glial cell strain in tissue culture. *Science*, *161*(3839), 370-371. https://doi.org/10.1126/science.161.3839.370

[11] Gutteridge, J. M. C., & Halliwell, B. (2010). Antioxidants: Molecules, medicines, and myths. *Biochemical and Biophysical Research Communications*, *393*(4), 561-564. https://doi.org/10.1016/j.bbrc.2010.02.071

[12] Karademir M., Öztürk, A., Yulak, F., Özkaraca, M., & Taskiran, A. S. (2024). Unveiling the protective potential of sugammadex against ptz-induced epileptic seizures in mice: A comprehensive study on oxidative stress, apoptosis, and autophagy. *Neurochemical Journal*, *18*(2), 338-347. https://doi.org/10.1134/s1819712424020181

[13] Azimullah, S., Meeran, M. F., Ayoob, K., Arunachalam, S., Ojha, S., & Beiram, R. (2023). Tannic acid mitigates rotenone-induced dopaminergic neurodegeneration by inhibiting inflammation, oxidative stress, apoptosis, and glutamate toxicity in rats. *International Journal of Molecular Sciences*, *24*(12), 9876. https://doi.org/10.3390/ijms24129876

[14] Brocardo, P. S., Gil-Mohapel, J., & Christie, B. R. (2011). The role of oxidative stress in fetal alcohol spectrum disorders. *Brain Research Reviews*, *67*(1-2), 209-225. https://doi.org/10.1016/j.brainresrev.2011.02.001

[15] Javed, H., Azimullah, S., Haque, M. E., & Ojha, S. K. (2016). Cannabinoid type 2 (CB2) receptors activation protects against oxidative stress and neuroinflammation associated dopaminergic neurodegeneration in rotenone model of parkinson's disease. *Frontiers in Neuroscience*, *10*. https://doi.org/10.3389/fnins.2016.00321

[16] Ergül, M., & Taşkıran, A. Ş. (2021). Thiamine protects glioblastoma cells against glutamate toxicity by suppressing oxidative/endoplasmic reticulum stress. *Chemical and Pharmaceutical Bulletin*, *69*(9), 832-839. https://doi.org/10.1248/cpb.c21-00169

[17] Salim, S. (2017). Oxidative stress and the central nervous system. *The Journal of Pharmacology and Experimental Therapeutics*, *360*(1), 201-205. https://doi.org/10.1124/jpet.116.237503

[18] Nielsen, F. H. (2008). Is boron nutritionally relevant? *Nutrition Reviews*, *66*(4), 183-191. https://doi.org/10.1111/j.1753-4887.2008.00023.x

[19] Qiu, L., Zhu, C.-L., Wang, X.-Y., & Xu, F.-L. (2007). Changes of cell proliferation and differentiation in the developing brain of mouse. *Neuroscience Bulletin*, *23*(1), 46-52. https://doi.org/10.1007/s12264-007-0007-0

[20] Barrón-González, M., Montes-Aparicio, A. V., Cuevas-Galindo, M. E., Orozco-Suárez, S., Barrientos, R., Alatorre, A., … & Soriano-Ursúa, M. A. (2023). Boron-containing compounds on neurons: Actions and potential applications for treating neurodegenerative diseases. *Journal of Inorganic Biochemistry*, *238*, 112027. https://doi.org/10.1016/j.jinorgbio.2022.112027

[21] Barranco, W. T., & Eckhert, C. D. (2006). Cellular changes in boric acid-treated DU-145 prostate cancer cells. *British Journal of Cancer*, *94*(6), 884-890. https://doi.org/10.1038/sj.bjc.6603009

[22] Sogut, I., Oglakcı, A., Kartkaya, K., Ol, K. K., Sogut, M. S., Kanbak, G., & Inal, M. E. (2014). Effect of boric acid on oxidative stress in rats with fetal alcohol syndrome. *Experimental and Therapeutic Medicine*, *9*(3), 1023-1027. https://doi.org/10.3892/etm.2014.2164

[23] Ince, S., Kucukkurt, I., Cigerci, I. H., Fatih Fidan, A., & Eryavuz, A. (2010). The effects of dietary boric acid and borax supplementation on lipid peroxidation, antioxidant activity, and DNA damage in rats. *Journal of Trace Elements in Medicine and Biology*, *24*(3), 161-164. https://doi.org/10.1016/j.jtemb.2010.01.003

[24] Yousefzadehmoghaddam, R., Hassanpour, M., Öztürk, A., & Karabulut, S., (2023). Investigation of the effect of galium aparine extract on glutamate excitotoxicity induced in C6-glioma cell line. *Health Sciences Student Journal*, *3*(1), 8-18. Retrieved from https://journals.indexcopernicus.com/api/file/viewByFileId/1773565

[25] Taskiran, A. S., & Ergul, M. (2021). The effect of salmon calcitonin against glutamate-induced cytotoxicity in the C6 cell line and the roles the inflammatory and nitric oxide pathways play. *Metabolic Brain Disease*, *36*(7), 1985-1993. https://doi.org/10.1007/s11011-021-00793-6

[26] Dirik, H., & Joha, Z. (2023). Investigation of the effect of sugammadex on glutamate-induced neurotoxicity

in C6 cell line and the roles played by nitric oxide and oxidative stress pathways. *Fundam Clin Pharmacol*, *37*(4), 786-793. https://doi.org/10.1111/fcp.12890

[27] Gömeç, M., İpek, G., Öztürk, A., & Şahin İnan, D. (2022). Effect of wheat germ oil on wound healing: An *in vitro* study in fibroblast cells. *Turkish Journal of Science and Health*, *3*(3), 230-235. https://doi.org/10.51972/tfsd.1128533

[28] Erel, O. (2004). A novel automated method to measure total antioxidant response against potent free radical reactions. *Clinical Biochemistry*, *37*(2), 112-119. https://doi.org/10.1016/j.clinbiochem.2003.10.014

[29] Taşkıran, A. Ş., & Topçu, A. (2023). Investigation of the protective role of quercetin on oxidative stress and endoplasmic stress pathway in 4-aminopyridine-induced neuronal damage. *Turkish Journal of Agriculture - Food Science and Technology*, *11*(1), 2505-2511. https://doi.org/10.24925/turjaf.v11is1.2505-2511.6413

[30] Filiz, A. K., Joha, Z., & Yulak, F. (2021). Mechanism of anti-cancer effect of β-glucan on SH-sy5y cell line. *Bangladesh Journal of Pharmacology*, *16*(4), 122-128. https://doi.org/10.3329/bjp.v16i4.54872

[31] Gavande, N., Kim, H.-L., Doddareddy, M. R., Johnston, G. A., Chebib, M., & Hanrahan, J. R. (2013). Design, synthesis, and pharmacological evaluation of fluorescent and biotinylated antagonists of ρ1 GABAC Receptors. *ACS Medicinal Chemistry Letters*, *4*(4), 402-407. https://doi.org/10.1021/ml300476v

[32] Soriano-Ursúa, M. A., Bello, M., Hernández-Martínez, C. F., Santillán-Torres, I., Guerrero-Ramírez, R., Correa-Basurto, J., … & Trujillo-Ferrara, J. G. (2018). Cell-based assays and molecular dynamics analysis of a boron-containing agonist with different profiles of binding to human and guinea pig beta2 adrenoceptors. *European Biophysics Journal*, *48*(1), 83-97. https://doi.org/10.1007/s00249-018-1336-9

[33] Vernekar, S. K., Hallaq, H. Y., Clarkson, G., Thompson, A. J., Silvestri, L., Lummis, S. C., & Lochner, M. (2010). Toward biophysical probes for the 5-HT3 receptor: Structure−activity relationship study of granisetron derivatives. *Journal of Medicinal Chemistry*, *53*(5), 2324-2328. https://doi.org/10.1021/jm901827x

[34] Çolak, S., Geyikoğlu, F., Keles, O. N., Türkez, H., Topal, A., & Unal, B. (2011). The neuroprotective role of boric acid on aluminum chloride-induced neurotoxicity. *Toxicology and Industrial Health*, *27*(8), 700-710. https://doi.org/10.1177/0748233710395349

[35] Kar, F., Hacioğlu, C., & Kaçar, S. (2022). The dual role of boron *in vitro* neurotoxication of glioblastoma cells via SEMA3F/NRP2 and ferroptosis signaling pathways. *Environmental Toxicology*, *38*(1), 70-77. https://doi.org/10.1002/tox.23662

[36] Kizilay, Z., Erken, H., Çetin, N., Aktaş, S., Abas, B., & Yılmaz, A. (2016). Boric acid reduces axonal and myelin damage in experimental sciatic nerve injury. *Neural Regeneration Research*, *11*(10), 1660. https://doi.org/10.4103/1673-5374.193247

[37] Zafar, H., & Ali, S. (2013). Boron inhibits the proliferating cell nuclear antigen index, molybdenum containing proteins and ameliorates oxidative stress in hepatocellular carcinoma. *Archives of Biochemistry and Biophysics*, *529*(2), 66-74. https://doi.org/10.1016/j.abb.2012.11.008

[38] Ince, S., Kucukkurt, I., Demirel, H. H., Acaroz, D. A., Akbel, E., & Cigerci, I. H. (2014). Protective effects of boron on cyclophosphamide induced lipid peroxidation and genotoxicity in rats. *Chemosphere*, *108*, 197-204. https://doi.org/10.1016/j.chemosphere.2014.01.038

[39] Ayhanci, A., Tanriverdi, D. T., Sahinturk, V., Cengiz, M., Appak-Baskoy, S., & Sahin, I. K. (2019). Protective effects of boron on cyclophosphamide-induced bladder damage and oxidative stress in rats. *Biological Trace Element Research*, *197*(1), 184-191. https://doi.org/10.1007/s12011-019-01969-z

[40] Coban, F. K., Ince, S., Kucukkurt, I., Demirel, H. H., & Hazman, O. (2014). Boron attenuates malathion-induced oxidative stress and acetylcholinesterase inhibition in rats. *Drug and Chemical Toxicology*, *38*(4), 391-399. https://doi.org/10.3109/01480545.2014.974109

[41] Acaroz, U., Ince, S., Arslan-Acaroz, D., Gurler, Z., Kucukkurt, I., Demirel, H. H., … & Zhu, K. (2018). The ameliorative effects of boron against acrylamide-induced oxidative stress, inflammatory response, and metabolic changes in rats. *Food and Chemical Toxicology*, *118*, 745-752. https://doi.org/10.1016/j.fct.2018.06.029

[42] Ataizi, Z. S., Ozkoc, M., Kanbak, G., Karimkhani, H., Burukoglu Donmez, D., Ustunisik, N., & Ozturk, B. (2019). Evaluation of the neuroprotective role of boric acid in preventing traumatic brain injury-mediated oxidative stress. *Turkish Neurosurgery*, *31*(4). https://doi.org/10.5137/1019-5149.jtn.25692-18.4

[43] Yavuz, E., Çevik, G., Çevreli, B., & Serdaroğlu Kaşıkçı, E. (2023). Effect of boric acid and quercetin combination on oxidative stress/ cognitive function in parkinson model. *Journal of Boron*, *8*(3), 85-91. https://doi.org/10.30728/boron.1215949

[44] Filiz, A. K., Öztürk, A. (2021). The effect of carbamazepine against glutamate-induced cytotoxicity in the C6 cell line. *International Journal of Scientific and Technological Research*, *7*(8). https://doi.org/10.7176/jstr/7-08-09

[45] Yıldızhan, K., & Öztürk, A. (2022). Quipazine treatment exacerbates oxidative stress in glutamate-induced HT-22 neuronal cells. *The European Research Journal*, *8*(4), 521-528. https://doi.org/10.18621/eurj.1027423

[46] Çakır Çanak, T., Akpınar, S., & Serhatlı, E. (2017). Homopolymerization and synthesis of a new methacrylate monomer bearing a boron side group: Characterization and determination of monomer reactivity ratios with styrene. *Turkish Journal of Chemistry*, *41*, 209-220. https://doi.org/10.3906/kim-1603-106

[47] Şahin, B., & Karabulut, S. (2022). Sugammadex causes C6 glial cell death and exacerbates hydrogen peroxide-induced oxidative stress. *Cumhuriyet Medical Journal*, *44*(1), 22-27. https://doi.org/10.7197/cmj.1069629

[48] Dohi, K., Satoh, K., Nakamachi, T., Yofu, S., Hiratsuka, K., Nakamura, S., … & Aruga, T. (2007). Does Edaravone (MCI-186) act as an antioxidant and a neuroprotector in experimental traumatic brain injury? *Antioxidants & Redox Signaling*, *9*(2), 281-287. https://doi.org/10.1089/

ars.2007.9.281

[49] Topal Canbaz, G., Keskin, Z. S., Yokuş, A., & Aslan, R. (2023). Biofabrication of copper oxide nanoparticles using solanum tuberosum L. var. Vitelotte: Characterization, antioxidant and antimicrobial activity. *Chemical Papers*, *77*(8), 4277-4284. https://doi.org/10.1007/s11696-023-02776-6

[50] Sahin, N., Akdemir, F., Orhan, C., Aslan, A., Agca, C. A., Gencoglu, H., … & Sahin, K. (2012). A novel nutritional supplement containing chromium picolinate, phosphatidylserine, docosahexaenoic acid, and boron activates the antioxidant pathway Nrf2/HO-1 and protects the brain against oxidative stress in high-fat-fed rats. *Nutritional Neuroscience*, *15*(5), 42-47. https://doi.org/10.1179/1476830512y.0000000018

[51] Hazman, Ö., Bozkurt, M. F., Fidan, A. F., Uysal, F. E., & Çelik, S. (2018). The effect of boric acid and borax on oxidative stress, inflammation, er stress and apoptosis in cisplatin toxication and nephrotoxicity developing as a result of toxication. *Inflammation*, *41*(3), 1032-1048. https://doi.org/10.1007/s10753-018-0756-0

[52] Hacioglu, C., Kar, F., Kar, E., Kara, Y., & Kanbak, G. (2020). Effects of curcumin and boric acid against neurodegenerative damage induced by amyloid beta (1-42). *Biological Trace Element Research*. *199*, 3793-3800. https://doi.org/10.1007/s12011-020-02511-2

BOR DERGİSİ
JOURNAL OF BORON
https://dergipark.org.tr/boron

A novel boron nitride quantum dots-based fluorescent sensing platform for selective detection of Fe^{3+}

Duygu Kuru [1,*]

[1]*Bilecik Seyh Edebali University, Faculty of Engineering, Department of Chemical Engineering, Bilecik, 11100, Türkiye*

ARTICLE INFO

Article history:
Received September 25, 2024
Accepted January 15, 2025
Available online March 31, 2025

Research Article

DOI: 10.30728/boron.1556075

Keywords:
Boron nitride quantum dots
Fluorescent sensing platform
Metal ion sensing
Nanocomposite film
PMMA

ABSTRACT

In this study, boron nitride quantum dots (BNQDs) and polymethyl methacrylate (PMMA) nanocomposite films were produced to be used as a metal sensing material. BNQDs were synthesized from boric acid and urea using the hydrothermal method. The selectivity of PMMA/BNQDs nanocomposite films as fluorescent sensing platforms was tested for different metal ions (Fe^{3+}, Na^{+} Zn^{2+}, Mg^{2+}, and Ca^{2+}). The morphological, structural, and chemical properties of the produced films were determined by scanning electron microscope (SEM), high-resolution transmission electron microscopy (HRTEM), Fourier transform infrared (FT-IR) spectroscopy, and atomic force microscopy (AFM) analyses. The optical properties of the films were determined by ultraviolet-visible spectrophotometer (UV-Vis). Fluorescence and sensing properties were determined using photoluminescence (PL) spectroscopy analysis. SEM and transmission electron microscopy (TEM) analyses confirmed the strong bonding and homogeneous distribution between the BNQDs and the PMMA. FT-IR and TEM analyses proved the formation of BNQDs. PMMA-BNQDs nanocomposite film showed selective fluorescence quenching properties for Fe^{3+} ions. The fluorescence intensity of the nanocomposite films showed a good linear relationship between 0-60 µM for Fe^{3+}. In addition, it showed good sensitivity to detect Fe^{3+} ions in drinking water. Thus, this fluorescent sensing platform can be selective and sensitive in the 0-60 µM concentration range with a limit of detection (LOD) of 4.06 µM.

1. Introduction

The growth in the industrial area and the rapid increase in the population bring about water pollution [1]. Heavy metal ions in water negatively impact the environment and human health [2]. As it is known, it is impossible to live without water consumption, and for this reason, so much research is carried out to ensure that the water is clean and does not threaten human health. Polluted water can contain a wide variety of ions such as Cu^{2+}, Cd^{2+}, Co^{2+}, Ni^{2+}, Al^{3+}, Pb^{2+}, Hg^{2+}, Fe^{3+}, Fe^{2+}, and these ions can combine to form more dangerous compounds [3]. These highly toxic compounds cannot decompose and, as a result, continue accumulating on the earth, causing harm to the human body [4]. This situation has encouraged researchers to find new materials to remove and sense metal ions.

Quantum dots are used not only in bio-imaging or solar cells but also frequently in chemical sensor applications [5]. Boron nitride quantum dots (BNQDs) are promising sensor materials, especially in detecting fluorescent-based metal ions or gases, due to their photoluminescence emission, good solution dispersion, tunable band gap, and biocompatibility [6]. There are several studies in the literature in which BNQDs are used as metal ion-selective in solution form. However, BNQDs, unlike carbon quantum dots, are still open to development as metal sensors, as they are newly discovered. Huo et al. used BNQDs, which were produced by hydrothermal synthesis methods using boric acid and melamine to detect ferric ions in aqueous solutions. They concluded that prepared quantum dots could be effectively used as a valuable fluorochrome [7]. Liu et al. similarly used BNQDs produced by hydrothermal synthesis to detect different concentrations of Fe^{2+} and Fe^{3+} ions in the aqueous medium. In their study, they also simulated hydrothermal reaction and fluorescence properties using density simulated functional theory (DFT). They concluded that as the concentration of Fe^{2+} and Fe^{3+} increased, the fluorescence intensity of BNQDs was quenched [8]. Peng et al. exfoliated hexagonal boron nitride treated with hydrazine (N_2H_4) in an ethanol-water mixture and then obtained BNQDs by hydrothermal synthesis. The obtained BNQDs-based sensor material shows potential for selectively detecting 2,4,6-trinitrophenol in natural water without

*Corresponding author: duygu.gokdai@bilecik.edu.tr

any pretreatment process [9]. Wang et al. used hexagonal boron nitride quantum dot probes for the detection of Hg^{2+} ions. In the presence of Hg^{2+} ions in the medium, BNQDs created a peak at 560 nm under 280 nm excitation [10]. In the study of Han et al., the fluorescence effects of BNQDs on different metal ions were determined. It was observed that fluorescence peaks of both Fe^{3+} and Cu^{2+} ions could be quenched in the presence of BNQDs [11].

While there are several studies in the literature investigating the fluorescence properties of BNQDs in solution, no study has been found in which BNQDs/polymer nanocomposite films are used as test surfaces for metal ion detection. While metal ions can be detected in an aqueous solution or with the help of probes or devices, the fact that these methods are expensive, and the sensor materials can be prepared as a result of complex processes. This situation has led researchers to find practical and disposable economic methods such as fluorescent test papers or composite films [12-14]. In this method, chemical ions on the surface interact chemically with metals when test papers are immersed in a solution including metal ions. As a result of this interaction, the color change on the test paper can instantly detect metal ions. In their study, Wang et al. showed the sensor activity of the graphene quantum dots by coating them on the surface with the polyvinyl alcohol (PVA) polymer in different metal solutions [15]. Dalal et al. developed a sensor for detecting Fe^{3+} ions doped with polymer-based carbon dots. These sensors based on polyether amine showed high sensitivity in aqueous media with a limit of detection (LOD) value of 162 nm [16]. In 2021, Shirani et al. developed a polymer-integrated silica quantum dot-based sensor with a 1 nm LOD for indoxacarb [17].

Polymethyl methacrylate (PMMA) has a hydrophilic structure with a water contact angle of 68°. PMMA has many advantages over other polymers, such as superior environmental stability and scratch and UV resistance [18]. In addition, there are also studies showing that it is produced as a composite with boron nitride and that boron nitride is effectively distributed in this polymer [19,20]. Wang et al. also used $CsPbBr_3$ perovskite quantum dot/PMMA fiber structures in the detection of Cu^{2+} ions from water in their study [21]. In another study, PMMA films were produced using the electrospun method with fluorescent poly(amidoamine) to detect heavy Co^{2+} ions in water [22].

Some properties of polymers, such as low selectivity and sensitivity and weak photoluminescence properties, may limit their use, especially in heavy metal detection. Low-dimensional quantum dots are very effective in creating metal detection platforms due to their superior optical-electronic and chemical diversity properties. In addition, polymers provide an excellent matrix for the dispersion of these low-dimensional nanoparticles and enable them to use their properties as nanocomposite films [23]. Based on this motivation, in this study, after the BNQDs were formed by the hydrothermal synthesis method, they were incorporated into the PMMA polymer to produce nanocomposite film, and fluorescence properties were determined for different metal ions (Fe^{3+}, Na^{+}, Zn^{2+}, Mg^{2+}, and Ca^{2+}) for the first time. In addition, the effect of different concentrations of Fe^{3+} aqueous solutions (0-100 µM) on the fluorescence properties of nanocomposite films was also investigated. This test surface has been developed as an environmentally friendly, economical, and practical sensor material that detects metal contamination in aqueous solutions.

2. Materials and Methods

2.1. BNQDs and PMMA/BNQDs Fluorescent Sensing Platform Preparation

BNQDs were produced using the hydrothermal synthesis method. Here, the dispersant phase in the BNQD solution is 10 mL of ethanol, 5 mL of distilled water for boric acid, and 10% ammonia solution for urea. Details of the synthesis of BNQDs were given in our previous work [24]. A certain amount of PMMA (Sigma-Aldrich, US) was dissolved to form the composite films in 50 mL acetone. Then, the PMMA solution was added to the BNQDs solution at a weight ratio of 1:0.2. The solution was sonicated for 1 hour and stirred for 6 hours using a magnetic stirrer. The resulting mixture was kept in the beaker and dried completely under ambient conditions, and then it was obtained as BNQDs-doped PMMA composite films. The flow chart of the experimental method is shown in Figure 1.

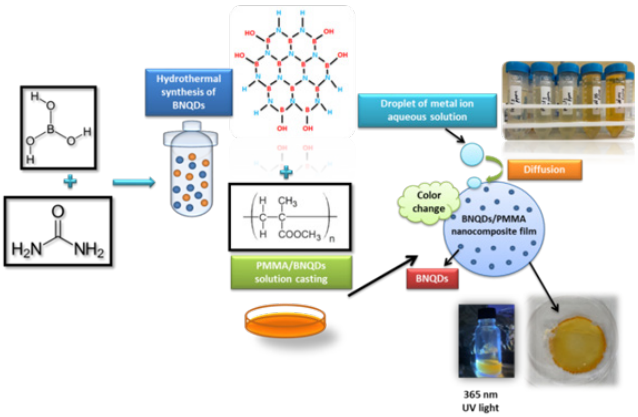

Figure 1. Schematic flow chart of the process

2.2. Metal Ion Detection of PMMA/BNQDs Fluorescent Sensing Platform

Heavy metal solutions were prepared from their salts and nitrates. Fe^{3+} prepared from $FeCl_3$, Na^{+} from NaCl, Zn^{2+} from $Zn(NO_3)_2$, Mg^{2+} from $MgCl_2$ and Ca^{2+} from $CaCl_2$. In a typical process, a certain amount of (100 µM) metal ions (Fe^{3+}, Na^{+}, Zn^{2+}, Mg^{2+}, and Ca^{2+}) were added into water, and then the PMMA/BNQDs films were immersed in the different metal ions aqueous solutions. Different concentrations (0, 20, 45, 60,

80, and 100 μM) of Fe^{3+} aqueous solutions were prepared, and the films were immersed for 3 minutes. PL measurements were carried out after the films were removed from the solution.

2.3. Characterization

The morphological and chemical analysis was performed using SEM (Zeiss Supra 40VP, Germany) at different magnifications (25 and 75 kX for PMMA and 10 and 40 kX for PMMA-BNQDs composite film), high-resolution TEM (HRTEM) (FEI TALOS F200S TEM, 200 kV, US), and FT-IR (Agilent Technologies, Cary 630, between 400-4000 cm^{-1}, US) analysis. Optical properties of the composites were determined by UV-Vis spectrophotometer (Agilent Technologies, Cary 60 UV-Vis, US) and photoluminescence properties were determined by PL spectroscopy (Dongwoo optron, matched with maple II HeCd laser, 532 nm, between 200 and 800 nm, South Korea). AFM analyzed the size of the produced composite with the scan size fixed to 1 μm × 1 μm (Park Systems, South Korea).

3. Results and Discussion

The most priority analyses to define the optical properties of quantum dots are the determination of absorption and fluorescence spectrum. Figure 2a shows the UV-Vis spectrum of pure and composite samples.

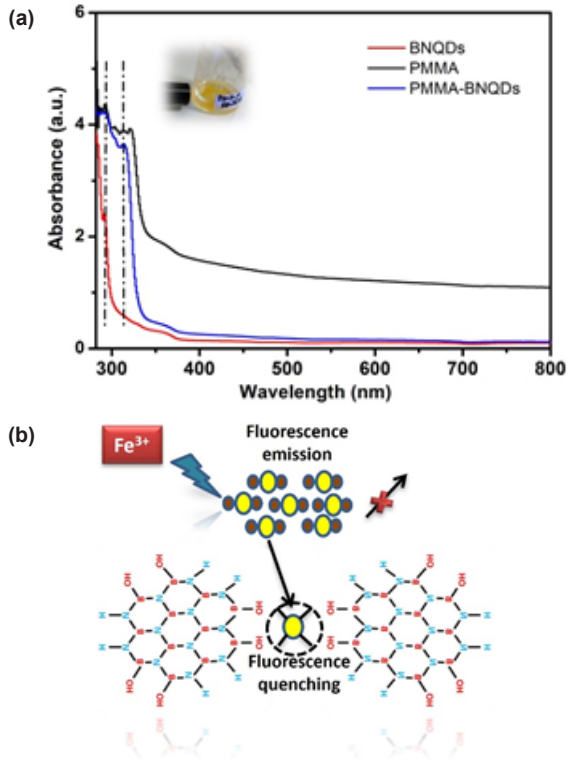

Figure 2. UV-Vis spectrum of the pure and composite samples; inset: PMMA-BNQDs composite solution appears as a blue-green color under 365 nm UV light (a), possible fluorescence quenching mechanism of PMMA/BNQDs film by Fe^{3+} (b)

Two main peaks appear around 280 and 290 nm in the absorption spectrum of the obtained BNQDs. While the intense peak at 280 nm is defined as the peak arising due to band transitions in quantum dots, the weak peak at 290 nm is due to the change in the band gap. The main reason for this band gap change is the functional groups attached to the surface of the quantum dots [25-27]. Two different peaks occur at 280 and 315 nm in the absorption spectrum of the PMMA-BNQDs composite film. These are the peaks from BNQDs and PMMA polymer, respectively. Compared with the absorption spectrum of BNQDs, the peak at 280 nm in the composite sample did not show any shift, indicating that the quantum dots were distributed homogeneously in the PMMA [28]. Figure 2b shows the possible fluorescence capture mechanism of iron ions by the PMMA-BNQDs composite film.

Boron nitride has an electron affinity towards metal ions thanks to the abundance of hydroxyl and amino groups at the corners of the quantum dots. When metal ions form a complex with the surface of BNQDs, the basic level of fluorescence is quenched and turns into a non-fluorescent compound. After photoexcitation, the BNQDs metal ion complex returns to its ground state by absorbing the blocked light and emission [29]. Figure 3a includes the IR spectrum of the produced BNQDs. FT-IR analysis is one of the most effective methods for determining the chemical structure and analysis of functional groups in the sample.

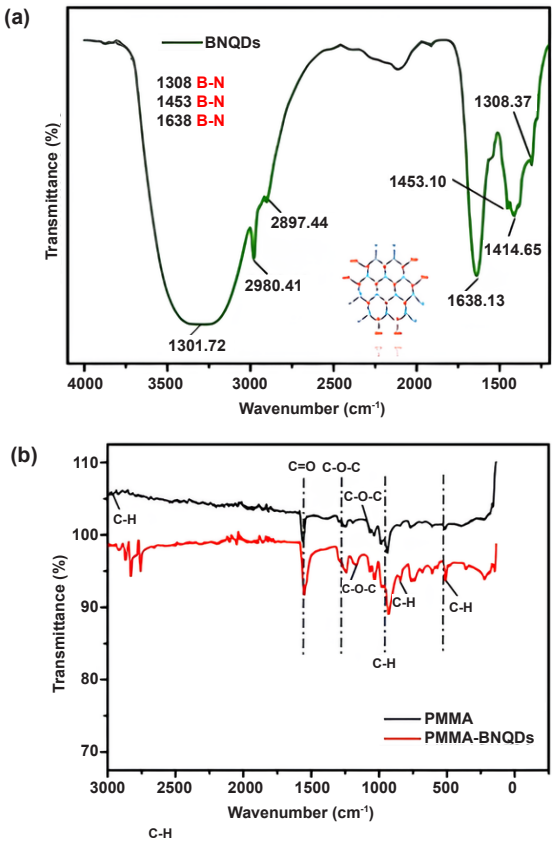

Figure 3. IR spectrum of BNQDs (a) and IR spectrum of PMMA and PMMA-BNQDs nanocomposite film (b)

BNQDs showed absorption bands at 1308, 1453, and 1638 cm^{-1}, respectively, due to the B-N stretching modes [8]. The band at 1414 cm^{-1} belongs to C-O bending [30]. The broad tensile band at 3300 cm^{-1} can be explained as the tensile band belonging to the N-H or O-H stretching. The appearance of the strains in the boron and nitrogen bonds and also functional groups such as -OH and $-NH_2$ in the IR spectra indicates that boron nitride was formed. FT-IR analysis is not sufficient to prove this. Therefore, the formation of quantum dots was supported by high-resolution TEM images. Figure 3b represents the IR spectrum of pure polymer and BNQDs polymer composite film. A sharp peak around 1730 cm^{-1} is consistent with the C=O stretching and stretching or deformation of C-O-C vibration peaks observed at 1249, 1164, and 1069 cm^{-1}. The peaks around 933 cm^{-1} and 844 cm^{-1} belong to the bending vibrations of C-H. The polymer chains have an absorption band around 750 cm^{-1} [31].

FTIR spectra of the PMMA-BNQDs nanocomposite film showed an absorption band at nearly 2970 cm^{-1} due to the C-H stretching vibration. Compared to the pure polymer, the peak intensities increased with the inclusion of boron nitride quantum dots into the structure at the stress intensity of 508 cm^{-1}, 928 cm^{-1}, and 1553 cm^{-1}, respectively. As a result of the modification of the polymer structure with the coating of boron nitride nanoparticles, the stretching band of the C-O-C shifted [32]. This shows that boron nitride nanoparticles are effectively incorporated into the PMMA polymer structure.

Figure 4 contains SEM images of PMMA and PMMA-BNQDs nanocomposite film at different magnifications. Figure 4 a,b shows the morphology of the PMMA polymer at magnifications of 25 and 75 kX, respectively. PMMA particles show a single type of morphology with a spherical shape and narrow size distribution [33]. Spherical particles are distributed with an average diameter of 0.15 μm. Figure 4 c,d contains the morphology of PMMA-BNQDs nanocomposite films at different magnifications. While some particles have smooth surfaces, some are coated with agglomerated BNQDs nanoparticles. The average size of these particles is 1.45μm, and it is clearly observed that they are larger than the pure PMMA polymer. This confirms a strong chemical electron affinity between BNQDs and PMMA, facilitating the formation of the core and shell [34].

Figure 5 shows the TEM image of the pure PMMA and PMMA-BNQDs nanocomposite film. In Figure 5a, PMMA shows a well-dispersed and forms an interconnected network-like structure [35]. In Figure 5b, the dark region refers to fluorescent particles and holes due to particle aggregation [36]. BNQDs have a significant agglomeration in some places in the polymer matrix. However, it is generally possible to say that the quantum dots are distributed homogeneously within the polymer. Figure 5c contains the HRTEM image of the obtained BNQDs. The average size

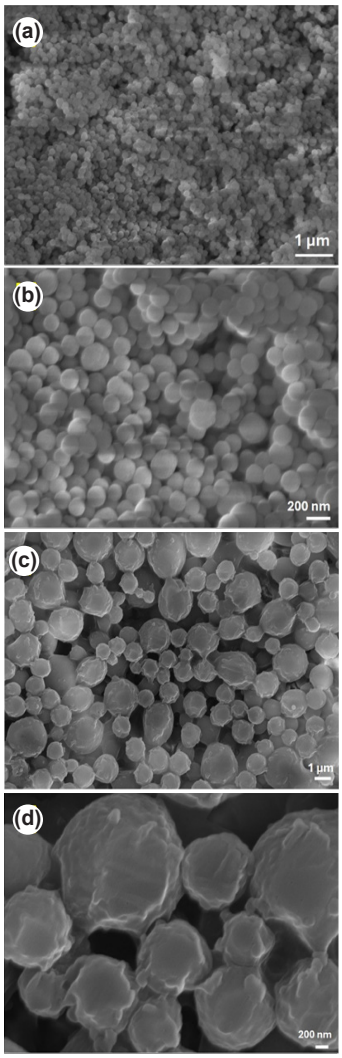

Figure 4. SEM images of the samples at different magnifications PMMA- 25 kX (a), PMMA-75 kX (b), PMMA-BNQDs-10 kX (c), PMMA-BNQDs-40 kX (d)

of quantum dots is 4.5 nm. High-resolution TEM images represent hexagonal boron nitride with high crystallinity and (002) the plane which confirms the production of BNQDs [37]. The surface morphology of PMMA-BNQDs nanocomposite film was identified by AFM with the scan size fixed to 1 μm × 1 μm (Figure 5d). The surface texture of polymer composites and the average size of the particles are also consistent with SEM and TEM images. The dispersed inorganic parts are homogeneously embedded in the polymer film. PMMA/BNQDs composite film comprises microspheres, as shown in the AFM histogram. The average size of BNQDs incorporated PMMA macro spheres is calculated as 1.6 μm. The size of these particles means that several interconnected quantum dots are embedded in the polymer [38].

Figure 6a shows the PL spectrum of PMMA-BNQDs nanocomposite film for 100 μM of different metal ions. In the spectrum, the emission peak for Ca^{2+}, Mg^{2+}, and Na^{+} was around 510 nm, while for Fe^{3+} and Zn^{2+}, this emission peak was observed around 538 and 540 nm, respectively.

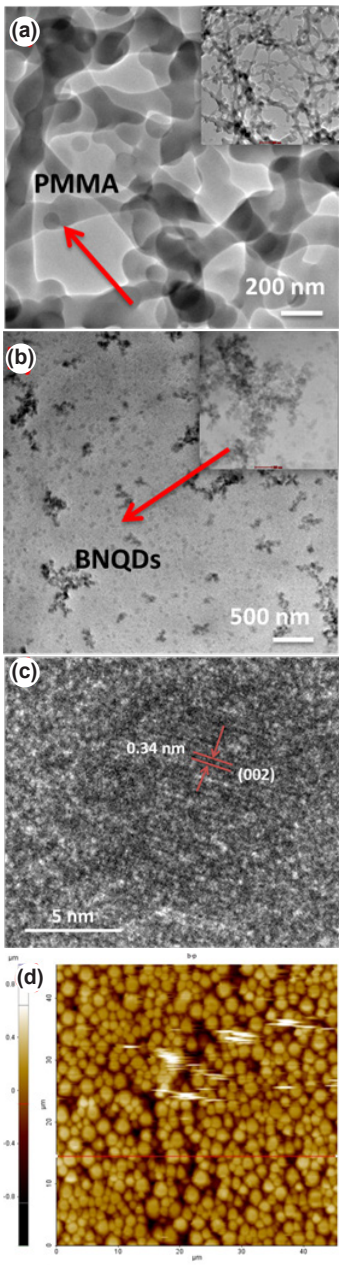

Figure 5. TEM image of pure PMMA sample (a), TEM image of PMMA-BNQDs nanocomposite film (b), HRTEM image of the BNQDs (c), and AFM image of the PMMA-BNQDs nanocomposite film (d)

This shift is seen more clearly in the normalized PL spectrum (Figure 6b). Here, the functional groups at the ends of BNQDs interact with metal ions and want to form stronger complexes with these metals [39]. Although there is no clear information about the fluorescence quenching mechanism for each metal, we assume that differences in the intermolecular interactions between different metals and composite films lead to different emission peaks in the fluorescence spectrum [40]. In their study, Wang et al. similarly observed that while the emission peak of BNQDs was observed at 461 nm, in the environment of Hg^{2+} ions, this emission peak shifted to 560 nm and created a fluorescence response against these ions. They interpreted the reason for this shift as the absorption of fluorescence from parts not connected to Hg^{2+} ions through induced electron transfer and internal filter effect [10]. There are many studies in the literature where BNQDs are used as sensors in liquid solution form in the detection of heavy metals, and it is clearly stated in these studies that the possible fluorescence response of the BNQDs against the Fe^{3+} ion is due to electron transfer [9, 11]. Boron nitride quantum dots interact with Fe^{3+} ions thanks to their rich amine groups and transfer the excited electrons to the half-filled orbitals of the Fe^{3+} ion. As a result of this excitation, the electron/hole part disappears, and fluorescence quenching occurs [41]. This quenching is apparently due to the affinity relationship of Fe^{3+} ions with the functional groups of BNQDs.

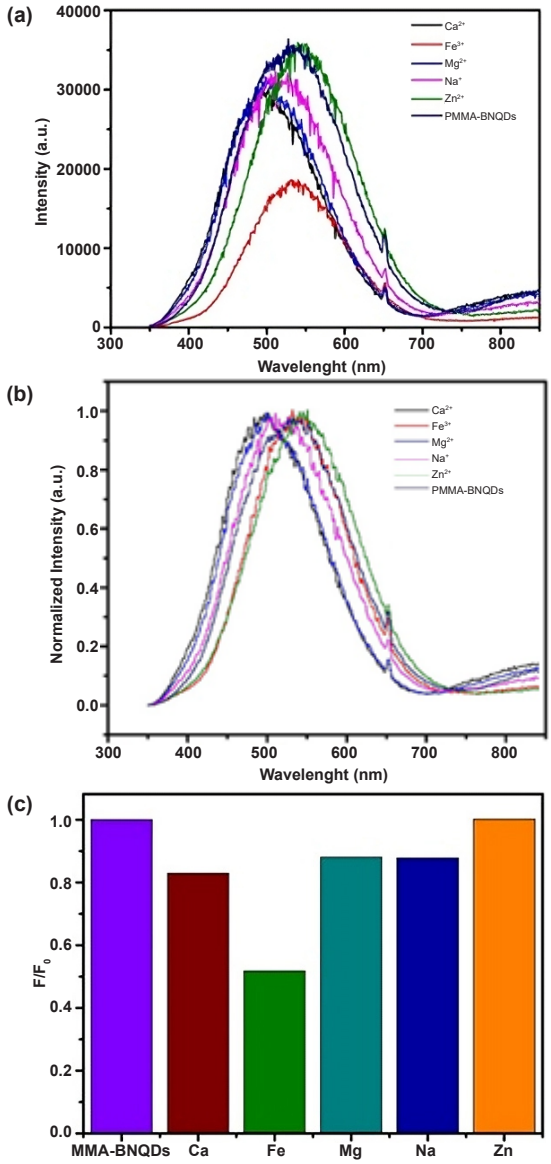

Figure 6. PL spectrum of PMMA-BNQDs nanocomposite film for 100 µM of different metal ions (a),normalized PL spectrum of PMMA-BNQDs nanocomposite film for 100 µM of different metal ions (b), selective fluorescence response of PMMA-BNQDs film towards 100 µM of different metal ions. F_0 and F represent the fluorescence intensity of PMMA/BNQDs film in the absence and presence of metal ions (c), respectively

The main reason for this affinity is that Fe^{3+} ions, which have paramagnetic properties, compensate for the electron deficiency on the surface of BNQDs. Due to the paramagnetic property of Fe^{3+}, it has high bonding interaction with electron-rich -OH or $-NH_2$ groups on the surface of BNQDs. These half-filled orbitals of the Fe^{3+} ion are very suitable for the transfer. The filling of these empty holes by these electrons results in the quenching of the fluorescence of the quantum dots [42,43]. In order to determine the selectivity of the obtained nanocomposite films, F/F_0 values were calculated for each metal using the PL spectra obtained in different metal ion solutions prepared at 100 µM concentration (Figure 6c). Zn^{2+} did not show any quenching effect. It can be seen clearly from Figure 6c that Ca^{2+}, Mg^{2+}, and Na^{+} show a slight quenching effect compared to Fe^{3+}. It is observed that the obtained PMMA-BNQDs nanocomposite sample has selectivity towards Fe^{3+} ion due to its high damping effect. For this reason, different concentrations of Fe^{3+} ions between 0-100 µM were prepared, and their absorbance and PL spectra were recorded.

Figure 7a shows the UV-Vis spectrum of PMMA-BNQDs nanocomposite film for different (0, 20, 45, 60, 80 and 100 µM) concentrations of Fe^{3+} ion. When nanocomposite films were immersed in Fe^{3+} solutions of different concentrations, it was observed that their absorbance values increased as the concentration of the metal ion increased. The linear increase in absorption intensity is related to the increase in complex formation, which leads to an increase in nanoparticle concentration. In general, this change in absorption intensity can be associated with an increase in particle size [44]. More importantly, it was observed that when the composites were immersed in Fe^{3+} solution, the peak of around 280 nm belonging to BNQDs disappeared, and the films showed a peak of around 260 nm. The disappearance of this peak compared to Figure 2a shows that the BNQDs surfaces are modified with Fe^{3+} ions and the films form complexes with Fe^{3+} ions [45]. Figure 7b represents the PL spectrum of PMMA-BNQDs nanocomposite film for different concentrations of Fe^{3+} ions. The fluorescence intensity of the nanocomposite films decreased with the increase in the concentration of Fe^{3+} ions. This can be associated with the fact that as the amount of Fe^{3+} ions in the medium increases, the empty orbitals of the Fe^{3+} ions are filled by electron transfer by quantum dots, thus increasing the damping demand and quenching of the films [42]. Figure 7c includes the relationship between F_0/F and Fe^{3+} ion concentration between 0-60 µM. While the calibration curve shows a linear trend between 0-60 µM, this trend does not exist between 0-100µM (Inset of Figure 7c). This shows that the sensitivity of the composite film above 60 µM is relatively low. For this reason, the LOD value and standard deviation were calculated for the 0-60 µM sensitivity level. The LOD value is the lowest value of a quantitatively specified signal, such as concentration and activity. In other words, it is known as the lowest

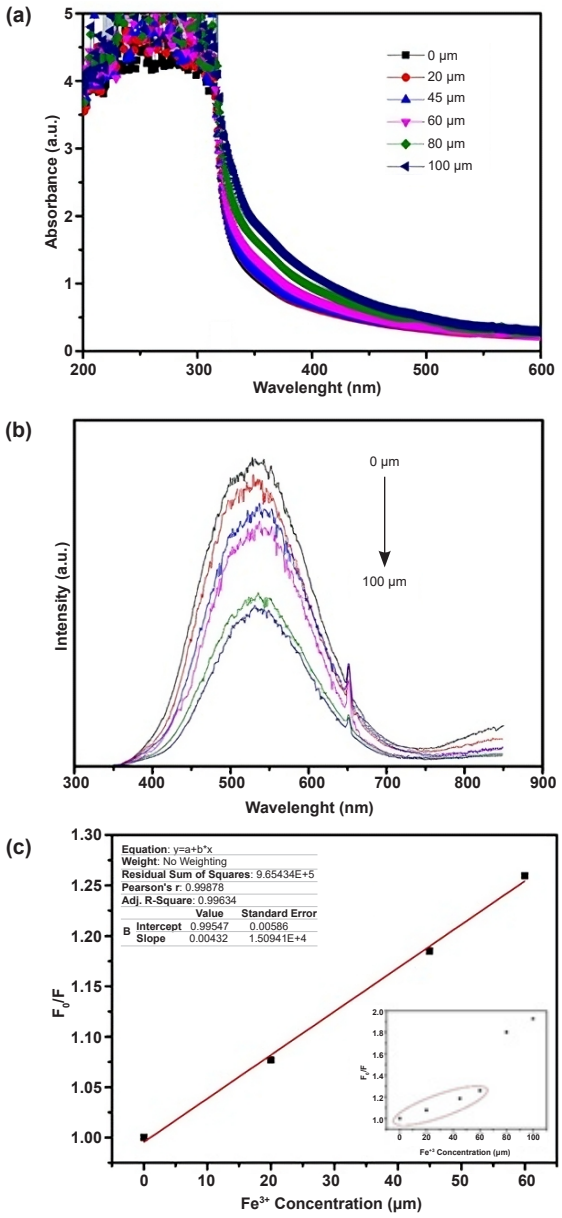

Figure 7. UV-Vis spectrum of PMMA-BNQDs nanocomposite film for different concentrations of Fe^{3+} ion (a), PL spectrum of PMMA-BNQDs nanocomposite film for different concentrations of Fe^{3+} ion (b), Calibration curve to present the relationship between fluorescence emission peak and Fe^{3+} concentration between 0-60 µM where F_0 and F are the fluorescence intensities in the absence and presence of Fe^{3+} ions (c), inset: calibration curve to present the relationship between fluorescence emission peak and Fe^{3+} concentration between 0-100 µM

amount of a matter that can be separated from the failure of that matter and identified within a given confidence interval [46]. According to the graph, the change in Fe^{3+} ion concentration between 0-60 µM showed a linear relationship, confirmed by the R^2 value of 0.99634. In addition, the standard deviation value of the linear curve is quite low (0.000150), which shows that the data points are distributed closer to the mean, the data set is not scattered, and small deviations are present [47].

This stable complex of Fe^{3+} with BNQDs confirms the static fluorescence quenching relationship.

On the other hand, the limit of detection (LOD) was calculated according to the following formula, where δ is the standard deviation [48]:

$$LOD = \frac{3\delta}{slope} \quad (1)$$

Using the data in Table 1, LOD was determined as 4.06 μM, lower than the Environmental Protection Agency (EPA) guidelines for drinking water of 5.37 μM [49].

Lv et al. obtained films from PVA and sulfur quantum dots that detected Fe^{3+} ions and found a limit of detection value of 0.69 μM. The stabilization of the polymer used here was quite effective. The fact that the sulfur quantum dots did not agglomerate in the polymer caused them to exhibit strong photoluminescence properties [28]. In another study, Gogoi et al. showed that the hydrogels they prepared using chitosan and carbon quantum dots had a detection limit of 0.0005 μM in detecting Fe^{3+} ions [50]. Compared with the results found here, the agglomeration and concentration of BNQDs in some areas within PMMA negatively affected the photoluminescence properties and LOD value. The sensor sensitivity ranges of composite materials can be improved by using different polymers. The results obtained were guiding in terms of directing the use of BNQDs in the detection of heavy metals in water by forming films with different polymers.

Table 1. Calibration data of PMMA-BNQDs nanocomposite film with Fe^{3+}

Parameter	Fe^{3+}
Regression equation	F_0/F=0.00432[μM]+0.99547
Slope	0.00432
Intercept	0.99547
R^2	0.99634
Correlation coefficient (r)	0.99878
Linear range	0-60 μM
SD of intercept	0.00586
SD of slope	0.000150
LOD	4.06 μM

4. Conclusions

Herein, PMMA-BNQDs nanocomposite film was successfully synthesized as a fluorescence test surface to identify metal ions in water selectively. Various characterization techniques have demonstrated the morphological structure of nanocomposite films and the chemical groups they contain. While FT-IR and HR-TEM analysis proved the existence of BNQDs, the structural analysis of the films was supported by FT-IR, SEM, TEM, and AFM analyses. It was determined that the obtained films showed selective fluorescence quenching properties against Fe^{3+}. The fluorescence intensities of the films showed a linear relationship between 0-60 μM and were calculated to have a LOD value of 4.06 μM. This reveals that this fluorescence sensing platform can selectively and sensitively detect Fe^{3+} ions in drinking water between 0-60 μM. Fluorescence quenching is apparently due to the affinity relationship of Fe^{3+} ions with the functional groups of BNQDs. These groups attached to the surface of BNQDs are electron-rich groups and show high interaction due to the paramagnetic properties of Fe^{3+} ions. This study has guided the use of boron nitride quantum dot-based polymer nanocomposite films as fluorescence sensing platforms, and it also offers an innovative and practical application approach for the use of polymer-based composite structures in the detection of metal ions.

5. Author Contribution Statement

Duygu Kuru: Conceptualization, methodology, data curation, writing-original draft preparation, visualization, investigation, validation, writing-review, and editing.

References

[1] Dawoud, H. D., Saleem, H., Alnuaimi, N. A., & Zaidi, S. J. (2021). Characterization and treatment technologies applied for produced water in Qatar. *Water*, *13*(24), 3573. https://doi.org/10.3390/w13243573

[2] Soliman, M.N., Guen, F.Z., Ahmed, S.A., Saleem, H., & Zaidi, S.J. (2002) Environmental impact assessment of desalination plants in the gulf region. In V. Naddeo, K. H. Choo, M. Ksibi (Eds.), *Water-energy-nexus in the ecological transition*. Advances in science, technology & innovation (pp. 173-177). Springer, Cham.. https://doi.org/10.1007/978-3-031-00808-5_41

[3] Saleem, H., Zaidi, S. J., Ismail, A. F., Goh, P. S., & Vinu, A. (2022). Recent advances in the application of carbon nitrides for advanced water treatment and desalination technology. *Desalination*, *542*, 116061. https://doi.org/10.1016/j.desal.2022.116061

[4] Saud, A., Saleem, H., Munira, N., Shahab, A. A., Siddiqui, H. R., & Zaidi, S. J. (2023). Sustainable preparation of graphene quantum dots for metal ion sensing application. *Nanomaterials*, *13*(1), 148. https://doi.org/10.3390/nano13010148

[5] Li, Q., Zhou, W., Yu, L., Lian, S., & Xie, Q. (2021). Perovskite quantum dots as a fluorescent probe for metal ion detection in aqueous solution via phase transfer. *Materials Letters, 282*, 128654. https://doi.org/10.1016/j.matlet.2020.128654

[6] Bian, S., Shen, C., Hua, H., Zhou, L., Zhu, H., Xi, F., … & Dong, X. (2016). One-pot synthesis of sulfur-doped graphene quantum dots as a novel fluorescent probe for highly selective and sensitive detection of lead(II). *RSC Advances*, *6*(74), 69977-69983. https://doi.org/10.1039/C6RA10836A

[7] Huo, B., Liu, B., Chen, T., Cui, L., Xu, G., Liu, M., & Liu, J. (2017). One-step synthesis of fluorescent boron

nitride quantum dots via a hydrothermal strategy using melamine as nitrogen source for the detection of ferric ions. *Langmuir*, *33*(40), 10673-10678. https://doi.org/10.1021/acs.langmuir.7b01699

[8] Liu, B., Yan, S., Song, Z., Liu, M., Ji, X., Yang, W., & Liu, J. (2016). One-step synthesis of boron nitride quantum dots: Simple chemistry meets delicate nanotechnology. *Chemistry A European Journal*, *22*(52), 18899-18907. https://doi.org/10.1002/chem.201603935

[9] Peng, D., Zhang, L., Li, F., Cui, W., Liang, R., & Qui, J. (2018). Facile and green approach to the synthesis of boron nitride quantum dots for 2,4,6-trinitrophenol sensing. *ACS Applied Materials Interfaces*, *10*(8), 7315-7323. https://doi.org/10.1021/acsami.7b15250

[10] Wang, L., Zhang, Q., Su, P., Yu, L., Bu, Y., Yuan, C., & Wang, S. (2022). Excitation-dependent ratiometric fluorescence response to mercury ion based on single hexagonal boron nitride quantum dots. *Analytica Chimica Acta*, *1236*, 340585. https://doi.org/10.1016/j.aca.2022.340585

[11] Han, Y., Niu, Y., Liu, M., Niu, F., & Xu, Y. (2019). A rational strategy to develop a boron nitride quantum dot-based molecular logic gate and fluorescent assay of alkaline phosphatase activity. *Journal of Materials Chemistry B*, *7*(6), 897-902. https://doi.org/10.1039/C8TB02948B

[12] Yu, X., Yang, L., Zhao, T., Zhang, R., Yang, L., Jiang, C., … & Zhang, Z. (2017). Multicolorful ratiometric-fluorescent test paper for determination of fluoride ions in environmental water. *RSC Advances*, *7*(5), 53379-53384. https://doi.org/10.1021/am506558d

[13] Cheng, Z., Liu, X., Zhao, B., Liu, X., Yang, X., Zhang, X., & Feng, X. (2024). A portable europium complex-loaded fluorescent test paper combined with smartphone analysis for the on-site and visual detection of mancozeb in food samples. *Food Chemistry*, *458*, 140311. https://doi.org/10.1016/j.foodchem.2024.140311

[14] Huang, T., Xu, Y., Meng, M., & Li, C. (2022). PVDF-based molecularly imprinted ratiometric fluorescent test paper with improved visualization effect for catechol monitoring. *Microchemical Journal*, *178*, 107369. https://doi.org/10.1016/j.microc.2022.107369

[15] Wang, C., Sun, Y., Jin, J., Xiong, Z., Li, D., Yao, J., & Liu, Y. (2018). Highly selective, rapid-functioning and sensitive fluorescent test paper based on graphene quantum dots for on-line detection of metal ions. *Analytical Methods*, *10*(10), 1163-1171. https://doi.org/10.1039/C7AY02995K

[16] Dalal, C., Garg, A. K., Mathur, M., & Sonkar, S. K. (2022). Fluorescent polymer carbon dots for the sensitive-selective sensing of Fe3+ metal ions and cellular imaging. *ACS Applied Nano Materials*, *5*(9), 12699-12710.https://doi.org/10.1021/acsanm.2c02544

[17] Shirani, M. P., Rezaei, B., Ensafi, A. A., & Ramezani, M. (2021). Development of an eco-friendly fluorescence nanosensor based on molecularly imprinted polymer on silica-carbon quantum dot for the rapid indoxacarb detection. *Food Chemistry*, *339*, 127920.https://doi.org/10.1016/j.foodchem.2020.127920

[18] Ma, Y., Cao, X., Feng, X., Ma, Y., & Zou, H. (2007). Fabrication of super-hydrophobic film from PMMA with intrinsic water contact angle below 90. *Polymer*, *48*(26), 7455-7460. https://doi.org/10.1016/j.polymer.2007.10.038

[19] Cui, Z., Martinez, A. P., & Adamson, D. H. (2015). PMMA functionalized boron nitride sheets as nanofillers. *Nanoscale*, *7*(22), 10193-10197.https://doi.org/10.1039/C5NR00936G

[20] Liu, F., Li, Q., Li, Z., Liu, Y., Dong, L., Xiong, C., & Wang, Q. (2017). Poly(methyl methacrylate)/boron nitride nanocomposites with enhanced energy density as high temperature dielectrics. *Composites Science and Technology*, *142*, 139-144.https://doi.org/10.1016/j.compscitech.2017.02.006

[21] Wang, Y., Zhu, Y., Huang, J., Cai, J., Zhu, J., Yang, X., & Li, C. (2017). Perovskite quantum dots encapsulated in electrospun fiber membranes as multifunctional supersensitive sensors for biomolecules, metal ions and pH. *Nanoscale Horizons*, *2*(4), 225-232. https://doi.org/10.1039/C7NH00057J

[22] Wang, Q., Sun, G., Wei, S., Hao, W., & Yang, W. (2021). HPAMAM/PMMA composite electrospun film for cobalt ion detection in water environments. *Materials Letters*, *299*, 130115. https://doi.org/10.1016/j.matlet.2021.130115

[23] Tajik, S., Beitollahi, H., Nejad, F. G., Dourandish, Z., Khalilzadeh, M. A., Jang, H. W., … & Shokouhimehr, M. (2021). Recent developments in polymer nanocomposite-based electrochemical sensors for detecting environmental pollutants. *Industrial & Engineering Chemistry Research*, *60*(3), 1112-1136. https://doi.org/10.1021/acs.iecr.0c04952

[24] Emir, P., & Kuru, D. (2024). Boron nitride quantum dots/polyvinyl butyral nanocomposite films for the enhanced photoluminescence and UV shielding properties. *Journal of Applied Polymer Science*, *141*(13), e55171. https://doi.org/10.1002/app.55171

[25] Yang, Y., Zhang, C., Huang, D., Zeng, G., Huang, J., Lai, C., … & Xiong, W. (2019). Boron nitride quantum dots decorated ultrathin porous g-C3N4: Intensified exciton dissociation and charge transfer for promoting visible-light-driven molecular oxygen activation. *Applied Catalysis B: Environmental*, *245*, 87-99. https://doi.org/10.1016/j.apcatb.2018.12.049

[26] Liu, M., Xu, Y., Wang, Y., Chen, X., Ji, X., Niu, F., Song, Z., & Liu, J. (2017). Boron nitride quantum dots with solvent-regulated blue/green photoluminescence and electrochemiluminescent behavior for versatile applications. *Advanced Optical Materials*, *5*(3), 1600661. https://doi.org/10.1002/adom.201600661

[27] Abdelsalam, H., & Zhang, Q. F. (2022). Properties and applications of quantum dots derived from two-dimensional materials. *Advances in Physics: X*, *7*(1), 2048966. https://doi.org/10.1080/23746149.2022.2048966

[28] Lv, G., Dai, X., Lu, G., Ye, L., Wang, G., & Zhou, L. (2023). Facile fabrication of portable electrospun poly(vinyl alcohol)/sulfur quantum dots film sensor for sensitive and selective detection of Fe3+. *Optical Materials*, *135*, 113227.https://doi.org/10.1016/j.optmat.2022.113227

[29] Sekar, A., Yadav, R., & Basavaraj, N. (2021). Fluorescence quenching mechanism and the application of green carbon nanodots in the detection of heavy metal ions: A review. *New Journal of Chemistry*, *45*(5), 2326-2360. https://doi.org/10.1039/D0NJ04878J

[30] Mohan Babu, M., Syam Prasad, P., Venkateswara Rao, P., Hima Bindu, S., Prasad, A., Veeraiah, N., & Özcan, M. (2020). Influence of ZrO2 addition on structural and biological activity of phosphate glasses for bone regeneration. *Materials*, *13*(18), 4058.https://doi.org/10.3390/ma13184058

[31] Mthethwa, T. P., Moloto, M. J., Vries, A. D., & Matabola, K. P. (2011). Properties of electrospun CdS and CdSe filled poly(methyl methacrylate) (PMMA) nanofibres. *Materials Research Bulletin*, *46*(4), 569-575. https://doi.org/10.1016/j.materresbull.2010.12.022

[32] Alqahtani, M. (2020). Effect of hexagonal boron nitride nanopowder reinforcement and mixing methods on physical and mechanical properties of self-cured PMMA for dental applications. *Materials*, *13*(10), 2323. https://doi.org/10.3390/ma13102323

[33] Khan, F. A., Akhtar, S., Almohazey, D., Alomari, M., Almofty, S. A., Badr, I., & Elaissari, A. (2019). Targeted delivery of poly (methyl methacrylate) particles in colon cancer cells selectively attenuates cancer cell proliferation. Artificial Cells, *Nanomedicine, and Biotechnology*, *47*(1), 1533-1542. https://doi.org/10.1080/21691401.2019.1577886

[34] Meng, X., Cui, H., Dong, J., Zheng, J., Zhu, Y., Wang, Z., … & Zhu, Z. (2013). Synthesis and electrocatalytic performance of nitrogen-doped macroporous carbons. *Journal of Materials Chemistry A*, *1*, 9469-9476. https://doi.org/10.1039/C3TA10306D

[35] Pawar S., Rzeczkowski P. P., Pötschke P., Krause B., & Bose S. (2018). Does the processing method resulting in different states of an interconnected network of multiwalled carbon nanotubes in polymeric blend nanocomposites affect EMI shielding properties? *ACS Omega*, *3*(5), 5771-5782. https://doi.org/10.1021/acsomega.8b00575

[36] Yoon, C., Yang, K. P., Kim, J., & Shin, K. (2020). Fabrication of highly transparent and luminescent quantum dot/polymer nanocomposite for light emitting diode using amphiphilic polymer-modified quantum dots. *Chemical Engineering Journal*, *382*, 122792. https://doi.org/10.1016/j.cej.2019.122792

[37] Lin, L., Xu, Y., Zhang, S., Ross, I. M., Ong, A. C. M., & Allwood, D. A. (2014). Fabrication and luminescence of monolayered boron nitride quantum dots. *Small*, *10*(1), 60-65. https://doi.org/10.1002/smll.201301001

[38] Poderys, V., Matulionyte, M., Selskis, A., & Rotomskis, R. (2011). Interaction of water-soluble cdte quantum dots with bovine serum albumin. *Nanoscale Research Letters*, *6*(9). https://doi.org/10.1007/s11671-010-9740-9

[39] Wu, F., Tong, H., Wang, K., Wang, Z., Li, Z., Zhu, X., … & Wong, W. K. (2016). Synthesis, structural characterization and photophysical studies of luminescent Cu(I) heteroleptic complexes based on dipyridylamine. *Journal of Photochemistry and Photobiology A: Chemistry*, *318*, 97-103. https://doi.org/10.1016/j.jphotochem.2015.12.003

[40] Upadhyay, P. K., Marpu, S. B., Benton, E. N., Williams, C. L., Telang, A., & Omary, M. A. (2018). A phosphorescent trinuclear gold(I) pyrazolate chemosensor for silver ion detection and remediation in aqueous media. *Analytical Chemistry*, *90*(8), 4999-5006. https://doi.org/10.1021/acs.analchem.7b04334

[41] Yao, Q., Feng, Y., Rong, M., He, S., & Chen, X. (2017). Determination of nickel(II) via quenching of the fluorescence of boron nitride quantum dots. *Mikrochima Acta*, *184*, 4217-4223. https://doi.org/10.1007/s00604-017-2496-5

[42] Chen, Y., Wu, Y., Bo, W., Wang, B., & Li, C. (2016). Facile synthesis of nitrogen and sulfur co-doped carbon dots and application for Fe(III) ions detection and cell imaging. *Sensors and Actuators B: Chemical*, 223, 689-696. https://doi.org/10.1016/j.snb.2015.09.081

[43] Ahmadian-Fard-Fini, S., Ghanbari, D., Amiri, O., & Salavati-Niasari, M. (2020). Electro-spinning of cellulose acetate nanofibers/fe/carbon dot as photoluminescence sensor for mercury (ii) and lead (ii) ions. *Carbohydrate Polymers*, *229*, 115428-115428. https://doi.org/10.1016/j.carbpol.2019.115428

[44] Islam, N. U., Amin, R., Shahid, M., Amin, M., Zaib, S., & Iqbal, J. (2017). A multi-target therapeutic potential of Prunus domestica gum stabilized nanoparticles exhibited prospective anticancer, antibacterial, urease-inhibition, anti-inflammatory and analgesic properties. *BMC Complementary and Alternative Medicine*, *17*(1), 276. https://doi.org/10.1186/s12906-017-1791-3

[45] Zhao, L., Wang, Y., Zhao, X., Deng, Y., & Xia, Y. (2019). Facile synthesis of nitrogen-doped carbon quantum dots with chitosan for fluorescent detection of Fe3+. *Polymers*, *11*(11), 1731. https://doi.org/10.3390/polym11111731

[46] Rajaković, L. V., Marković, D. D., Rajaković-Ognjanović, V. N., & Antanasijević, D. Z. (2012). The approaches for estimation of limit of detection for ICP-MS trace analysis of arsenic. *Talanta*, *102*, 79-87. https://doi.org/10.1016/j.talanta.2012.08.016

[47] Armbruster, D. A., & Pry, T. (2008). Limit of blank, limit of detection and limit of quantitation. *The Clinical Biochemist Reviews*, *29*(Suppl 1), 49-52. Retrieved from https://pubmed.ncbi.nlm.nih.gov/18852857/

[48] Khairy, G. M., Amin, A. S., Moalla, S. M. N., Medhat, A., & Hassan, N. (2022). Fluorescence determination of Fe(III) in drinking water using a new fluorescence chemosensor. *RSC Advances*, *12*(42), 27679-27686. https://doi.org/10.1039/d2ra05144c

[49] Liu, X., Li, N., Xu, M., Wang, J., Jiang, C., Song, G., & Wang, Y. (2018). Specific colorimetric detection of Fe3+ ions in aqueous solution by squaraine-based chemosensor. *RSC Advances*, *8*(61), 34860-34866. https://doi.org/10.1039/C8RA07345G

[50] Gogoi, N., Barooah, M., Majumdar, G., & Chowdhury, D. (2015). Carbon dots rooted agarose hydrogel hybrid platform for optical detection and separation of heavy metal ions. *ACS Applied Materials & Interfaces*, *7*(5), 3058-3067.https://doi.org/10.1021/am506558d

BOR DERGİSİ
JOURNAL OF BORON
https://dergipark.org.tr/boron

Ethyl vinyl acetate (EVA) composites with nanoclays and boric acid: Thermal and mechanical properties

İlker Erdem [1,*], **Şeyma Avcı** [2], **Mehmet Fazıl Kapçı** [2]

[1]*Abdullah Gül University, Faculty of Engineering, Materials Science and Nanotechnology Engineering Department, Kayseri, 38080, Türkiye*
[2]*Abdullah Gül University, Graduate School, Materials Science and Mechanical Engineering, Kayseri, 38080, Türkiye*

ARTICLE INFO

Article History:
Received October 16, 2024
Accepted January 17, 2025
Available online March 31, 2025

Research Article

DOI: 10.30728/boron.1568002

Keywords:
Boric acid
Ethyl vinyl acetate
Flame retardancy
Mechanical properties
Nanoclay

ABSTRACT

The polymers are widely used materials in various applications. Their flammability is a concern when the material will be facing high temperatures and/or conditions resulting in the incidence of ignition. The flame resistance of the polymers tends to be enhanced by the utilization of inorganic materials as additives. Versatile inorganic materials can be used for this purpose, e.g., ceramics (oxides, hydroxides, clays, etc.). The addition of inorganic additives could alter the mechanical properties of the polymer-inorganic composite structure, which should be considered during composite preparation as well. In this study, two different nanoclays (up to 20/100 by weight) and boric acid (BA) were added to ethyl vinyl acetate (EVA) to investigate possible enhancement in flame retardancy of the polymer. The mechanical properties were also determined for the neat polymer and polymer-inorganic composites to determine the effect of nanoclay and BA addition. The prepared nanocomposites were evaluated in terms of their chemical structures (Fourier transform infrared spectroscopy and X-Ray diffraction analysis), thermal characteristics (thermogravimetric analysis), mechanical properties (tensile test), and flammability behaviours. The NC 1.4 sample containing the highest amount of nanoclay had the longest burning time and Young's modulus. The NC 2.3 and NC 1.3-BA samples had relatively higher stress-bearing capabilities. The addition of BA enhanced the stress-bearing capability of NC 1 containing samples and it slightly increased the burning time for NC 2 containing composites. The organic surface modifiers of nanoclays and BA addition were effective on the thermal and mechanical characteristics of the nanoclay/EVA composites.were effective on the thermal and mechanical characteristics of the nano-clay/EVA composites.

1. Introduction

Polymer materials are widely used in various applications due to their distinctive qualities, such as light weight, mechanical strength, viscoelasticity, and chemical durability [1]. However, because of their chemical composition and organic content, they are flammable, which limits the areas of application [2]. Research has been focused on developing environmentally friendly techniques and materials for preventing or retarding the ignition of fire in recent years. The utilization of alternative materials as flame retardant additives instead of halogenated chemicals is preferred due to the environmental and health concerns [3]. The inorganic/ceramic additives (oxides like silicates, clays), hydroxides like ($Mg(OH)_2$) are promising candidates which are environmentally friendly options, but their effect on the mechanical properties of the polymer composite should also be considered. The high loadings of inorganic fillers are adversely affect the mechanical properties of the composite.

The combustion process of the polymers should be examined to determine the flammability of them or their composites. The combustion occurs when there is heat, oxygen, and combustible material [4]. The polymers release degradation products with increasing temperature which are highly combustible. The oxidation will initiate if there is enough heat for ignition, and combustion would continue if the energy released during the process is enough to proceed with the combustion. There are several ways to prevent the initiation and progress of combustion for polymers. The diffusion of flammable disintegration components from polymer and oxygen from air can be blocked by barrier layer formation on polymer surface. The energy released during combustion are used for some side reactions (e.g., oxidation, phase transformation of fillers) which will hamper the process of combustion. The release of non-combustible gases (e.g., water vapour) from additives can dilute the oxygen and combustible gases which are stop combustion. The free radicals are be trapped by additives to decrease the rate of thermal degradation and consequently

*Corresponding author: ilker.erdem@agu.edu.tr

combustion. The most common flame retardants can be classified as halogenated additives, metal hydroxides, P, N and Si containing additives [5]. The halogen-containing additives are not healthy or environmentally friendly, and their usage was banned by Environmental Protection Agency (EPA) [6]. Current research efforts are concentrated on the other healthier and environmentally friendly alternatives [3]. Different inorganic fillers like metal hydroxides and silica-containing ceramics (e.g., clays) are promising flame-retardant additives. The mechanical properties of the composite materials prepared with inorganic fillers would be another concern. The inorganic fillers should be added at levels which wouldn't adversely affect the mechanical properties of the polymer.

Nanotechnology and nanomaterials may present promising enhancements in many applications, since the physicochemical properties of materials are superior when they are in nanosize. The decreasing size and increasing surface area make the nanomaterials more reactive. The effects of atomic/molecular interactions (e.g., interactions among charged groups like dipoles) with neighbouring materials become more abundant in the material characteristics. These new characteristics of nanocomposites result in enhanced properties. Possible enhancements can be observed for the thermal and mechanical properties of the composites with relatively lower filler content [7,8].

Nanoclays which are composed of alternating layers of tetrahedral silicate (SiO_4^{4-}) and octahedral aluminium oxide-hydroxide ($[AlO_3(OH)_3]_6$) are attracting the attention of researchers for the preparation of polymer nanocomposites [7]. They were reported to enhance the nanocomposite properties in terms of mechanical characteristics, ultraviolet (UV) resistance, and flame retardancy more than macro/micro forms of clays [8]. These enhancements are consequences of the larger surface area of nanoclay platelets interacting with the polymer matrix. Increased interaction of nanoclay with the polymer matrix decreases the necessary amount of clay to possess the enriched property levels (e.g., flame retardancy, mechanical properties). These clay-polymer nanocomposites can be used in different fields like packaging, electronics, automotive, aerospace, water treatment, construction, and biomedical applications [9].

Montmorillonite (MMT) is a widely used plate-like (2D) clay with a chemical formula of $(Na,Ca)_{0.33}(Al,Mg)_2Si_4O_{10}(OH)_2.nH_2O$ [7]. Its availability, high surface area (up to 750 m^2/g) and plate-like structure with a high aspect ratio (100-500) are some of its advantageous properties [10]. The negative charge of the alternating layers of tetrahedral SiO_2 and octahedral AlO_6 are compensated by the cations (e.g. Al^{+3}, Mg^{2+}) to have charge neutrality [9]. It can act as a thermal barrier in the polymer composite to prevent combustion and it tends to improve the mechanical properties of the polymer composite [5]. The mechanism of flame retardancy of MMT-like nanoclays are expected to take place by the formation of a barrier layer during the combustion process with the contribution of non-flammable nanoclay platelets and carbonaceous residues of polymer oxidation (i.e., formation of an improved char layer) [5]. The better dispersed the nanoclay platelets in the polymer, the better barrier formation for oxygen and combustible gases diffusion and consequently better flame retardancy. The nano form of clays can be loaded in lower ratios than micro/macro forms to provide flame retardancy (e.g. 5-15 % instead of 50%), potentially preserving or even improving the mechanical characteristics of the polymer [2]. The plate-like structure with a high surface area and aspect ratio of MMT also makes it a good candidate to increase the mechanical properties of the nanoclay polymer composites since it increases the possibility of stress transfer from the polymer matrix [10]. The Young's modulus values for MMT were reported as 51 GPa (via extrapolation using epoxy/clay data) and 14 GPa (via extrapolation using acoustic data) [8].

The nanoclay polymer composites can be prepared by different methods like the solvent solution method, melt mixing and in situ polymerization [11], and sol-gel technique [8]. In the solvent solution method, the polymer is dissolved in the proper solvent, and nanoclay is dispersed. The nanoclay platelets swell in the solvent, and polymer with solvent penetrates among the layers forming the nanoclay [8]. The penetration of polymer-solvent among the layers happens at different levels; the ultimate penetration results in total separation of the layers (Figure 1).

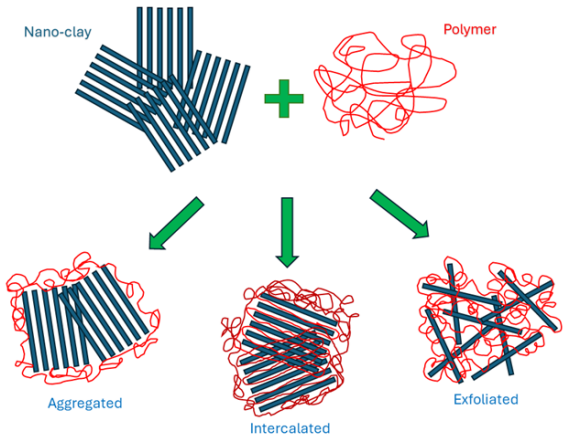

Figure 1. Nano-clay morphologies in polymer blends

The level of penetration can be affected by many parameters like interactions in the polymer/nanoclay/solvent system (e.g., type and ratios of clay, polymer, and solvent). The polymer/nanoclay surface characteristics (e.g,. polarity) in the presence of solvent could be determining on the separation of layers of nanoclay and penetration of polymer among them. The microstructure and properties of the composite after evaporation of the solvent are a result of these interactions among the polymer, nanoclay and the solvent. The surface of the nanoclay can be modified to enhance its compatibility with the polymer.

The organic chains added to the nanoclay surface change its surface polarity and tend to increase its affinity to the polymer chains. These surface modifications are aiming for better compatibility between the nanoclay and the polymer to suspend the nanoclay more efficiently to end up with a more homogeneous structure after solvent evaporation [9]. The aggregated clay particles become either intercalated (polymer penetrates in between the layers) or exfoliated (the layers are mostly separated from each other with the excess penetration of polymer) in the nanoclay/polymer suspension, resulting in more homogeneous suspension of nanoclay the parameters are optimized (Figure 1) [9]. The local aggregations of nanoclay result in a non-homogeneous composite structure with possibly worse mechanical properties and vice versa. Other properties of the nanocomposite can be affected by the distribution of nanoclay within the polymer matrix as well.

Ethylene vinyl acetate (EVA) copolymer is widely used in many sectors, including the wire and cable sector [11]. It possesses advantageous physicochemical characteristics and ease of compounding different additives or polymers (e.g., even with hydrophilic polymers like polylactic acid (PLA) with some fillers) [12]. The relatively low tensile strength and thermal stability of EVA copolymers could potentially considered disadvantageous [11]. The varying vinyl acetate (VA) content (e.g., 10-40%) has an influence on the properties of the EVA copolymer [10]. EVA copolymers with varying VA content are reported to cover the largest market share of the ethylene copolymers [13]. The VA content in EVA was reported to be effective on its physicochemical properties (e.g., crystallinity [13], polarity, and elastic characteristics [14]). The increased VA content in the copolymer (EVA) results in higher polarity but lower crystallinity, which can affect the mechanical behaviour of the polymer (or its composites) [15]. Also, the increasing polarity with a high VA content in the polymer was reported to improve its interaction with the clay which enhance the mechanical properties (e.g., Young's modulus, yield strength) of the EVA/nanoclay composite [15]. Moreover, inorganic fillers (e.g., clays, layered double hydroxides (LDHs)) can be used to enhance the flame retardancy of EVA copolymers [11]. The EVA and nanoclay combination has numerous industrial uses, including packaging films, adhesives and cables [16].

Boron compounds (e.g., boric acid (BA) (H_3BO_3) [17]) have significant potential as flame retardant ingredients in polymer-based products because of their low toxicity, chemical structure, and variety of flame retardant mechanisms [18]. They can act as flame retardants and smoke suppressors [19]. They are environmentally friendly and present synergistic effects with other flame retardant additives [18]. Therefore, they can be used in polymer composites either separately or with other additives [17]. Their utilization (e.g., boric acid and boron oxide) in textile materials as flame retardant additives was also reported [20]. BA was reported to degrade in 2 steps: first it was dehydrated forming meta boric acid (HBO_2) and then again dehydrated to form boron oxide (B_2O_3) resulting in 56% of mass left as char [21]. It was noted to act as a cross-linking agent hindering the oxidation of polymer during decomposition and preventing dripping (keeping the burnt material intact) [22]. Besides, the high char residue acts as a barrier and consequently hamper the combustion process [23]. BA was reported to increase the char yield and even stop afterglow when used >10% in cellulose-based films [18]. The beneficial effect of BA addition (2%) on bending strength of polymer composites prepared by using paper mill sludge (PMS) was reported [24].

Even though EVA copolymer is one of the most important copolymers which are used in various applications in different industries thanks to superior and adjustable physicochemical properties (e.g., by adjusting VA content), the studies about EVA copolymer and increasing its flame retardancy are limited in the literature. The studies about enhancing flame retardancy of polymers are not investigating the effects of flame retardant additives on the mechanical characteristics of the composite, in general. The boron-containing compounds are drawing attention as additives to be used in polymer composites for enhanced flame retardancy. In the current study, EVA/nanoclay composites were prepared by using two different organo-modified nanoclays (montmorillonite-MMT) by using the solvent solution method. The effects of clay type/content and presence/absence of boric acid (BA) on the flame retardancy and mechanical properties of the composites were investigated. The current study is expected to supply data for possible use of nanoclays and BA in the enhancement of the flame retardancy of EVA copolymer while considering the mechanical characteristics of the composite as well.

2. Materials and Methods

2.1. Materials

EVA (containing 26 wt. % of VA) was kindly supplied by HES Cable Company (Kayseri, Türkiye). Surface-modified nanoclays were products of Sigma-Aldrich Co., Ltd. (USA). The nanoclay with the code 682632 contains 15-35 wt.% octadecylamine (Figure 2a),

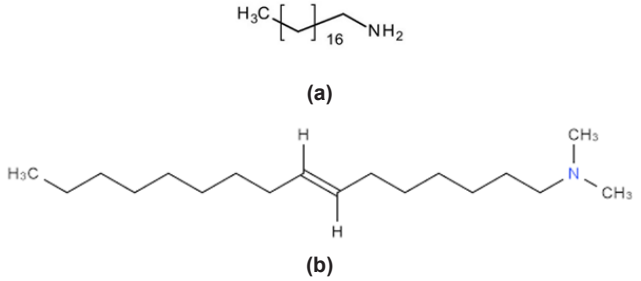

Figure 2. Chemical structure of a) octadecylamine and b) dimethyl dialkyl (C14-C18) amine

0.5-5 wt.% aminopropyltriethoxysilane, and the nanoclay with the code 682624 contains 35-45 wt.% dimethyl dialkyl (C14-C18) amine (Figure 2b). The boric acid used in the study was a product of Amresco Co. Ltd. (USA) Other chemicals and solvents were products of Merck Co. (Germany). All materials were used in their original form.

2.2. Preparation of EVA/NC and the EVA/NC/BA Nanocompositess

35 ml of chloroform were added to 3.5 g of ethyl vinyl acetate (EVA) polymer in the capped glass jar. The polymer was dissolved in chloroform using a heated magnetic stirrer (T_{mix}: 40-50 °C) keeping it stirred overnight. To avoid flocculation, the additives in powder form were added gradually. The amounts of additives are given in Table 1. NC 1 and NC 2 are nanoclays with codes 682632 and 682624, respectively. The samples prepared with BA addition were coded with -BA extension.

Table 1. Samples and their contents

Sample	Polymer (g)	Nano-Clay (g)	Boric Acid (g)	Polymer / Nano-Clay / BA
Control	3.5	0	0	100 / 0 / 0
NC 1.1	3.5	0.035	0	100 / 1 / 0
NC 1.2	3.5	0.07	0	100 / 2 / 0
NC 1.3	3.5	*0.35*	0	100 / 10 / 0
NC 1.4	3.5	0.7	0	100 / 20 / 0
NC 2.3	3.5	0.35	0	100 / 10 / 0
NC 1.3-BA	3.5	*0.35*	0.0175	100 / 10 / *0.5*
NC 2.3-BA	3.5	*0.35*	0.0175	100 / 10 / *0.5*

The mixtures were promptly put into glass petri dishes after being mixed and homogenized, where they were dried in the hood. The dried films were sliced into strips of 1-1.25 cm width and 10-12.5 cm length for the mechanical (tension) test and burning test, respectively. The remaining parts were used for further characterization.

2.3.Characterization of the EVA/NC and the EVA/NC/BA Nanocomposites.

2.3.1. Fourier transform infrared (FTIR) spectroscopy

FTIR technique was used to characterize the chemical structure of the prepared nanocomposite materials (Thermo Scientific Nicolet 6700). The ATR crystal module was used in the analysis.

2.3.2. Thermal analysis (TGA)

The thermal behaviour of the samples with or without the additives (nanoclay/BA) was determined by using a multipurpose thermal analysis instrument (Perkin Elmer, STA 8000, USA). The analysis was performed under nitrogen flow (20 mL/min.) in the temperature range of 30-800 °C with an increment rate of 10°C/ minute.

2.3.3. X-Ray diffraction (XRD) analysis

The crystallinity of the samples was analysed by using X-ray diffraction analysis (Bruker D8 Discover, USA) (2θ: 0° to 50°, Cu Kα radiation (α = 0.15406 nm)).

2.3.4. Mechanical properties

According to ASTM D882 standard for thin plastic specimens, the tensile properties were assessed on specimens cut out from dried composite sheets (100 mm × 10 mm, thin films) using SHIMADZU AG-X 50 kN universal testing equipment (Japan). The strain rate and load cell capacity were 15 mm × s^{-1} and 50 kN, respectively.

2.3.5. Flammability tests

Flammability tests in vertical configuration for thin material were performed via samples prepared with respect to the UL-94 VTM standard. The samples were exposed to flame for 3 seconds, and combustion times including the ignition time were recorded (Figure 3).

Figure 3. Flammability test

3. Results and Discussion

3.1. FTIR Spectroscopy

FTIR spectroscopy is the measurement technique for the identification of organic and inorganic materials by scanning samples and collecting infrared spectra [25]. The purpose of using FTIR was to identify compounds/bonding by investigating the IR absorption/ transmission spectrum with the presence/absence of peaks on the IR plot. The comparison of the IR spectra enables determining the resemblance/difference of the bonding and possible impurities in the material. The FTIR spectra of the samples are shown in Figure 4. The spectra of neat EVA (control) and all other samples with varying ratios of different additives are almost similar, indicating the additives are physically blended but didn't form new bonds with the EVA matrix.

The only exceptional IR absorption peak was for sample NC 1.3 at 1590.77 cm^{-1} (Figure 4), which may be attributed to the increased additive (NC 1) content which has considerable organic surface modifier (15-35 wt.% (Figure 2a)). FTIR bands between 3250-3400 cm-1 and 1580-1650 cm^{-1} were reported to be related with the NH stretching and bending, respectively [26]. The broadening and decreasing intensity for the NH stretching band was claimed to be an indicator of hydrogen bonding formation between the organic modifier octadecylamine and the nanoparticles [27]. The molecular formula of EVA is $(C_2H_4)_n(C_4H_6O_2)_m$. The structure of EVA appears to have ketone, alkene and alcohol functional groups. The peaks at wavenumbers of 1236 and 2916 cm^{-1} was attributed to vibrations of C=O (1240 cm^{-1}) and aliphatic CH_2 group (2920 cm^{-1}), respectively [28]. The peak at 1733 cm^{-1} (1735 cm-1 for the current study) was attributed to C=O vibration [29] while peaks at 1240 cm^{-1} (1236-7 cm^{-1} for the current study) and 1019 cm^{-1} were related with C-O stretching due to the presence of polar VA groups in the EVA [30]. C-H asymmetric and symmetric stretching and bending were attributed to the peaks 2914 cm^{-1} (2916 cm^{-1} for the current study), 2816 cm^{-1} (2849 cm^{-1} for the current study) and 1469 cm^{-1} (1464-7 cm^{-1} for the current study) [30]. The peaks at 1365 cm^{-1} (1371 cm^{-1} for the current study) and 717 cm^{-1} (719 cm^{-1} for the current study) were related to $-CH_3$ symmetric vibration and C-H rocking vibration, respectively [30]. Bartolomei et al. also reported the inorganic nano-filler addition did not change the FTIR spectra which is in accordance with the results of the current study [30].

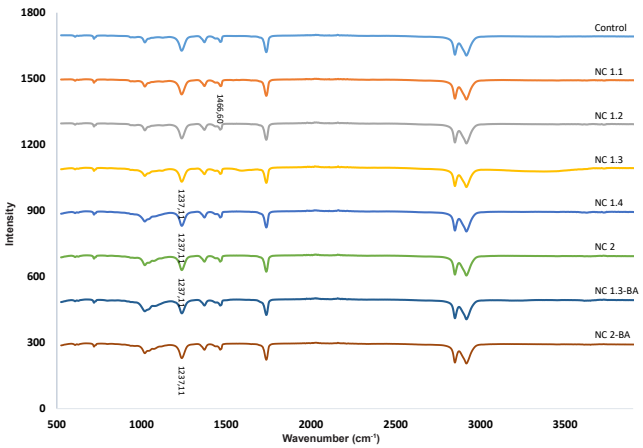

Figure 4. The FTIR spectra of neat EVA (control) and EVA with additives

3.2. X-Ray Diffraction (XRD) Analysis

The X-ray diffractograms of the neat EVA and the samples with additives are shown in Figure 5. Neat EVA has a peak at a 2θ value of 21° and there is a shouldering peak at around 23°, which were attributed to (110) and (200) planes, respectively [13, 30]. The peak intensities of these peaks were decreasing with the addition of nanoclays (especially for NC 1 addition) which can be indicating a possible decrease in the crystallinity of EVA. The crystallinity of the EVA copolymers with 24 and 28 wt. % VA was reported to be 19% and 13%, respectively [13]. The neat EVA copolymer used in this study with 26 wt. % VA content may have a crystallinity among these values, since the crystallinity of EVA was reported to decrease with increasing VA (vinyl acetate) content [13]. It was mentioned that the crystallinity of the melt-blended EVA (9, 18 or 28% VA) with surface modified MMT (Cloisite 15 A or 30 B) was decreasing with increasing nanoclay content (0, 2.5, 5 or 7.5 %) (and with the increasing VA%) [15]. There are no other characteristic peaks for NC 1 added samples, indicating the nanoclay is well-exfoliated in the polymer matrix. It was mentioned the characteristic peaks of nanoclay were absent when it is totally intercalated/exfoliated in the composite [31]. There is a peak at a 2θ value of 6.9° for the NC 2 added samples with relatively lower intensity which may be attributed to the presence of agglomerated or intercalated nanoclay/polymer morphology in the polymer matrix (i.e., the nanoclay NC 2 was not totally exfoliated) (Figure 5). The peaks for the (001) plane for montmorillonites (MMTs) were reported with 2θ values of 7.4° and 5.6° for Na- and Ca-MMT which were in accordance with the 2θ value in the current study [32].

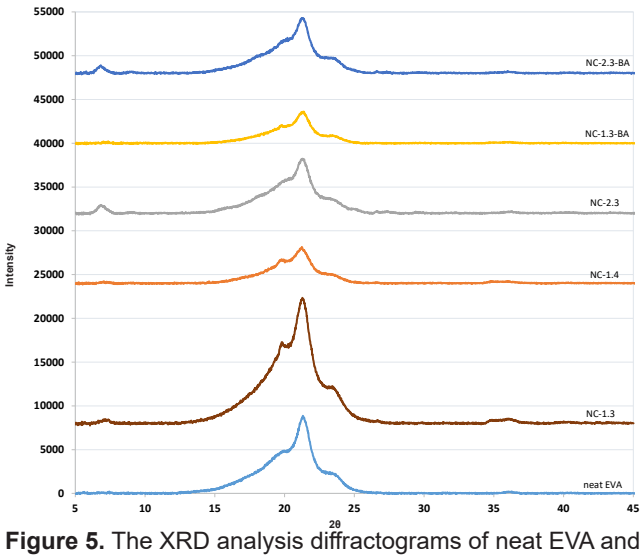

Figure 5. The XRD analysis diffractograms of neat EVA and nano-clay and/or BA added samples

3.3. Thermal Analysis (TGA/D-TGA)

Thermal behaviour of the neat EVA and the selected composites prepared by adding nanoclay 1 and 2 (NC 1 and NC 2) and/or BA were investigated via a multipurpose thermal analyser. TGA (thermogravimetric analysis) was also performed for the organically surface modified neat nanoclay (NC 1 and NC 2) samples.

The TGA (thermogravimetric analysis) results are shown in Figure 6a (for the temperature range of 30-800 °C) and in Figure 6b (for the temperature range of 200-550 °C). The onset and offset temperatures of the neat EVA (control) and EVA with additives are tabulated in Table 2 and Figure 6c.

Table 2. The onset, offset temperature values, % weight loss values between onset temperatures and residual weight (%) from TGA for the control (neat EVA) and the EVA composites with different additives

Sample	onset T1	Δ1 (mass%)	onset T1a	Δ1a (mass%)	onset T2	Δ2 (mass%)	offset T	residue (mass%)
Control (neat EVA)			326.07	25.238	448.69	73.596	525.53	1.801
NC 1.3	280.29	7.465	334.75	13.159	454.41	69.538	533.24	9.669
NC 1.4	280.83	13.676	359.96	7.025	448.00	64.994	506.86	15.537
NC 2.3			314.40	20.175	441.38	72.514	494.68	8.223
NC 1.3-BA	280.43	8.235	334.02	13.45	457.92	71.605	513.95	9.298
NC 2.3-BA			319.76	20.104	443.42	72.299	495.78	8.135

Table 3. The 5%, 10% and 50% weight loss temperature values from TGA for the control (neat EVA) and the EVA composites with different additives

Sample	T (-5%)	T (-10%)	T (-50%)
Control (neat EVA)	333.2	346.9	459.3
NC 1.3	293.7	329.9	468.5
NC 1.4	293.1	305.6	461.3
NC 2.3	325.5	*338.9*	457
NC 1.3-BA	294.3	323.5	468.7
NC 2.3-BA	347.3	*363.6*	458

The temperature values for 5%, 10% and 50% weight loss are shown in Table 3 and illustrated in Figure 6c. The TGA graphs for the nanoclays NC 1 and NC 2 are shown in Figure 7.

The neat EVA (control) has 2 main steps of weight loss as was reported in the literature [13, 33]. The first was attributed to the deacetylation (removal of acetate groups from the backbone) and the second was related to the chain scission of the polymer backbone taking place at relatively higher temperatures [13, 21, 29]. It was the case for the TGA analysis of the neat EVA (control) (Figures 6a and 6b). The onset temperature for the first step (onset T1) was 326.07°C ended and after 25.2% weight loss. The second step initiated at (onset T2) 448.69°C and the weight loss was 73.6% (Table 2). Diez et al. performed TGA for EVA samples with varying acetic acid content (12.5-33% (w/w)) and showed the correlation of the weight loss at the first step with the acetic acid content of the EVA copolymer [13]. Luna et al. mentioned the first weight loss step was between 330-390 °C, and the second step was above 430°C for the neat EVA, which is in accordance with the current data [29].

3.3.1. Effect of nanoclay addition on thermal stability

The thermal degradation profile of EVA was considerably changed, especially with the addition of NC 1 (Figures 6a and b). Interestingly, the addition of both nanoclays resulted in thermal instability for the EVA composites. The first onset temperature (onset T1) for the EVA/nanoclay composites were lower than the value for the neat EVA (326.07°C) (Table 2, Figure 6c).

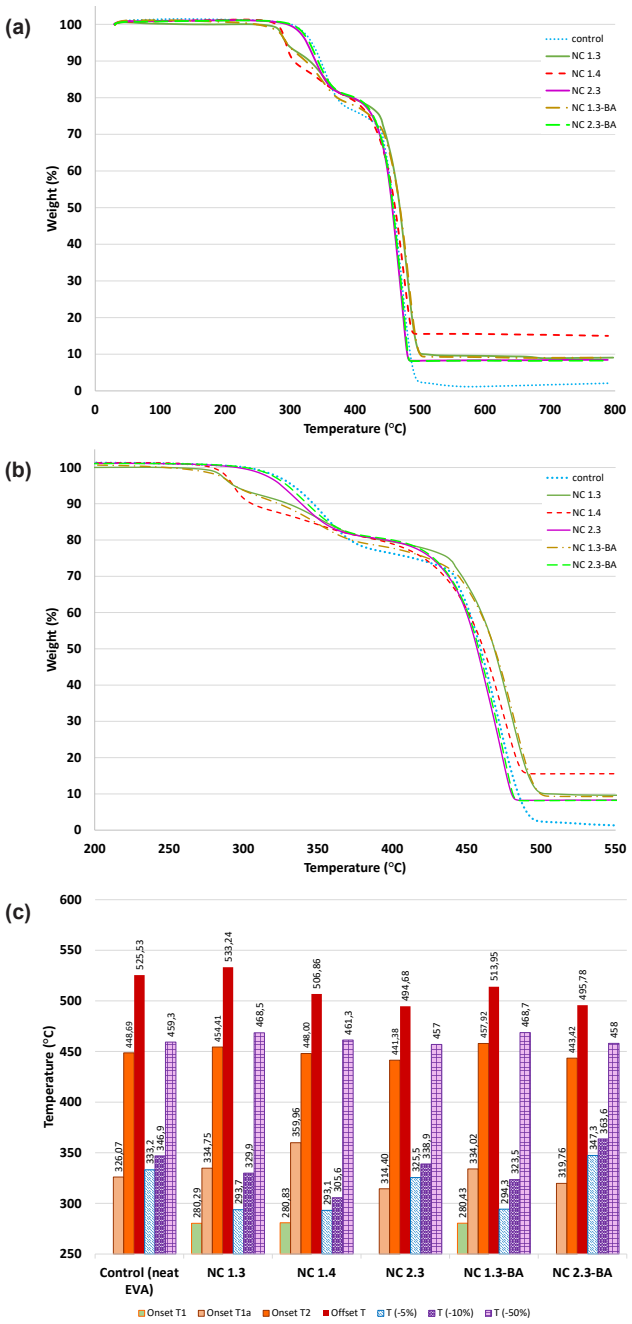

Figure 6. a. TGA graphs for the samples neat EVA (control), NC1.3, NC 1.4, NC 2.3, NC 1.3-BA and NC 2.3-BA (30-800°C), b. TGA graphs for the samples neat EVA (control), NC1.3, NC 1.4, NC 2.3, NC 1.3-BA and NC 2.3-BA (200-550°C), c. The onset, offset, 5, 10 and 50% weight loss temperature values from TGA for the neat EVA and the EVA composites with different additives

The organic surface modifiers of the nanoclays may be the reason for the initiation of the thermal degradation at relatively lower temperatures. The TGA results for the neat nanoclay samples (NC 1 and NC 2) also showed that the thermal degradation initiated at relatively lower temperatures (Figure 7).

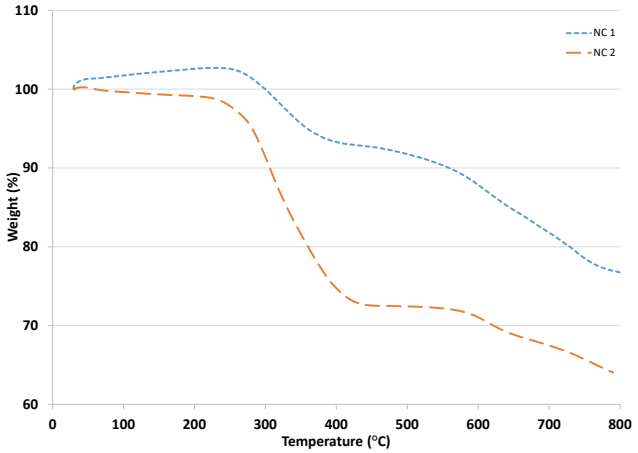

Figure 7. The TGA results for the neat nano-clays (NC 1 and NC 2)

TGA result for NC 1 showed that it was gaining some weight at relatively lower temperatures indicating a probable nitrogen adsorption/binding (Figure 7) followed by weight loss with increasing temperature. The onset temperatures were 264°C and 269°C for NC 1 and NC 2, respectively. The effect of thermal instability was more severe for the EVA/nanoclay samples with NC 1, which were with exfoliated morphology. The homogeneously distributed nanoclay platelets in the exfoliated morphology of the EVA/NC 1 composites let the organic surface modifier on the nanoclay surface more exposed to surface reactions which resulted in thermal degradation at relatively lower temperatures. The thermal degradation took place in 3 main steps (i.e., there was one additional step at relatively lower temperatures compared to neat EVA degradation) (Figures 6a and b). The weight loss at lower temperatures was increasing with increasing NC 1 content. NC 1.4 (nanoclay/polymer: 20/100) lost more weight (%) than NC 1.3 (and NC 1.3-BA) (nanoclay/polymer: 20/100) at these lower temperatures showing the effect of nanoclay (i.e. organic surface modifier) ratio (Figures 6a and b).

The onset temperature for the second step of degradation (onset T1a) was higher for NC 1.3 (334.75°C) than neat EVA (326.07°C) (Table 2). The weight loss at this step was relatively lower for NC 1.3 (13%) compared to the neat EVA (25%). The total weight losses at steps 1 and 2 were 7.5 and 13% (21.5 5 in total) for NC 1.3, and this was lower than the weight loss of neat EVA in that temperature range (25%)(Table 2). This may indicate the mass loss was hampered with the addition of NC 1 during TGA. The increasing amount of NC 1 resulted in an even a higher onset T1a which was 359.96°C for NC 1.4. The weight loss ratios for the first and second step were 13.7% and 7% for the sample NC 1.4 (20.7% in total), indicating the higher NC 1 content (i.e., higher organic surface modifier) resulted in higher weight loss at lower temperatures compared to NC 1.3. The total mass loss was slightly lower for NC 1.4 (20.7%) than NC 1.3 (21.5%) which may indicate an increasing resistance against mass transfer with increasing NC 1 content in the EVA/nanoclay composite.

The onset T2 for NC 1.4 was (448°C) almost similar to the value for the neat EVA (448.7°C), while it was slightly higher for NC 1.3 (454.4°C) (Table 2). The weight loss (%) values for this step of thermal degradation were decreasing with NC 1 addition. The neat EVA sample lost 73.6% of its weight, while NC 1.3 lost 69.5% and NC 1.4 (with higher NC 1 content) lost 65% of its weight at this step (Table 2). The offset T value was the highest for NC 1.3 (533.2°C) among all samples. It was 506.9°C for NC 1.4 and 525.5°C for the neat EVA (Table 2). The residual weight was 1.8% for the neat EVA, while it was 9.7% and 15.5% for NC 1.3 and NC 1.4, respectively, showing the residual mass increased with increasing nanoclay addition to EVA/NC 1 composites.

The NC 2.3 sample had 2-step thermal degradation like EVA, which may be attributed to its morphology (intercalated or partially aggregated). The onset temperatures (onset T1a and T2) were lower for NC 2.3 than the neat EVA, indicating NC 2 resulted in some thermal instability for EVA composites. The weight loss(%) ratios were lower for NC 2.3 compared to the neat EVA, indicating the resistance against mass loss was increased by NC 2 addition. The weight loss (%) was even lower for NC 1.3 (69.5%) (with a similar EVA/nanoclay ratio) than NC 2.3 72.5%) (Table 2). That lower weight loss value may be attributed to higher mass transfer resistance by NC 1.3 which was with exfoliated morphology (i.e. well-separated, more homogeneously distributed platelets in the EVA/nanoclay composite).

The temperatures for certain mass loss ratios (e.g., 5% or 10%) are also used to monitor the thermal characteristics of the composites [23, 29]. The temperatures at which there was a mass loss of 5, 10 and 50% are tabulated in Table 3 and illustrated in Figure 6c.

The samples with NC 1 were with the lowest T (-5%) and T (-10%) values which were considerably lower than the values for the control (the neat EVA: T (-5%): 333.2°C and T (-10%): 346.9°C), which may be attributed to the thermal instability due to the organic surface modifier on NC 1. Yao et al. reported a T (-5%) value for the neat EVA (14% VA) of 349.6°C, which was higher than the value determined in the current study [23]. That higher value may be attributed to the lower acetate content of the copolymer (14 vs. 26%). Luna et al. reported a T (-10%) value of 337.7°C for the neat EVA (28% VA) which was slightly lower than the

current result, and it may be attributed to the different (higher) acetate content (28 vs. 26%) [29]. Nyambo et al. reported a T (-10%) value of 351°C, which was slightly higher than the value in the current study [21]. The EVA they used had a lower acetate content (18%) which may explain the higher T (-10%) value [21]. Sample with NC 2 (NC 2.3) had T (-5%) and T (-10%) values relatively closer to the values of the control (Table 3, Figure 6c).

Ryu et al. also observed different TGA curves for MMT-EVA composites which were prepared either with MMT without surface modification or surface-modified using different organics, which was the case observed in the current study for 2 different nanoclays (NC1 and 2) with different surface modifications [11]. Ryu et al. used the T (-50%) for comparing the thermal stability of the EVA composites prepared by different inorganic fillers which were either surface modified or not [11]. They reported a T (-50%) value of 432°C for the neat EVA (28% VA) which was lower than the value in the current study (459°C). The difference may be attributed to TGA parameters and VA %. They reported surface-modified montmorillonite (MMT) added to EVA at a ratio of 6% (among the samples 1-12%) resulted in the highest T (-50%) (ΔT=28°C, higher than T (-50%) value of the neat EVA) and claimed to be the best sample in terms of thermal durability [11]. In the current study, the T (-50%) values were slightly lower than the value of the neat EVA for NC 2.3 while it was higher for NC 1.3 (ΔT = 9°C), which may be indicating the NC 1.3 had a higher mass transfer resistance hampering the thermal degradation (i.e. weight loss).

3.3.2. Effect of BA addition on thermal stability

BA addition to the samples with NC 1 did not affect the thermal degradation behaviour of the samples drastically, considering the TGA results. The TGA profiles of samples NC 1.3 and NC 1.3-BA coincide with each other considerably (Figures 6a and 6b). The onset temperatures T1 and T1a were almost similar, while onset T2 was slightly higher for NC 1.3-BA, and offset T was slightly higher for NC 1.3 (Table 2). Weight loss(%) values were also comparable for the 3 weight loss steps for NC 1.3 and NC 1.3-BA, which were slightly higher for NC 1.3-BA, and the mass residue(%) was slightly higher for NC 1.3, indicating the BA addition slightly decreased the resistance to mass transfer during thermal decomposition.

The thermal degradation behaviour of NC 2.3 and NC 2.3-BA was almost similar considering the TGA profiles for these samples (Figures 6a and 6b). The thermal degradation occurred in 2 main steps, like neat EVA (i.e., the step at relatively lower temperatures observed for the samples with NC 1 was not observed for the samples with NC 2). The onset temperatures (T1a and T2) were slightly higher for NC 2.3-BA (Table 2), which may indicate BA addition slightly increased thermal durability. The weight losses(%), offset T and residual weight (%) values were comparable for NC 2.3 and NC 2.3-BA (Table 2). Nyambo et al. reported a residue % of 6 for the EVA-BA (10%) sample and of 1% for the neat EVA after reaching 800°C, which were comparable with the current results [21].

The T (-5%) value of the sample NC 1.3 (293.7°C) was close to the value of sample NC 1.3-BA (294.3°C), while T (-10%) values were different for these samples with NC 1. It was 305.6°C for the sample NC 1.3 and was higher for the sample NC 1.3-BA (323.5°C), which may indicate the effect of BA in the suppression of thermal decomposition at relatively lower temperatures (Table 3 and Figure 6c). The T (-5%) value for the sample NC 2.3 was 325.5°C and it was 329.5°C for the sample NC 2.3-BA, showing the possible effect of BA in suppressing the thermal degradation at relatively lower temperatures. T (-10%) values for NC 2.3 and NC 2.3-BA were 338.9°C and 363.6°C, respectively. The T (-10%) value of the control sample (the neat EVA) was in between these values (346.9°C). the presence of BA in composites with NC 2 may be hindering the weight loss with increasing temperature (at relatively lower temperatures). Nyambo et al. reported T (-10%) value for the neat EVA as 351°C, which was comparable with the current result (347°C) [21]. They reported 10% BA addition resulted in thermal instability for EVA-BA composite at relatively lower temperatures (100-350°C), which was attributed to degradation of boric acid to form water and B_2O_3, resulting in a 4°C increase in T (-10%) value compared to neat EVA [21]. In the current study, NC 2.3-BA also had a higher T (-10%) value (343°C) than NC 2.3 (339°C) where ΔT was also 4°C, but the BA amount (used with NC 2) was relatively lower.

The BA addition (with NC 2) did not affect the thermal decomposition temperature (T (-50%)) of the EVA/nanoclay composite considerably. The T (-50%) values were comparable for the neat EVA and for both NC 2 containing samples with and without BA addition (Table 2 and Figure 6c).

3.3.3. Derivative TGA (D-TGA) results

The D-TGA (derivative weight loss %, i.e., weight loss per time (%/min)) graphs are shown in Figure 8a. The peak temperatures at which the weight loss(%) with increasing temperature in time was maximized can be seen in Table 4 (and in Figure 8b). There were 2 peak temperatures (peak T1a and peak T2) for the control (neat EVA) and samples with NC 2 (with 35-45 wt.% dimethyl dialkyl (C14-C18) amine (Figure 2b) as an organic surface modifier) and 3 peak temperatures (peak T1, peak T1a and peak T2) for samples with NC 1 (with 15-35 wt.% octadecylamine, Figure 2a).

The first peak temperature (peak T1a) values were 351.19, 336.59, and 340.95°C for the control (neat EVA), NC 2.3, and NC 2.3-BA samples, respectively. The peak temperature values (Peak T1a) for the samples with NC 2 were lower than the value for the control sample. The second peak temperature (peak

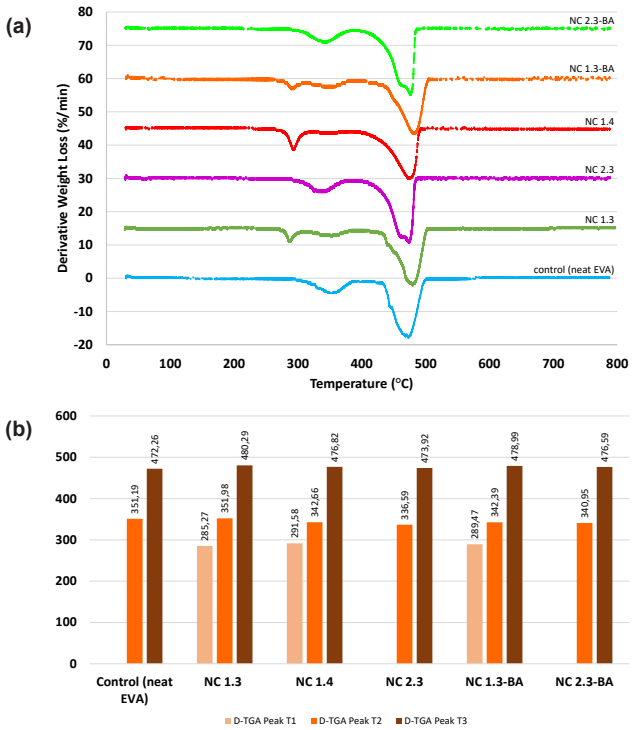

Figure 8. a. The TGA results for the neat nano-clays (NC 1 and NC 2), b. The peak temperature values for D-TGA graphs for the control (neat EVA) and the EVA composites with different additives

T2) values were 472.26, 473.92, and 476.59°C for the control (neat EVA), NC 2.3, and NC 2.3-BA samples, respectively. The peak T2 values for the samples with NC 2 were slightly higher than the value for the control sample. Nyambo et al. reported a peak T value for the second step of neat EVA (VA 18%) thermo-degradation as 456°C [21], which was lower than the value for the copolymer (EVA, 26%) in the current study. The peak T value for a lower acetate content was expected to be a higher value, but it was lower, probably because of TGA parameters (e.g., the heating rate was higher: 20 [21] vs. 10°C/min for the current study). Yao et al. reported the peak temperature for the second step of neat EVA degradation as 474.7°C, which was slightly higher than the value reported 472.3°C in the current study [23]. The difference may be attributed to the lower acetate content in the study by Yao et al. [23]. Osman et al. reported the peak temperature values of the first

Table 4. The peak temperature values for D-TGA graphs for the control (neat EVA) and the EVA composites with different additives (na: not available)

Sample	D-TGA Peak T1	D-TGA Peak T1a	D-TGA Peak T2
Control (neat EVA)	na	351.19	472.26
NC 1.3	285.27	351.98	480.29
NC 1.4	291.58	342.66	476.82
NC 2.3	na	*336.59*	473.92
NC 1.3-BA	289.47	342.39	478.99
NC 2.3-BA	na	*340.95*	476.59

step (deacetylation) as 350, 346 and 348°C for neat EVA (18% VA), EVA with 5% MMT, and EVA with 5% pretreated MMT, respectively [33]. The peak T values for MMT-added samples (composites) were lower than the neat EVA (as was in the current study) which was attributed to the catalytic effect of degradation products (of the surface modifier) [33]. For the second step of the degradation compared to neat EVA (449°C) higher peak temperatures were reported by Osman et al. for the samples with 5% MMT addition [33]. The pretreated MMT was reported to increase the peak temperature more (495°C) than the untreated MMT (470°C) [33]. They attributed the better exfoliation of pretreated nanoclay in the composite resulted in higher thermal durability (i.e., increased the second step peak T) [33]. The peak T for the second step of degradation (peak T2) for EVA/nanoclay composites was also higher than the value for the neat EVA in the current study, but the differences were smaller (only 2°C for NC 2.3), which may be attributed to scissoring (defragmentation) of the polymer backbone being slightly hampered in the presence of nanoclay (NC 2) addition.

The BA addition decreased the peak temperature value at relatively lower temperature (peak T1a) and slightly increased the peak temperature at relatively higher temperature (peak T2) for the samples with NC 2 compared to the control sample. The first peak temperature (peak T1a) may be related to the removal of acetate groups from the polymer matrix which took place at relatively lower temperatures with the presence of NC 2. It was suggested that the unknown acetic acid content of a copolymer (EVA) could be determined by using D-TGA data, mentioning the correlation between the intensity of the D-TGA value for the first peak (at relatively lower temperature) and the acetic acid content in the EVA copolymers [13]. The peak temperature (peak T1a) for the sample with BA was slightly higher than the value for the sample only with NC 2. The peak temperature value at relatively higher temperature (peak T2) was also slightly higher for NC 2.3-BA compared to NC 2.3. Yao et al. also reported a slight increase in the peak temperature (Tmax2, peak T2 in the current study) with the addition of BA in the presence of some other additives [23].

There were 3 peak temperatures for the samples prepared via NC 1 (with 15-35 wt.% octadecylamine (Figure 2a), 0.5-5 wt.% aminopropyltriethoxysilane as an organic surface modifier). The additional peak temperature (peak T1) values were 285.27, 291.58, and 289.47°C for the samples NC 1.3, NC 1.4, and NC 1.3-BA, respectively (Table 4). This additional peak may be related to the relatively less thermostable character of the surface modifier used for NC 1 and the exfoliated morphology of the EVA/NC 1 composite. The peak T1 value was slightly higher for the sample with higher nanoclay addition (NC 1.4), which may be attributed to the possible additional mass transfer resistance with increased nano clay content. The peak T1a for NC 1.3 was slightly higher than neat EVA (Table 4). Increasing the NC 1 content decreased the

peak T1a from 351.19°C to 342.66°C for NC 1.3 and NC 1.4, respectively, which may be attributed to the increasing organic modifier content with the increase in the NC 1 content. The peak T1a values were 351.98 and 342.39°C for NC 1.3 and NC 1.3-BA (Table 4). BA addition to EVA/NC 2 composite decreased the peak T1a, indicating a possible catalytic effect of BA in VA group removal from the EVA copolymer. The nanoclay addition at higher content (NC 1.4 with EVA/nanoclay: 100/20) and BA addition resulted in decreasing thermal stability at the relatively lower temperatures (i.e., the removal of acetate groups was happening at relatively lower temperatures). The peak T2 values for NC1 and BA-added samples were all higher than the peak T2 of the neat EVA (Table 4). The value increased from 472.26°C to 480.29°C for NC 1.3 (the highest among NC 1 containing samples). The increasing nanoclay content resulted in a relatively lower peak T2 (476.82°C for NC 1.4) which was still higher than the value for the neat EVA. BA addition to EVA/NC 1 composite resulted in peak T2 value of 478.99°C (NC 1.3-BA), which was lower than peak T2 for NC 1.3 (480.29°C), but was still higher than the value for the neat EVA (472.26°C). The NC 1.3 having the highest peak T2 indicates that certain EVA/NC 1 ratio may supply better thermal stability for the defragmentation (scissoring) of main backbone of EVA copolymer and BA addition (NC 1.3-BA) may have some adverse effect on the copolymer's thermostability at this step of thermal degradation.

3.4. Mechanical Properties

3.4.1. Effect of nano-clay content

The effect of nanoclay content in the EVA/nanoclay composites on the mechanical properties of the composites was determined by performing tensile tests using EVA/NC 1 samples. The stress-strain graphs for the neat EVA and EVA with varying NC 1 ratios are shown in Figure 9. The addition of NC 1 at a lower ratio (NC 1.1, nanoclay/polymer: 1/100) worsens the mechanical durability of the composite under stress when compared to the control sample (neat EVA), while a higher amount of NC 1 addition (NC 1.2, nanoclay/polymer: 2/100) resulted in a composite with comparable stress-bearing capability with the control. Further increase in NC 1 content enhanced the mechanical durability. NC 1.3 (nanoclay/polymer: 10/100) and NC 1.4 (nanoclay/polymer: 20/100) had higher stress-bearing capacity compared to neat EVA and EVA with relatively lower nano-filler content (Figure 9). It was reported that the increasing inorganic filler content (1-12%) enhanced the stress-bearing characteristics of the EVA composites prepared with different inorganic fillers including montmorillonite (MMT) [11]. It was. also mentioned the decreasing mechanical strength when a small quantity of nanoclay (e.g., 1%) was used, and they attributed this to the dominance of the debonding phenomenon at lower nanoclay concentrations [12]. The results were in accordance with the former studies. The maximum sample elongation was higher for the neat EVA

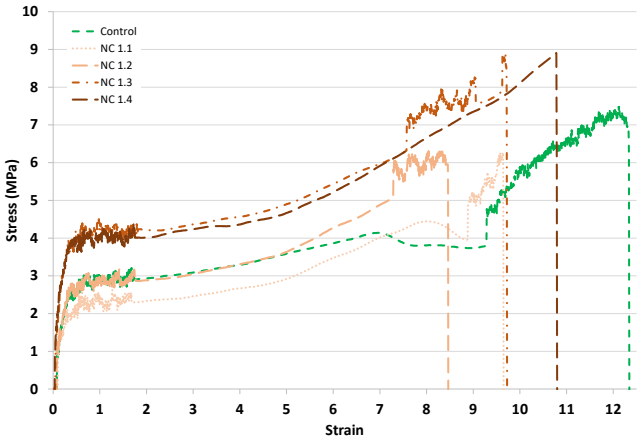

Figure 9. The stress-strain curves for neat EVA (control) and EVA with varying nano-clay (NC 1) content

(control), indicating the nanoclay addition resulted in relatively more brittle characteristics.

3.4.2. Effect of nanoclay type and boric acid (BA) addition

The effect of nanoclay type (i.e., the type of organic surface modifier on the nanoclay surface) on the mechanical characteristics of EVA/nanoclay composites was determined by applying tensile tests using EVA/NC 1 and EVA/NC 2 composites. The stress-strain curves for this analysis are shown in Figure 10. Both sample NC 1.3 (nanoclay/polymer: 10/100) and NC 2.3 (nanoclay/polymer: 10/100) could bear higher stress values than the control (neat EVA). Sample NC 2.3 was superior to sample NC 1.3. This difference may be attributed to the morphology of the composites. Sample NC 1.3 was totally exfoliated, as was determined via XRD analysis, that there were no peaks of nanoclay on the XRD diffractogram (Figure 5). But sample NC 2.3 had either agglomerated or intercalated nanoclay/polymer morphology. The morphology of the polymer/filler nanocomposites (e.g., exfoliated, intercalated, agglomerated) were reported to affect mechanical properties [34]. The more homogeneous distribution of nanoclay platelets in the EVA matrix for the sample NC 1.3 might result in higher stress-bearing characteristics, but it was not the case. Sample NC 2.3 with intercalated (or partially agglomerated) morphology could bear higher stress values (Figure 10). The mechanical characteristics of EVA/nanoclay composites may be affected not only by the morphology of the composite but also by the interaction of EVA and the organic surface modifier on the nanoclay. The higher stress-bearing capacity of the sample NC 2.3 may be attributed to a better surface interaction of the polymer and the organic surface modifier on NC 2 (Figure 2b) which has a double bond in the middle and two methyl groups at the end of the polymer chain that may form secondary bonding more efficiently with the EVA copolymer (e.g., hydrogen bonding with the oxygen at the VA groups of the EVA copolymer).

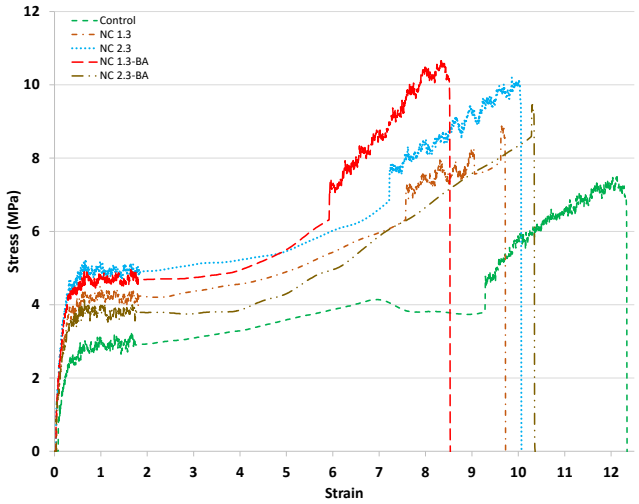

Figure 10. The stress-strain curves for neat EVA (control) and EVA with additives (lower stress-strain region)

The possible effect of BA addition on the mechanical properties of EVA/nanoclay composites was investigated by using samples with both NC 1 (NC 1.3, nanoclay/polymer: 10/100) and NC 2 (NC 2.3, nanoclay/polymer: 10/100) either with or without BA addition. The stress-strain curves for these samples are shown in Figure 10. Both samples NC 1.3-BA and NC 2.3-BA could bear higher stress than the neat EVA (like the samples NC 1.3 and NC 2.3 without BA addition). The stress-bearing capacity of the sample NC 1.3-BA was superior to NC 1.3. The NC 1 nanoclay was determined to have a totally exfoliated structure in the EVA matrix with respect to XRD analysis where peaks for the nanoclay were missing in the diffractogram (Figure 5). BA addition did not change the morphology. But the hydroxyl groups of boric acid may serve as extra sites to form hydrogen bonds with the organic surface modifier on the nanoclay with the amine group (N element) (Figure 2a) and EVA copolymer (vinyl acetate group, O and H elements). There was no considerable new primary bonding formation observed with the nanoclay and/or boric acid addition to the EVA copolymer (determined via FTIR analysis, Figure 4), but the strong hydrogen (secondary) bonding formation with the presence of BA might be increasing the stress-bearing capacity of the composite (NC 1.3-BA) (Figure 10). The homogeneous (exfoliated) morphology might be supporting the surface interaction of the nanoclay (i.e., organic surface modifier) with the BA and EVA (i.e., increasing the surface area for interaction). BA addition did not enhance the stress-bearing capacity of the sample with NC 2 (NC 2.3-BA) as it did for NC 1.3-BA. The stress-bearing capacity was still better than the control (neat EVA) but not as satisfactory as the sample without BA (NC 2.3). The reason may be related to the morphology of the sample. Samples with NC 2 (with or without BA addition) had intercalated (or partially agglomerated) morphology (considering the XRD analysis, Figure 5). The nanoclay was not exfoliated in the EVA copolymer, and the surface interaction between filler and polymer is limited compared to the exfoliated morphology. It may be expected that BA will not be as effective as in an exfoliated morphology to enhance bonding, but the negative effect (decreasing the stress-bearing capability) of BA addition was not expected. The organic modifier of NC 2 and EVA had a better bonding capability in the absence of BA, which adversely affected the secondary bonding in the EVA/NC 2/BA matrix.

3.4.3. Mechanical characteristics at elastic region

The Young's modulus (elastic modulus) values for the neat EVA and the composites with a different additives are shown in Figure 11.

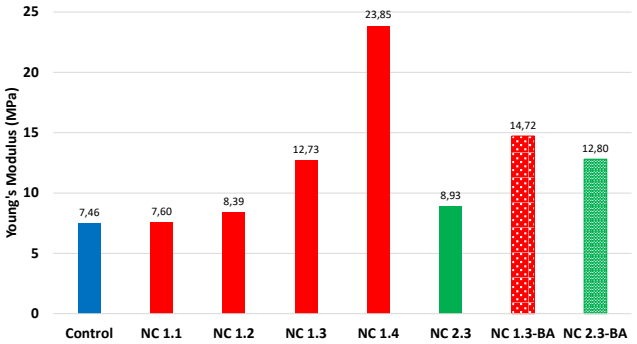

Figure 11. The elastic moduli of the neat EVA (control) and EVA with additives

The elastic modulus of the control sample (neat EVA) was 7.46 MPa, which was the lowest among all samples. It was slightly higher for the sample NC 1.1 (nanoclay/polymer: 1/100) with relatively low nanoclay addition (7.46 MPa). The Young's modulus value was increasing with increasing nanoclay (NC 1) content in the composite (almost linearly, Figure 11). Osman et al. reported a slight decrease in the Young's modulus value compared to neat EVA (18% VA) with the addition of 5% surface-modified MMT pretreated either with water or toluene and dried before melt mixing (at 160°C) with EVA [33]. They commented the pretreated surface-modified nanofiller resulted in some plasticizing effect which was attributed to possible interaction of the EVA copolymer and surface modifier of the nanoclay [33]. The numerical values of Young's modulus for neat and 5% MMT-added composites were relatively lower (less than 2.5 MPa) which may be related to the difference in material preparation (melt mixing vs. solvent solution method) [33]. The Young's modulus values for higher NC 1 content were 8.39, 12.73, and 23.85 MPa for the samples NC 1.2, NC 1.3, and NC 1.4, respectively (which had 2/100, 10/100, and 20/100 nanocaly/EVA ratios, respectively). The increase of Young's modulus with increasing NC 1 addition in comparison to the control's value was considerable (e.g., 71% for NC 1.3 and 220% for NC 1.4). Ryu et al. determined the mechanical characteristics of the EVA composites prepared by using different inorganic fillers (including MMT) [11]. It was mentioned that the Young's modulus of the neat EVA (12 MPa) increased with increasing amounts of MMT addition (26 MPa (117% higher) for

12% MMT) [11]. It was also reported the inorganic filler (MMT) addition to EVA increased the Young's modulus value compared to the neat EVA (13 MPa) [2]. The values were 17.1 MPa and 19.3 MPa for the MMT without and with surface modification (via low MW DNA strands) [2]. Aforementioned studies were comparable with the Young's modulus values determined in the current study (Figure 11) [2, 11]. The Young's modulus values for neat EVA were reported as 44 MPa (18% VA) [12] and less than 2.5 MPa (18% VA) [33], which were not that comparable with the values determined in the current study, which may be related to the used EVA copolymer and sample preparation/testing parameters.

The nanoclay type (i.e., the organic modifier on the nanoclay surface) was effective on the Young's modulus values of the nanoclay/EVA composites. The Young's modulus values for NC 1.3 and NC 2.3 (which were both with a nanoclay/EVA ratio of 10/100) were 12.73 and 8.93 MPa, respectively. The possible reason might be the morphological and chemical differences of the composites. NC 1 samples were exfoliated while NC 2 samples were intercalated (or partially agglomerated) with respect to XRD analysis. The exfoliated NC 1-containing sample was lacking the peaks for the nanoclay in the XRD diffractogram while the peak was observed for the NC 2-containing samples (Figure 5). The separated platelets of NC 1 were forming a more homogeneous distribution in the EVA matrix with an enhanced surface interaction between the nanoclay (i.e., organic surface modifier) and the EVA copolymer. That strong interaction between the nanofiller and the polymer might result in a higher Young's modulus value for NC 1.3 compared to NC 2.3 (Figure 11). The difference in the chemical structure of the different organic surface modifiers for NC 1 and NC 2 may also be partially effective on the Young's modulus values. BA addition to EVA/nanoclay composites was increasing the Young's modulus values for both NC1 and NC 2 containing samples (Figure 11). The moduli were 14.72 MPa for NC 1.3-BA (16% higher than NC 1.3) and 12.8 MPa for NC 2.3-BA (44% higher than NC 2.3). The increasing Young's modulus for the EVA/nanoclay composites may be attributed to extra secondary bonding formation between organic surface modifiers on the nanoclay surface and the EVA copolymer due to BA presence in the matrix. Tambe et al. reported even the addition sequence of components in the composite preparation was influential on mechanical characteristics of EVA (28% VA)/LDPE (low density polyethylene)/NC (nanoclay: MMT) composites, indicating the composites composed of EVA/nanoclay/other additives should be prepared and characterized diligently [31].

3.5. Flammability Tests

The fire durability of the neat EVA and its composites prepared via nanoclays (NC 1 and NC 2) and BA was determined by using samples prepared with respect to the UL94 VTM standard test. The time for complete burnout (including the 3 seconds for ignition) was determined for each sample. The samples were not self-extinguishing in the time limits of the UL94 VTM test, and drippings were observed (i.e., the samples failed in the UL94 VTM test). The burning time of samples was recorded for comparing the relative contribution of different additives on flame retardancy (Figure 12). It was 29 seconds for the neat EVA.

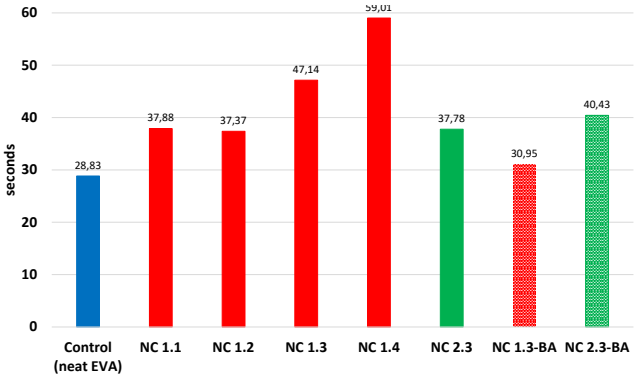

Figure 12. Burning durations for the control (neat EVA) and samples with NC and/or BA

3.5.1. Effect of nanoclay addition

The nanoclay addition was observed to increase the burning time. The increasing amount of NC 1 addition (from NC 1.1 (nanoclay/polymer: 1/100) to NC 1.4 (nanoclay/polymer: 20/100)) resulted in an increase in burning time from 38 seconds to 59 seconds (which were 31% and 105% higher than the time for the neat EVA). The addition of 20 parts of NC 1 in the EVA matrix increased the burning time for the composite by 105% (i.e., more than double). NC 2 addition was also beneficial in the elongation of the burnout time. The sample NC 2.3 (nanoclay/polymer: 10/100) had a burning time of 38 seconds which was 31% higher than the time for the neat EVA. The enhancement was not as high as NC 1 addition at a similar ratio. The sample NC 1.3 (nanoclay/polymer: 10/100) had a burning time of 47 seconds, which was 64% higher than the time for the neat EVA. Therefore, the NC 1 is more effective at elongating the burnout time (i.e., suppressing the burning process) than NC 2.

3.5.2. Effect of BA addition

The effect of BA addition was also investigated. Co-utilization of BA with NC 1 did not elongate the burning time. The sample NC 1.3-BA (nanoclay/polymer: 10/100) had a burning time of 31 seconds, which was slightly higher (7%) than the time of the neat EVA (29 seconds) and lower than the NC 1.3. sample (47 seconds) without BA. The contribution of BA addition in the composite prepared by using NC 2 elongated the burning time relatively. The burning time for the sample NC 2.3-BA (nanoclay/polymer: 10/100) was 40 seconds (40% higher than the time for the neat EVA). It was slightly higher than the NC 2.3 sample

(38 seconds) without BA. BA was reported to enhance flame retardancy [23]. It was claimed that BA may result in crosslinking during combustion which may hinder dripping [22]. It was also mentioned boron containing additives may form a glassy layer and create an extra resistance against heat transfer and mass transfer of flammable components [23]. The enhancing effect of BA as a boron-containing additive was observed for the composites prepared via NC 2 slightly, but it was not enhancing the flame durability of composites prepared by using NC 1. The difference in organic surface modifiers for NC 1 and NC 2 may be adversely affecting the possible crosslinking contribution of BA in NC 1 composites, while it was possible for NC 2, which has a different surface modifier.

3.5.3. Effect of additives (nano-clays with and without BA)

The additives (nanoclays with and without BA) increased the burn-out time for the EVA composites. But they were not able to prevent the burning out of the composites. There were drippings during the burning test. The burning tests showed that the current amounts/ratios of additives are not supplying total flame retardancy for the prepared composites, but they were resulting in some considerable enhancements in burning time. The amounts of the additives may be altered to investigate a better flame retardancy. NC 1 was more effective in terms of flame retardancy for EVA composites than NC 2. Increasing NC 1 content in the EVA composite was increasing the burning time. BA addition was slightly beneficial for NC 2-containing composites, but not for NC 1-containing samples (Figure 12). Different BA amounts/ratios may be investigated for better flame retardancy performance. 30% and 40% of BA addition were reported to result in epoxy composites with V1 and V0 score for the UL-94 V test, respectively, indicating the higher BA content may be used for better flame retardancy [35]. The burning times were not totally in accordance with the TGA data. The sample NC 1.3-BA had the highest temperature values during thermal degradation analysis (e.g., D-TGA peak T3, T (-50%)), which were higher/slightly higher than the values for the sample NC 2.3 which had the longest burning time. This may be due to the difference in testing/analysis conditions and may be indicating the importance of using different characterization methods for evaluating the performance of composite materials.

4. Conclusion

In the current study, the effects of the addition of two different nanoclays (NC 1 and NC 2) with different organic surface modifiers and boric acid (BA) on both the thermal characteristics/flame retardancy and mechanical characteristics were investigated. The morphology of the polymer/nanoclay composite was very effective on the characteristics of the composites. The nanoclay in the EVA/NC 1 composites was more exfoliated, while the EVA/NC 2 samples were either intercalated (or aggregated). The more homogeneous mixing of nano platelets for the exfoliated morphology resulted in higher surface area and surficial interaction between the organically modified nanoclay surface and EVA matrix. Consequently, the mechanical and thermal characteristics were varying with the nanoclay type (and polymer/nanoclay ratio). The nanoclay type (i.e., with different surface modifiers) was effective on the thermal degradation characteristics of the nanoclay/EVA composites (Figure 6c). Samples with NC 1 had 3 thermal degradation steps in TGA, while neat EVA and samples with NC 2 had 2-step thermal degradation. Both nanoclays decreased the peak temperature for deacetylation of EVA (at 341-352°C) but increased the second peak temperature related to the defragmentation of the polymer backbone (at 474-480 °C) (Table 4). The higher temperatures for the second step degradation may be considered as an enhancement in the thermal durability of the composite [33]. BA addition increased both peak temperatures (for deacetylation and defragmentation of the EVA copolymer) for NC 2 added samples, which may be indicating a beneficial effect on flame retardancy. The nanoclay addition at a lower ratio (NC 1.1, EVA/nanoclay: 100/1) decreased the stress-bearing capability of the EVA/nanoclay composite, but increasing the nanoclay ratio to higher values increased the stress-bearing capability of the composite (Figure 9). The Young's (elastic) moduli increased with increasing nanoclay content. The increase was only 1.9% for NC 1.1 (EVA/NC 1: 100/1) while it was 220% for NC 1.4 (EVA/NC 1: 100/20) (Figure 10). The lower Young's modulus value of NC 1.1 may be interpreted as a higher ductility, which may be beneficial for certain applications (e.g., biomaterials), while a higher value of Young's modulus may be preferential for different applications. The nanoclay type (i.e., organic surface modifier) affected the mechanical characteristics of the EVA/nanoclay composite. The NC 1.3 and NC 2.3, both with a similar EVA/nanoclay ratio of 100/10, had elastic modulus values of 12.7 MPa and 8.9 MPa (which were 71% and 20% higher than the modulus of the neat EVA) (Figure 11). The considerable difference between the moduli of NC 1 and NC 2 containing EVA composites may be attributed to the difference in their morphology. BA addition to the EVA/nanoclay composites was effective on the mechanical characteristics of the composite. The stress-bearing of composites, either with or without BA addition, was better than the neat EVA (Figure 10). The stress-bearing capability was increased for the EVA/NC 1 composite, while it decreased for the EVA/NC 2 composites with BA addition (Figure 10). This may also be a consequence of having different morphologies in NC 1 and NC 2 containing composites. Increasing stress bearing capability of EVA/nanoclay composite with NC 1 (NC 1.3-BA) indicates the BA should be contributing to the interaction between the organic modifier on the nanoclay surface and the EVA matrix in an enhancing way. The enhancing effect of BA on stress bearing was not observed for NC 2.3-BA, which was with intercalated/partially agglomerated

morphology, which relatively decreased the surface area between the nanoclay (i.e., organic surface modifier) and the EVA matrix (Figure 10). The elastic moduli increased with BA addition for both composites with different nanoclays. The moduli for NC 2.3 and NC 2.3-BA were 8.9 and 12.8 MPa, respectively, showing the enhancing effect of BA addition on elastic modulus (44%) (Figure 11). The used additives (nanoclays: NC 1 and NC 2 and BA) at the ratios investigated were not sufficient to prepare self-extinguishing composites (i.e., the samples examined were all burnt out, dripped, and failed the UL94 VTM test). The additives and their ratio may/should be altered for higher flame resistance. The most effective nanoclay in terms of flame retardancy was NC 1. The burn-out time for NC 1.4 was 105% longer than the neat EVA (Figure 12). The burning time was increasing with the increasing nanoclay content (105% for NC 1.4) (Figure 12). Nanoclay type was effective on burning time, too. NC 1.3 with exfoliated morphology burnt out in 47.1 seconds, while it was 37.8 seconds for NC 2.3, indicating the exfoliated morphology of the EVA/NC 1 composite resulted in more hampering effect on burning process (Figure 12). BA addition was also effective on the burning characteristics of the EVA/nanoclay composites. The effect was adverse for NC 1.3-BA. The burning time of NC1.3-BA was 34% shorter than the time for NC 1.3 (and 7% longer than the time for the neat EVA) (Figure 12). The burning time for NC 2.3-BA was 7% longer than NC 2.3 (Figure 12). The burning times were not totally in accordance with the TGA data. The samples NC 1.3 and NC 1.3-BA had the highest temperature values during thermal degradation analysis (e.g., D-TGA peak T2, T (-50%)), which were higher/slightly higher than the values for the sample NC 1.4, but NC 1.4 had the longest burning time. This difference may be attributed to the steps of thermal degradation and differences in their progress under different conditions of TGA and burning tests. It was also showing that the composites should be characterized diligently to estimate their performance. The stress-bearing behaviour of the EVA composites was altered considerably with the additives, but the types and ratios of the additives should be revised to prepare composites with a better flame retardancy. The co-utilization of NC 1 (enhancing burning time) and NC 2 (enhancing stress-bearing) in the EVA composites may reveal a possible synergistic effect of two different nanoclays. The effect of a higher amount/ratio of the inorganic fillers (nanoclays) may be investigated. BA can be used at different (higher) ratios to investigate possible enhancement in flame retardancy of the composites. Different inorganic fillers, like metal hydroxides (e.g., magnesium hydroxide (MH), aluminium trihydroxide (ATH)), which are also environmentally friendly additives, may be used simultaneously with nanoclays and BA for possible enhancement in the flame retardancy. One of the important findings of the study may be the fact that additives may affect different properties of the composites in different ways, e.g., they may enhance the flame retardancy while not enhancing (or worsening) the mechanical properties. The EVA composites should be prepared and characterized diligently for the specific application, considering all important characteristics of the composites.

5. Acknowledgement

HES Kablo (Kayseri, TR) should be acknowledged for its kind and generous support by supplying EVA to this research.

6. Author Contribution Statement

İlke Erdem: Conceptualization, methodology, laboratory work, research, sources, data curation, manuscript-review and editing, supervision, project management.

Şeyma Avcı: laboratory work, manuscript-original draft research.

Mehmet Fazıl Kapçı: laboratory work, manuscript-original draft.

References

[1] Hou, Y., Xu, Z., Chu, F., Gui, Z., Song, L., Hu, Y., & Hu, W. (2021). A review on metal-organic hybrids as flame retardants for enhancing fire safety of polymer composites. *Composites Part B: Engineering*, *221*, 109014. https://doi.org/10.1016/j.compositesb.2021.109014

[2] Rajczak, E., Arrigo, R., & Malucelli, G. (2020). Thermal stability and flame retardance of EVA containing DNA-modified clays. *Thermochimica Acta*, *686*, 178546. https://doi.org/10.1016/j.tca.2020.178546

[3] Jeong, S. H., Park, C. H., Song, H., Heo, J. H., & Lee, J. H. (2022). Biomolecules as green flame retardants: Recent progress, challenges, and opportunities. *Journal of Cleaner Production*, *368*, 133241. https://doi.org/10.1016/j.jclepro.2022.133241

[4] Xu, Y. J., Qu, L. Y., Liu, Y., & Zhu, P. (2021). An overview of alginates as flame-retardant materials: Pyrolysis behaviors, flame retardancy, and applications. *Carbohydrate Polymers*, *260*, 117827. https://doi.org/10.1016/j.carbpol.2021.117827

[5] He, W., Song, P., Yu, B., Fang, Z., & Wang, H. (2020). Flame retardant polymeric nanocomposites through the combination of nanomaterials and conventional flame retardants. *Progress in Materials Science*, *114*, 100687. https://doi.org/10.1016/j.pmatsci.2020.100687

[6] Yılmaz Aydın, D., Gürü, M., Ayar, B., & Çakanyıldırım, Ç. (2016). Bor bileşiklerinin alev geciktirici ve yüksek sıcaklığa dayanıklı pigment olarak uygulanabilirliği [Applicability of boron compounds as flame retardant and high temperature resistant pigments]. *Journal of Boron*, *1*(1), 33-39. https://dergipark.org.tr/en/download/article-file/173986

[7] Das, P., Manna, S., Behera, A. K., Shee, M., Basak, P., & Sharma, A. K. (2022). Current synthesis and characterization techniques for clay-based polymer nano-composites and its biomedical applications: A

review. *Environmental Research*, *212*, 113534. https://doi.org/10.1016/j.envres.2022.113534

[8] Rafiee, R., & Shahzadi, R. (2019). Mechanical properties of nanoclay and nanoclay reinforced polymers: A Review. *Polymer Composites*, *40*(2), 431-445. https://doi.org/10.1002/pc.24725

[9] Guo, F., Aryana, S., Han, Y., & Jiao, Y. (2018). A review of the synthesis and applications of polymer-nanoclay composites. *Applied Sciences*, *8*(9), 1696. https://doi.org/10.3390/app8091696

[10] Chuayjuljit, S., & Worawas, C. (2011). Nanocomposites of EVA/polystyrene nanoparticles/montmorillonite. *Journal of Composite Materials*, *45*(6), 631-638. https://doi.org/10.1177/0021998310376116

[11] Ryu, H. J., Hang, N. T., Lee, J. H., Choi, J. Y., Choi, G., & Choy, J. H. (2020). Effect of organo-smectite clays on the mechanical properties and thermal stability of EVA nanocomposites. *Applied Clay Science*, *196*, 105750. https://doi.org/10.1016/j.clay.2020.105750

[12] Aghjeh, M. R., Nazari, M., Khonakdar, H. A., Jafari, S. H., Wagenknecht, U., & Heinrich, G. (2015). In depth analysis of micro-mechanism of mechanical property alternations in PLA/EVA/clay nanocomposites: A combined theoretical and experimental approach. *Materials and Design, 88*, 1277-1289. https://doi.org/10.1016/j.matdes.2015.09.081

[13] Díez, E., Rodríguez, A., Gómez, J. M., & Galán, J. (2021). TG and DSC as tools to analyse the thermal behaviour of EVA copolymers. *Journal of Elastomers and Plastics*, *53*(7), 792-805. https://doi.org/10.1177/0095244320988163

[14] Farias, G. M. G., Agrawal, P., Hanken, R. B. L., de Araújo, J. P., de Oliveira, A. D. B., & de Mélo, T. J. A. (2021). Effect of EVA copolymer containing different VA content on the thermal and rheological properties of bio-based high-density polyethylene/ethylene vinyl acetate blends. *Journal of Thermal Analysis and Calorimetry*, *146*(5), 2127-2139. https://doi.org/10.1007/s10973-020-10423-5

[15] Chaudhary, D. S., Prasad, R., Gupta, R. K., & Bhattacharya, S. N. (2005). Clay intercalation and influence on crystallinity of EVA-based clay nanocomposites. *Thermochimica Acta*, *433*(1-2), 187-195. https://doi.org/10.1016/j.tca.2005.02.031

[16] Beyer, G. (2009). Nanocomposites - A new class of flame retardants. P*lastics, Additives and Compounding*, *11*(2), 16-17, 19-21. https://doi.org/10.1016/S1464-391X(09)70048-0

[17] Erdem, A., & Dogan, M. (2023). Influence of boron bearing fillers on flame retardancy properties of huntite hydromagnesite filled ductile PLA biocomposites. *Journal of Boron*, *8*(1), 16-24. https://doi.org/10.30728/boron.1135702

[18] Dogan, M., Dogan, S. D., Savas, L. A., Ozcelik, G., & Tayfun, U. (2021). Flame retardant effect of boron compounds in polymeric materials. *Composites Part B: Engineering*, *222*, 109088. https://doi.org/10.1016/j.compositesb.2021.109088

[19] Uslu, B., Eskitoros-Togay, M., & Dilsiz, N. (2021). Improvement on flame retarding performance: Preparation and characterization of water-based indoor paints with addition of boric acid. *Journal of Boron*, *6*(2), 309-315. https://doi.org/10.30728/boron.865316

[20] Bozacı, E. (2018). Application of boron compounds to polyacrylonitrile fabrics by environmentally friendly methods. *Journal of Boron*, *3*(1), 17-23. https://doi.org/10.30728/boron.341441

[21] Nyambo, C., Kandare, E., & Wilkie, C. A. (2009). Thermal stability and flammability characteristics of ethylene vinyl acetate (EVA) composites blended with a phenyl phosphonate-intercalated layered double hydroxide (LDH), melamine polyphosphate and/or boric acid. *Polymer Degradation and Stability*, *94*(4), 513-520. https://doi.org/10.1016/j.polymdegradstab.2009.01.028

[22] Ozcelik, G., Elcin, O., Guney, S., Erdem, A., Hacioglu, F., & Dogan, M. (2022). Flame-retardant features of various boron compounds in thermoplastic polyurethane and performance comparison with aluminum trihydroxide and magnesium hydroxide. *Fire and Materials*, *46*(7), 1020-1033. https://doi.org/10.1002/fam.3050

[23] Yao, M., Wu, H., Liu, H., Zhou, Z., Wang, T., Jiao, Y., & Qu, H. (2021). In-situ growth of boron nitride for the effect of layer-by-layer assembly modified magnesium hydroxide on flame retardancy, smoke suppression, toxicity and char formation in EVA. *Polymer Degradation and Stability, 183*, 109417. https://doi.org/10.1016/j.polymdegradstab.2020.109417

[24] Çeliker, H. İ., Başbozkurt, A. Ç., & Yaraş, A. (2020). Mechanical and thermal properties of boric acid and paper mill sludge reinforced polyester composites. *Journal of Boron*, *5*(4), 163-169. https://doi.org/10.30728/boron.702466

[25] Titus, D., Samuel, E. J. J., & Roopan, S. M. (2019). Nanoparticle characterization techniques. In A. K. Shukla & Siavash Iravani (Eds.), G*reen Synthesis, Characterization and Applications of Nanoparticles* (pp. 303-319). Elsevier. https://doi.org/10.1016/b978-0-08-102579-6.00012-5

[26] Pedrosa, M. C. G., Filho, J. C. D., de Menezes, L. R., & da Silva, E. O. (2020). Chemical surface modification and characterization of carbon nanostructures without shape damage. *Materials Research*, *23*(2). https://doi.org/10.1590/1980-5373-MR-2019-0493

[27] Varlı, H. S., Akkurt Yıldırım, M., Kızılbey, K., & Türkoğlu, N. (2024). Gene delivery via octadecylamine-based nanoparticles for iPSC generation from CCD1072-SK fibroblast cells. *Current Issues in Molecular Biology*, *46*(11), 12588-12607. https://doi.org/10.3390/cimb46110747

[28] Ye, L., Miao, Y., Yan, H., Li, Z., Zhou, Y., Liu, J., & Liu, H. (2013). The synergistic effects of boroxo siloxanes with magnesium hydroxide in halogen-free flame retardant EVA/MH blends. *Polymer Degradation and Stability*, *98*(4), 868-874. https://doi.org/10.1016/j.polymdegradstab.2013.01.001

[29] Luna, C. B. B., da Silva Barbosa Ferreira, E., Siqueira, D. D., dos Santos Filho, E. A., & Araújo, E. M. (2022). Additivation of the ethylene-vinyl acetate copolymer (EVA) with maleic anhydride (MA) and dicumyl peroxide (DCP): The impact of styrene monomer on cross-linking

and functionalization. *Polymer Bulletin*, *79*(9), 7323-7346. https://doi.org/10.1007/s00289-021-03856-x

[30] Bartolomei, S. S., Santana, J. G., Valenzuela Díaz, F. R., Kavaklı, P. A., Guven, O., & Moura, E. A. B. (2020). Investigation of the effect of titanium dioxide and clay grafted with glycidyl methacrylate by gamma radiation on the properties of EVA flexible films. *Radiation Physics and Chemistry*, *169*, 107973. https://doi.org/10.1016/j.radphyschem.2018.08.022

[31] Tambe, S. P., Naik, R. S., Singh, S. K., Patri, M., & Kumar, D. (2009). Studies on effect of nanoclay on the properties of thermally sprayable EVA and EVAI coatings. *Progress in Organic Coatings*, *65*(4), 484-489. https://doi.org/10.1016/j.porgcoat.2009.04.003

[32] Zhang, X., Yi, H., Bai, H., Zhao, Y., Min, F., & Song, S. (2017). Correlation of montmorillonite exfoliation with interlayer cations in the preparation of two-dimensional nanosheets. *RSC Advances*, *7*(66), 41471-41478. https://doi.org/10.1039/c7ra07816a

[33] Osman, A. F., Tuty, T. F., Rakibuddin, M., Hashim, F., Tuan Johari, S. A. T., Ananthakrishnan, R., & Ramli, R. (2017). Pre-dispersed organo-montmorillonite (organo-MMT) nanofiller: Morphology, cytocompatibility and impact on flexibility, toughness and biostability of biomedical ethyl vinyl acetate (EVA) copolymer. *Materials Science and Engineering C*, *74*, 194-206. https://doi.org/10.1016/j.msec.2016.11.137

[34] Gianelli, W., Camino, G., Dintcheva, N. T., Lo Verso, S., & La Mantia, F. P. (2004). EVA-montmorillonite nanocomposites: Effect of processing conditions. *Macromolecular Materials and Engineering*, *289*(3), 238-244. https://doi.org/10.1002/mame.200300267

[35] Unlu, S. M., Dogan, S. D., & Dogan, M. (2014). Comparative study of boron compounds and aluminum trihydroxide as flame retardant additives in epoxy resin. *Polymers for Advanced Technologies*, *25*(8), 769-776. https://doi.org/10.1002/pat.3274

TENMAK BOREN BOR ARAŞTIRMA ENSTİTÜSÜ

BOR DERGİSİ
JOURNAL OF BORON
https://dergipark.org.tr/boron

Ni-Co-Ta-W-B metalik cam alaşımının metal matrisli kompozit üretiminde kullanım potansiyelinin arttırılması için camlaşma kabiliyetinin geliştirilmesi

Hakan Şahin [1,*], **Aytekin Hitit** [2]

[1]*Afyon Kocatepe Üniversitesi, Teknoloji Uygulama ve Araştırma Merkezi (TUAM), Afyonkarahisar, 03200, Türkiye*
[2]*Afyon Kocatepe Üniversitesi, Mühendislik Fakültesi, Malzeme Bilimi ve Mühendisliği Bölümü, Afyonkarahisar, 03200, Türkiye*

MAKALE BİLGİSİ

Makale Geçmişi:
İlk gönderi 27 Ekim 2024
Kabul 18 Ocak 2025
Online 31 Mart 2025

Araştırma Makalesi

DOI: 10.30728/boron.1573965

Anahtar kelimeler:
Cam oluşturma kabiliyeti
Co-W-B fazı
İri hacimli metalik cam
Mikrosertlik
Termal özellikler

ÖZET

Bu çalışmada, B açısından zengin Ni-Co-W-B metalik cam alaşımı ailesinin cam oluşturma yeteneği Fe ve Cr ilavesiyle arttırılmıştır. Bu alaşım ailesi, yüksek tokluk ve sertliğe sahip metal matrisli kompozit (MMC) malzemelerin üretiminde öncü olarak hizmet edebilecek umut verici bir malzeme grubunu temsil etmektedir. Alaşım ailesinin kristalleşmesi sonucunda yüksek tokluk sağlayabilen bir Ni katı çözeltisi ve çok yüksek sertliğe sahip bir borür fazı (CoWB) oluşmaktadır. Yüksek kristalleşme sıcaklığına sahip dökme metalik camlardan biri olan $Ni_{31,56}Co_{21,74}B_{15}W_{23,7}Ta_8$ alaşımının cam oluşturma yeteneği, termal özellikleri ve mikrosertlik özellikleri Fe ve Cr elementleri eklenerek incelenmiştir. Alaşımların yapısal ve termal özellikleri X-ışını kırınımı (XRD), diferansiyel taramalı kalorimetri (DSC), Vickers mikrosertliği ve taramalı elektron mikroskobu (SEM) analizleri kullanılarak araştırılmıştır. Analizler, Cr ilavesinin alaşımdaki kristalleşmeyi arttırdığını, dolayısıyla cam oluşturma yeteneğini olumsuz yönde etkilediğini ortaya çıkarmıştır. Buna karşılık, Fe'nin belirli seviyelerde eklenmesinin alaşımın cam oluşturma yeteneğini artırabileceği belirlenmiştir. $Ni_{21,5}Co_{21,5}Fe_{10,3}B_{15}W_{23,7}Ta_8$ alaşımı, 747°C'de ölçülen kristalizasyon sıcaklığı (T_x) ile 1 mm'lik kritik döküm kalınlığı sergilemiştir. Mikro sertlik ölçümleri alaşımın sertliğinin 1253 HV olduğunu ortaya çıkarmıştır. Uygun miktarlarda Fe eklenmesinin cam oluşturma yeteneğini artırabileceği, Cr eklenmesinin ise cam oluşturma eğilimini olumsuz yönde etkilediği gösterilmiştir.

Enhancing the glass-forming ability of Ni-Co-Ta-W-B metallic glass alloy to increase its potential use in metal matrix composite production

ARTICLE INFO

Article history:
Received October 27, 2024
Accepted January 18, 2025
Available online March 31, 2025

Research Article

DOI: 10.30728/boron.1573965

Keywords:
Glass-forming ability
Co-W-B phase
Bulk metallic glass
Microhardness
Thermal properties

ABSTRACT

In this study, the glass-forming ability of the B-rich Ni-Co-W-B metallic glass alloy family has been enhanced through the addition of Fe and Cr. This alloy family represents a promising group of materials that can serve as precursors for producing metal matrix composite (MMC) materials with high toughness and hardness. As a result of the crystallization of the alloy family, a Ni solid solution that can provide high toughness and a boride phase (CoWB) with very high hardness is formed. The glass-forming ability, thermal properties, and microhardness characteristics of the $Ni_{31.56}Co_{21.74}B_{15}W_{23.7}Ta_8$ alloy, one of the bulk metallic glasses with a high crystallization temperature, were investigated by adding Fe and Cr elements. The structural and thermal properties of the alloys were investigated using X-ray diffraction (XRD), differential scanning calorimetry (DSC), Vickers microhardness, and scanning electron microscopy (SEM) analyses. The analyses revealed that the addition of Cr increases crystallization in the alloy, thereby negatively impacting its glass-forming ability. In contrast, it was determined that incorporating Fe at certain levels can enhance the glass-forming ability of the alloy. The $Ni_{21.5}Co_{21.5}Fe_{10.3}B_{15}W_{23.7}Ta_8$ alloy exhibited a critical casting thickness of 1 mm, with a crystallization temperature (T_x) measured at 747°C. Micro-hardness measurements revealed that the hardness of the alloy is 1253 HV. It has been demonstrated that adding Fe in appropriate amounts can enhance the glass-forming ability, whereas the addition of Cr adversely affects the glass-forming tendency.

*Corresponding author: hakansahin@aku.edu.tr

1. Giriş (Introduction)

Metalik camlar 1960 yılında keşfedilmiş olup günümüzün ve geleceğin en önemli malzemelerinden birisidir [1]. Sahip oldukları fiziksel, kimyasal, mekanik ve manyetik özelliklerinden [2] dolayı savunma [3], havacılık [3], elektrik-elektronik [3], otomobil sanayi ve uzay araçları [4] gibi önemli endüstriyel sektörlerde kullanılan ve kullanılabilir önemli bir malzeme türüdür. Ayrıca metalik camlar yüksek tokluk ve yüksek sertliğe sahip metal matrisli kompozit (MMK) malzemeler elde etmek için öncül olarak kullanılabilecek en ideal malzeme tiplerinden biridir. MMK'lar, metal bir matris içerisinde dağıtılmış takviye malzemelerinden oluşan gelişmiş mühendislik malzemeleridir [5]. MMK'ların amacı, metalin yüksek mukavemet, süneklik ve tokluk gibi özelliklerini, seramik ya da elyaf gibi takviye malzemelerinin sertlik, yüksek sıcaklık dayanımı ve aşınma direnci gibi üstün özellikleriyle birleştirmektir. Bu tür kompozitler, gümüş, alüminyum, magnezyum, titanyum gibi hafif metallerin matris olarak kullanıldığı ve seramik parçacıklar (örneğin, SiC, Al_2O_3, BN) veya elyaflar (karbon, bor, silika) ile güçlendirilmiş yapılardır [6-8]. MMK'lar, geleneksel metallerin sahip olduğu sınırlamaları aşarak, daha yüksek mukavemet/ağırlık oranları, termal kararlılık, aşınma direnci ve korozyon dayanımı sunar. Bu nedenle, otomotiv, havacılık, uzay, savunma ve elektronik sektörlerinde yüksek performans gerektiren uygulamalarda tercih edilirler. MMK'ların üretimi genellikle toz metalürjisi, ergitme-döküm, sıvı infiltrasyon ve sıcak presleme gibi tekniklerle gerçekleştirilir. Ancak, matris ve takviye malzemeleri arasındaki ara yüzey bağlanma kalitesi, dağılım homojenliği ve üretim maliyetleri gibi zorluklar, MMK'ların geniş çapta endüstriyel uygulanabilirliğini sınırlayabilmektedir. Bu nedenle, son yıllarda nano-takviyeler, yüzey modifikasyon teknikleri ve yenilikçi üretim yöntemleri üzerinde çalışmalar yoğunlaşmıştır.

Uygun bileşimdeki amorf yapının kontrollü bir şekilde kristalizasyonu sonucunda yapıda hem yüksek tokluğa sahip hem de ultra sert fazlar çökeltebilmek mümkündür. Yüksek oranda B içeren Ni-Co-W-B metalik cam alaşım ailesi, bu tip malzemeleri geliştirmek için kullanılabilecek en iyi metalik cam alaşımlarından birisidir [9]. Bu alaşım ailesinin uygun sıcaklıklarda kristalize edildiğinde yapısında yüksek tokluğu sağlayabilecek yüzey merkezli kübik (YMK) yapıda Ni katı çözeltisi ve çok yüksek sertliğe sahip ortorombik kristal yapısında borür (CoWB) fazları çökelmektedir [10]. Metalik camların öncül olarak kullanımı ile yukarıda bahsedilen MMK' ların geniş çapta endüstriyel uygulanabilirliğini sınırlayan matris ve takviye malzemeleri arasındaki ara yüzey bağlanma kalitesi, dağılım homojenliği ve üretim maliyetleri gibi zorluklar aşılabilecektir. Yüksek sertliğe sahip borür fazlardan biri olan ve 4300 Vickers sertliği (HV) gibi ultra yüksek sertlik değerine sahip olan CoWB fazının [11] Ni-Co-W-B metalik cam alaşım ailesinin ısıl işlemi sonucunda yapıda çökelmesi ile oluşturulacak olan MMK malzemelerin yüksek tokluğun yanında yüksek sertlik özelliklerine de sahip olmalarında en önemli yapılardan biridir. Çalışma grubu tarafından Ni-Co-W-B alaşım ailesi üzerinde daha önce yapılan çalışmalarda alaşımın ısıl işlemi sonucunda elde edilen kompozit yapılarda 1400 HV sertlik değeri ile birlikte 6,45 MPa$\sqrt{m}$ tokluk değerleri elde edilmiştir [11]. Metalik camların yüksek tokluk ve yüksek sertliğe sahip MMK malzemelerin elde edilmesi için öncül olarak kullanılmasını engelleyen en önemli faktörlerden biri camlaşma kabiliyetlerinin sınırlı olmasıdır. Bu tip alaşımların yüksek tokluk ve sertliğe sahip MMK malzemelerin üretiminde öncül olarak kullanılabilmesi için alaşımlar öncelikle amorf yapıda toz olarak elde edilmelidir. Amorf olarak elde edilen bu tozlar eklemeli imalat veya çeşitli kaplama yöntemleri kullanılarak amorf yapılı malzemeler üretilmelidir [12-14]. Bu yöntemlerle kaplanmış veya eklemeli imalatla üretilmiş malzemelerin amorf yapılarını koruyabilmesi için kullanılan tozların camlaşma kabiliyeti yüksek olmalıdır. Ayrıca, kristalizasyon sıcaklıklarının da olabildiğince yüksek olması gerekmektedir [15-17]. Camlaşma kabiliyeti (GFA), bir malzemenin sıvı halden hızlı soğutma sırasında kristalleşmeden amorf bir yapıya geçebilme yeteneğini ifade etmektedir [18]. GFA, malzemelerin yüksek performanslı cam veya amorf alaşımlar olarak kullanılabilirliğini değerlendirmek açısından kritik bir parametredir. Bu bağlamda, camlaşma kabiliyetini belirlemek için çeşitli parametreler literatürde tanımlanmıştır. Makale kapsamında GFA'yı değerlendirmek için iki ana parametre kullanılmıştır. İndirgenmiş cam geçiş sıcaklığı (T_g/T_l) parametresi [19], cam geçiş sıcaklığı (T_g) ile sıvılaşma sıcaklığı (Tl) oranı olarak tanımlanmaktadır. Yüksek bir T_g / T_l oranı, malzemenin cam formda kalma olasılığının daha yüksek olduğuna işaret etmektedir. Çalışmamızda, bu parametre kullanılarak alaşımların camlaşma eğilimleri değerlendirilmiştir. Gama (γ) parametresi ise [20], cam geçiş sıcaklığı (T_g), sıvılaşma sıcaklığı (T_l) ve kristalizasyon sıcaklığı (T_x) gibi termal özelliklere dayalı olarak hesaplanmaktadır. Gama parametresinin hesaplanmasında $\gamma=T_x/(T_g+T_l)$ formülü kullanılmaktadır. Bu çalışmadaki amaç daha önceden geliştirilmiş yüksek kristalizasyon sıcaklığına sahip iri hacimli metalik cam alaşımlarından olan Ni-Co-W-Ta-B [21] alaşımının camlaşma kabiliyetini, kristalizasyon sıcaklığını ve mikrosertlik gibi özelliklerini arttırmaktır.

2. Malzeme ve Yöntemler (Materials and Methods)

2.1. Malzemeler (Materials)

Ana alaşımların hazırlanmasında Ni (%99,8, 3µm, Acros Organics, US), Co (%99,9, <2 µm, Sigma Aldrich, US), Fe (%99,9, <10 µm, Alfa Aesar, US), W (%99,9, 1-5 µm, Alfa Aesar, US), Ta (%99,9, <44 µm, Sigma Aldrich US), Cr (%99,9, <10µm, Alfa Aesar, US), B (%98, <44 µm, Alfa Aesar, US) kullanılmıştır. Saf toz halindeki elementler uygun kompozisyonlarda tartılıp hidrolik pres yardımı ile preslenerek tabletler halinde hazırlanmıştır. Presleme işlemi 80 MPa'lık bir basınç uygulanarak 10 mm çapında ve yaklaşık olarak 5-6 mm yüksekliğinde tabletler halinde

numuneler elde edilecek şekilde yapılmıştır. Ergitme ve döküm işlemleri için çalışma grubu tarafından tasarlanıp yaptırılan, 3,5x10^{-4} mbar vakum seviyesine düşebilen, inert atmosfer ortamında yaklaşık 3000°C sıcaklıklarda ergitme işlemi yapabilen vakum ark ocağı kullanılmıştır. Yüksek soğutma hızlarına ulaşabilmek için dökümler %99 saflıkta çok iyi termal iletkenliğe sahip olan bakır kalıplara yapılmıştır. Numunelerin kristalografik yapı incelemeleri için X-ışını kırınımı (XRD) cihazı (D8 Advanced model, Bruker, US), termal özelliklerini karakterize etmek için diferansiyel taramalı kalorimetre (DSC) cihazı (STA449 Jupiter F3 model, Netzsch, Germany), mikroyapı incelemeleri için taramalı elektron mikroskobu (SEM) cihazı (LEO 1430 VP, Zeiss, Germany) ve mikrosertlik değerlerinin belirlenmesi için de sertlik cihazı (HMV 2L, Shimadzu, Japan) kullanılmıştır.

2.2. Yöntemler (Methods)

Yüksek saflıktaki toz ham maddelerden presleme ile hazırlanan tablet halindeki numuneler vakum ark ocağında, cihaz 3,5x10^{-4} mbar vakum değerine alındıktan sonra yüksek saflıkta argon atmosferi altında homojenliği sağlamak açısından üçer kez ergitilerek alaşımlar hazırlanmıştır. Metalik cam çalışmalarında, hem ana alaşımların hazırlanması hem de alaşımların camlaşma kabiliyetinin belirlenmesi süreçlerinde, döküm esnasında oksitlenmenin camlaşma kabiliyetine olumsuz etkisini önlemek amacıyla mümkün olan en yüksek vakum seviyelerine inmek gerekmektedir [22,23]. Özellikle ana alaşımların ilk ergitilmesi sırasında, toz halinde preslenmiş numunelerin oksitlenme olasılığının yüksek olması nedeniyle, tasarlanan vakum ark ocağıyla mümkün olan en düşük vakum seviyesine inilerek alaşımlar ergitilmiştir. Metalik cam alaşımları elde etmek amacıyla hazırlanan alaşımlar, 0,3 mm ve 0,5 mm kalınlığında, 3 mm genişliğinde ve 5 mm uzunluğunda plaka ile 1 mm ve 1,5 mm kalınlığında, 15 mm uzunluğunda silindir numuneler olarak, bakır kalıba emme döküm yöntemi ile dökülmüştür. Emme döküm yöntemi, alaşımların hızlı katılaşmasını ve oksidasyon riskinin minimuma indirilmesini sağladığı için tercih edilmiştir [24]. Bu yöntem, özellikle metalik cam üretiminde homojen yapı elde etmek ve numune boyutlarında tutarlılık sağlamak amacıyla yaygın olarak kullanılmaktadır. Numunelerin dökümleri yapılırken vakum ark ocağı kullanılmış ve cihaz 3,5x10^{-3} mbar vakum değerine inilerek yüksek saflıkta argon atmosferi altında dökümler yapılmıştır. Hazırlanan alaşımların kompozisyonları Tablo 1'de verilmiştir. Alaşımların kompozisyonları, çalışma grubumuz tarafından daha önce geliştirilen Ni-Co-Ta-W-B alaşımı dikkate alınarak tasarlanmıştır. Önceki çalışmalarda, baz alaşımın camlaşma kabiliyetinin 1,5 mm ile sınırlı kalmasının, soğuma esnasında YMK yapıda çökelen Ni katı çözelti nano kristallerinin oluşumundan kaynaklandığı belirlenmiştir. Bu sorunu aşmak amacıyla, mevcut çalışmada ilk üç alaşımda Fe ve Cr elementleri, Ni ve Co elementleriyle eşit atomik yüzdelerde olacak şekilde alaşıma dahil edilmiştir. Bu yaklaşım, YMK yapıda kristalleşerek camlaşmayı bozan Ni bazlı katı çözeltilerin oluşumunu engellemeyi hedeflemiştir. Tasarım sürecinde, yüksek entropili metalik cam alaşımlarında izlenen yöntemlere benzer şekilde, alaşımın kristallenme eğilimini azaltmak için eş atomik oranlarda elementlerin kullanılması stratejisi benimsenmiştir. Elde edilen dökümler sonucunda numuneleri yapısal olarak inceleyebilmek için XRD analizleri yapılmıştır.

XRD analizleri 1,54 Å Cu-Kα dalga boyuna sahip X-ışını kaynağı kullanılarak 2θ açısı 10° ila 100° aralığında ve tarama hızı 2°/dk. olacak şekilde yapılmıştır. Analizlerin gerçekleştirilmesi için dökümü yapılan numunelerden yaklaşık 3-4 mm uzunluğunda parçalar kesilerek, bu numuneler öğütülmüş ve ardından detaylı analizler yapılmıştır. Elde edilen XRD verilerinde, amorf olmayan numunelerde tespit edilen piklerin hangi kristal yapıya ait olduğu, 2012 yılı Powder Diffraction File (PDF) veri tabanına sahip Diffract Suite değerlendirme programı kullanılarak belirlenmiştir. Bu yöntem, fazların kristal yapılarını doğru bir şekilde tanımlamak için kullanılan standart referans verileri ile karşılaştırma yapmamıza olanak tanımıştır. Alaşımların cam geçiş (T_g) ve T_x sıcaklıkları, 20°C/dk. ısıtma hızıyla DSC cihazı kullanılarak belirlenmiştir. Erime (T_m) ve likidüs (T_l) sıcaklıkları ise, yine aynı hızla yapılan soğutma sırasında ölçülmüştür. T_g, metalik camın amorf fazdan viskoelastik duruma geçişini temsil ederken, T_x, kristalleşmenin başladığı sıcaklığı ifade etmektedir. T_m, alaşımın katı fazdan sıvı faza geçişini tanımlarken, T_l, tamamen erimiş alaşımın sıvı fazda stabil hale geldiği noktadır. Bu kritik sıcaklıklar, alaşımların camlaşma kabiliyeti ve termal kararlılığı açısından belirleyicidir. Alaşımların mikroyapı analizleri, SEM cihazında geri yansıyan elektron (BSE) modunda gerçekleştirilmiştir. Bu mod, farklı elementlerin atom numarası farklarına dayalı olarak kontrast oluşturduğu için tercih edilmiştir. Böylece, metalik cam alaşımlarında olası farklı fazların tespiti ve element dağılımındaki homojenliğin değerlendirilmesi daha hassas bir şekilde yapılabilmektedir. Alaşımları mekanik özellikleri açısından inceleyebilmek için Vickers sertlik ölçümleri yapılmıştır.

Tablo 1. Hazırlanan alaşımların kompozisyonları (% atomik) (Compositions of the prepared alloys (atomic %)).

Kompozisyon	Ni	Co	Fe	Cr	Ta	W	B
$Ni_{13,25}Co_{13,25}Cr_{13,25}Fe_{13,25}B_{15}W_{23,7}Ta_8$	13,25	13,25	13,25	13,25	8,00	23,70	15,00
$Ni_{17,76}Co_{17,76}Cr_{17,76}B_{15}W_{23,7}Ta_8$	17,76	17,76	-	17,76	8,00	23,70	15,00
$Ni_{17,76}Co_{17,76}Fe_{17,76}B_{15}W_{23,7}Ta_8$	17,76	17,76	17,76	-	8,00	23,70	15,00
$Ni_{21,50}Co_{21,50}Fe_{10,30}B_{15}W_{23,7}Ta_8$	21,50	21,50	10,30	-	8,00	23,70	15,00

Ölçümler 2,94 N yük altında 15 sn süre uygulanarak yapılmıştır. Her alaşım için numune üzerinde 10 farklı noktadan ölçüm alınmış ve ölçümlerin aritmetik ortalamaları alınmıştır.

3. Sonuçlar ve Tartışma (Results and Discussion)

3.1. XRD Analiz Sonuçları (XRD Analysis Results)

Alaşımların camlaşma kabiliyetlerini ve termal özelliklerini ölçebilmek için ilk etapta cam numuneler elde edebilmek çok önemlidir. Farklı kalınlıklardaki dökümler sonucunda elde edilen numunelere XRD analizi yapıldığında Şekil 1'de görüldüğü üzere $Ni_{13,25}Co_{13,25}Cr_{13,25}Fe_{13,25}B_{15}W_{23,7}Ta_8$, $Ni_{17,76}Co_{17,76}Cr_{17,76}B_{15}W_{23,7}Ta_8$ ve $Ni_{17,76}Co_{17,76}Fe_{17,76}B_{15}W_{23,7}Ta_8$' alaşımlarının camlaşma kalınlıklarının 0,3 mm olduğu, $Ni_{21,50}Co_{21,50}Fe_{10,30}B_{15}W_{23,7}Ta_8$ alaşımının ise 1 mm camlaşma kabiliyetine sahip olduğu belirlenmiştir.

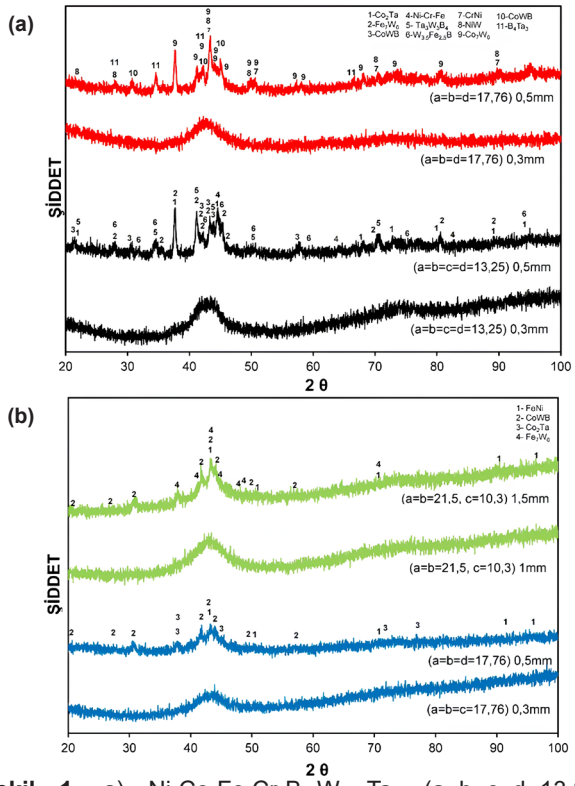

Şekil 1. a) $Ni_aCo_bFe_cCr_dB_{15}W_{23,7}Ta_8$ (a=b=c=d=13,25), (a=b=d=17,76, c=0), b) (a=b=c=17,76, d=0) ve (a=b=21,5, c=10,3, d=0) alaşımlarının farklı kalınlıklardaki dökümlerinin XRD analizi sonuçları (XRD analysis results of the castings with different thicknesses for the alloys: a) $Ni_aCo_bFe_cCr_dB_{15}W_{23,7}Ta_8$ (a=b=c=d=13.25), (a=b=d=17.76, c=0), b) (a=b=c=17.76, d=0), and (a=b=21.5, c=10.3, d=0)).

Yapılan XRD analizleri sonucunda $Ni_{13,25}Co_{13,25}Cr_{13,25}Fe_{13,25}B_{15}W_{23,7}Ta_8$ alaşımının 0,5 mm kalınlığındaki numunesinde rombohedral kristal yapıda Fe_7W_6, yüzey merkezli kübik (YMK) kristal yapıda Co_2Ta, ortorombik kristal yapıda CoWB, hacim merkezli kübik (HMK) kristal yapıda Ni-Cr-Fe, tetragonal kristal yapıda $Ta_3W_3B_4$ ve tetragonal kristal yapıda $W_{3,5}Fe_{2,5}B_4$ fazlarının çökeldiği belirlenmiştir. $Ni_{17,76}Co_{17,76}Cr_{17,76}B_{15}W_{23,7}Ta_8$ alaşımının 0,5 mm kalınlığındaki numunesinin XRD analizi sonucunda tetragonal kristal yapıda $Ni_{8,11}W_{1,89}$, YMK kristal yapıda CrNi, rombohedral kristal yapısında Co_7W_6, tetragonal kristal yapısında Cr_2B, ortorombik kristal yapıda CoWB ve hegzagonal kristal yapıda Ni kristallerinin çökeldiği belirlenmiştir. $Ni_{17,76}Co_{17,76}Fe_{17,76}B_{15}W_{23,7}Ta_8$ alaşımının 0,5 mm kalınlığındaki numunesinin XRD analizi sonucunda YMK kristal yapıda Co_2Ta, YMK kristal yapısında (Fe,Ni), ortorombik kristal yapıda CoWB fazlarının çökeldiği belirlenmiştir. $Ni_{21,50}Co_{21,50}Fe_{10,30}B_{15}W_{23,7}Ta_8$ alaşımının 1,5 mm kalınlığındaki numunesinin XRD analizi sonucunda $Ni_{17,76}Co_{17,76}Fe_{17,76}B_{15}W_{23,7}Ta_8$ alaşımının 0,5 mm kalınlığındaki numunesinde çökelen fazlar ile aynı fazların çökeldiği belirlenmiştir. Alaşımlarda camlaşma kabiliyetini artırmak amacıyla eklenen Cr ve Fe elementlerinin, XRD analizleri incelendiğinde, genel olarak kristallenmeyi teşvik edici bir etki gösterdiği tespit edilmiştir. Cr ve Fe elementlerinin Ni ile sıvı halde tam olarak karışabilmeleri, soğuma sırasında kristalleşmeyi kolaylaştırarak HMK yapısında Ni-Cr-Fe ve YMK yapısında NiCr, FeNi fazlarının çökelmesine yol açmıştır. Cr ve Fe elementlerinin çekirdeklenmeyi kolaylaştırarak yapıda nano çökeltilerin oluşumunu teşvik etmesi, alaşımda yüksek ergime sıcaklığına sahip Ta, W ve B gibi elementlerin farklı kristal yapılarda çökelmesini de kolaylaştırmıştır.

3.2. Termal ve Mikroyapı Analizleri Sonuçları (Thermal and Microstructure Analysis Results)

Alaşımların termal özelliklerini belirlemek amacıyla, amorf yapıdaki numunelere DSC/TG analizleri uygulanmıştır. Şekil 2'de, 0,3 mm kalınlığında amorf olarak elde edilen alaşımların DSC/TG analizi sonuçları sunulmaktadır. Yapılan analizlerde, alaşımlar arasında en yüksek Tx sıcaklığına sahip olanın $Ni_{17,76}Co_{17,76}Fe_{17,76}B_{15}W_{23,7}Ta_8$ alaşımı olduğu tespit edilmiştir. XRD analizlerine göre camlaşma kabiliyeti en iyi olan $Ni_{21,50}Co_{21,50}Fe_{10,30}B_{15}W_{23,7}Ta_8$ alaşımın T_g ve T_x sıcaklıkları sırası ile 629°C ve 747°C olarak ölçülmüştür. $Ni_{13,25}Co_{13,25}Cr_{13,25}Fe_{13,25}B_{15}W_{23,7}Ta_8$, $Ni_{17,76}Co_{17,76}Cr_{17,76}B_{15}W_{23,7}Ta_8$, $Ni_{17,76}Co_{17,76}Fe_{17,76}B_{15}W_{23,7}Ta_8$ kompozisyonlarına sahip alaşımların yapısal gevşeme, T_g ve T_x sıcaklıklarının çok yakın olması veya düşük serbest hacim gibi etkenlerden dolayı cam geçiş sıcaklıklarının belirlenmesini engelleyen geniş ekzotermik pikler görülmektedir. $Ni_{13,25}Co_{13,25}Cr_{13,25}Fe_{13,25}B_{15}W_{23,7}Ta_8$ alaşımı için belirlenen ekzotermik bölge 364°C ila 462°C, $Ni_{17,76}Co_{17,76}Cr_{17,76}B_{15}W_{23,7}Ta_8$ için belirlenen ekzotermik bölge 510°C ila 700°C $Ni_{17,76}Co_{17,76}Fe_{17,76}B_{15}W_{23,7}Ta_8$ için belirlenen ekzotermik bölge 360°C ila 476°C, dir. $Ni_{21,50}Co_{21,50}Fe_{10,30}B_{15}W_{23,7}Ta_8$ alaşımının cam geçiş sıcaklığı 629°C ve kristalizasyon sıcaklığı 747°C olarak belirlenmiştir. Yapılan XRD analizleri sonuçlarına göre camlaşma kabiliyetinin 1 mm olduğu belirlenen $Ni_{21,50}Co_{21,50}Fe_{10,30}B_{15}W_{23,7}Ta_8$ kompozisyonundaki alaşıma mikroyapı incelemesi yapılmıştır. Yapılan SEM mikro yapı görüntüleri Şekil 3'de verilmiştir. $Ni_{21,50}Co_{21,50}Fe_{10,30}B_{15}W_{23,7}Ta_8$ kompozisyondaki numunenin 1 mm kalınlığındaki örneklerinin 1000x büyütme oranındaki görüntülerine bakıldığında herhangi bir kristal yapıya

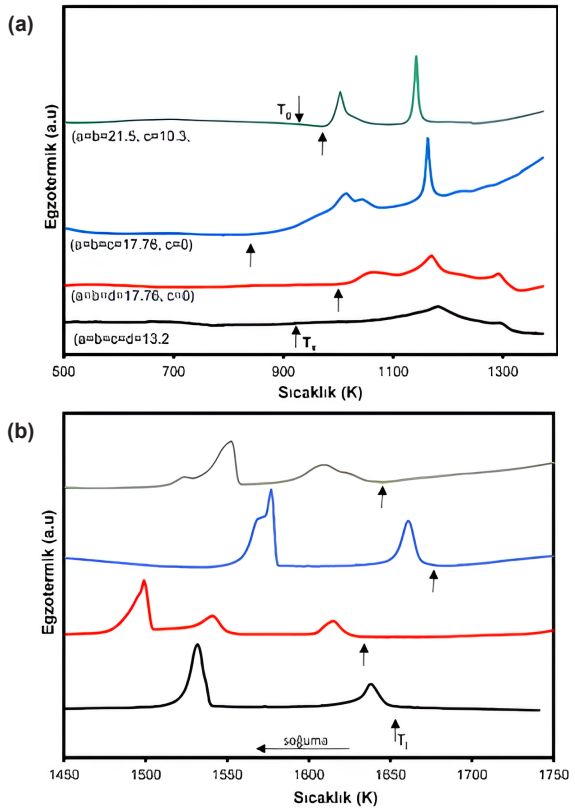

Şekil 2. $Ni_aCo_bFe_cCr_dB_{15}W_{23,7}Ta_8$ (a=b=c=d=13,25), (a=b=d=17,76, c=0), (a=b=c=17,76, d=0) ve (a=b=21,5, c=10,3, d=0) alaşımlarının DSC grafikleri, a) düşük sıcaklık b) yüksek sıcaklık (DSC graphs of the $Ni_aCo_bFe_cCr_dB_{15}W_{23,7}Ta_8$ alloys: (a=b=c=d=13.25), (a=b=d=17.76, c=0), (a=b=c=17.76, d=0), and (a=b=21.5, c=10.3, d=0), showing (a) low temperature and (b) high temperature).

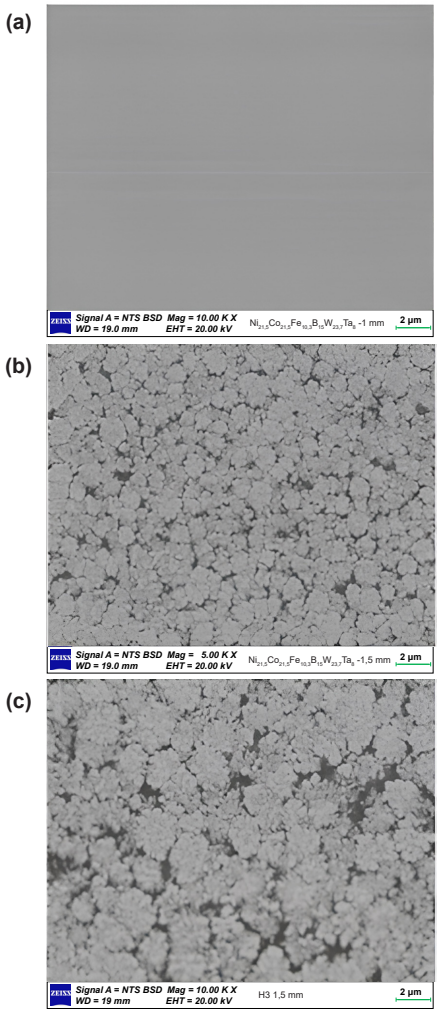

Şekil 3. $Ni_{21,50}Co_{21,50}Fe_{10,30}B_{15}W_{23,7}Ta_8$ alaşımının 1 mm ve 1,5 mm kalınlıktaki numunelerinin SEM görüntüleri (SEM images of the $Ni_{21,50}Co_{21,50}Fe_{10,30}B_{15}W_{23,7}Ta_8$ alloy samples with thicknesses of 1 mm and 1.5 mm).

rastlanmadığı görülmüştür. Alaşımın 1,5 mm döküm kalınlıklarındaki numunesinin 500X ve 1000X büyütme oranlarındaki görüntülerine bakıldığında yapılarda kristal fazların oluştuğu görülmüştür. Yapılan XRD analizlerinde de belirlendiği üzere alaşımın 1,5 mm kalınlığındaki numunesinin SEM görüntülerinde FeNi, Fe_7W_6 ve CoWB fazlarının varlığını gösteren 3 farklı faz bölgelerinin olduğu görülmektedir.

3.3. Mikrosertlik Analizi Sonuçları (Microhardness Analysis Results)

Yapılan Vickers mikrosertlik analiz sonucunda $Ni_{13,25}Co_{13,25}Cr_{13,25}Fe_{13,25}B_{15}W_{23,7}Ta_8$ alaşımının sertliğinin 1375 HV olduğu belirlenmiştir ve bu değer hazırlanan alaşımlar içerisinde ölçülen en yüksek değerdir (Şekil 4b). Camlaşma kabiliyeti en iyi olan $Ni_{21,50}Co_{21,50}Fe_{10,30}B_{15}W_{23,7}Ta_8$ alaşımının mikrosertlik değeri ise 1253 HV olarak ölçülmüştür (Şekil 4a). Alaşımların termal özellikleri, kritik döküm kalınlıkları, camlaşma parametreleri ve mikrosertlikleri Tablo 2'de verilmiştir.

Yüksek kristalizasyon sıcaklığına sahip ve camlaşma kabiliyeti 1,5 mm olan $Ni_{31,56}Co_{21,74}B_{15}W_{23,7}Ta_8$ alaşımının camlaşma kabiliyetini arttırabilmek için Fe ve Cr elementleri ilave edilmiştir. Elementlerin birbiri içerisinde çözünürlükleri ve atomik çapları dikkate alınarak 4 farklı alaşım tasarlanmıştır. Aynı şartlarda ve aynı numune miktarları ile yapılan ve Şekil 1' de gösterilen XRD analizleri sonuçları incelendiğinde baz alaşıma Cr ve Fe elementlerinin katkısı alaşımın camlaşma kabiliyetini negatif yönde etkilediği görülmektedir. Özellikle Cr elementi katkısının yapıyı Fe katkısının daha fazla olumsuz yönde etkilediği görülmüştür. Bunun sebebinin yapıya eklenen Cr elementinin özellikle alaşımda var olan B elementi ile bir araya gelerek küçük çapta nano-kristaller oluşturup alaşımın çekirdeklenmesini kolaylaştırdığı yönde bir etki yaptığı düşünülmektedir. Fe katkısı ise yapılan XRD analizi sonuçlarına göre yapıda Ni ve Co elementleri ile bir araya gelerek monoklinik yapıdaki kristallerin oluşumunu kolaylaştırdığı düşünülmektedir. Fe miktarının atomik %17,76 dan %10,3'e düşürüldüğünde camlaşma kabiliyetinin 0,3 mm'den 1 mm'ye kadar çıkması bunun bir göstergesidir. Fe ve Cr alaşımların kristalleşme eğilimlerini arttırmış ve camlaşma kabiliyetini olumsuz yönde etkilemişlerdir. DSC analiz sonuçlarına göre, hazırlanan yeni alaşımlar baz alaşımla kıyaslandığında, Tl sıcaklıklarındaki artış ve Tx sıcaklıklarındaki düşüş, alaşımların camlaşma kabiliyetlerini gösteren GFA (Glass Forming Ability) değerlerinin düşmesine neden olmuştur.

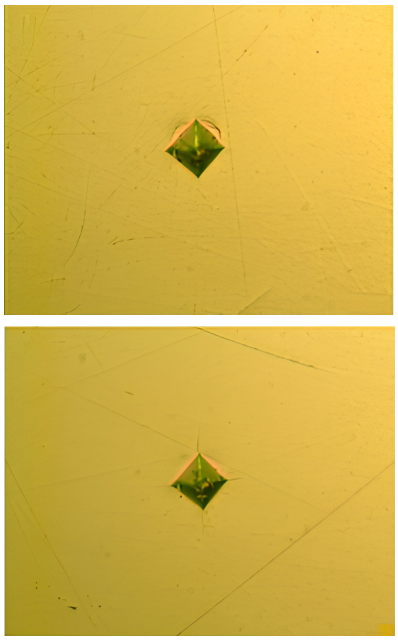

Şekil 4. a) $Ni_{21,50}Co_{21,50}Fe_{10,30}B_{15}W_{23,7}Ta_8$ kompozisyonundaki 0,3 mm kalınlığında amorf yapıdaki alaşımın ve b)Ni13,25 $Co_{13,25}Cr_{13,25}Fe_{13,25}B_{15}W_{23,7}Ta_8$ kompozisyonundaki 0,3 mm kalınlığında amorf yapıdaki alaşımın Vickers mikrosertlik ölçümü görüntüleri. (Vickers micro-hardness measurement images of (a) the amorphous alloy with a thickness of 0.3 mm and composition $Ni_{21.50}Co_{21.50}Fe_{10.30}B_{15}W_{23.7}Ta_8$ and (b) the amorphous alloy with a thickness of 0.3 mm and composition Ni13.25Co13.25Cr13.25Fe13.25B15W23.7Ta8.

Tablo 2'de, baz alaşım ile geliştirilen $Ni_{21,50}Co_{21,50}Fe_{10,30}B_{15}W_{23,7}Ta_8$ alaşımının GFA değerleri karşılaştırıldığında, geliştirilen alaşımın T_l sıcaklığının daha yüksek ancak T_x sıcaklığının daha düşük olduğu açıkça görülmektedir. Bu durum, GFA değerlerinin düşmesine neden olan temel faktörler arasında yer almaktadır.

Yapılan sertlik testleri sonucunda, alaşımların sertlik değerleri açısından incelendiğinde $Ni_{13,25}Co_{13,25}Cr_{13,25}Fe_{13,25}B_{15}W_{23,7}Ta_8$ alaşımının en yüksek sertlik değerine, buna karşın $Ni_{21,5}Co_{21,5}Fe_{10,3}B_{15}W_{23,7}Ta_8$ alaşımının ise en düşük sertlik değerine sahip olduğu tespit edilmiştir. Baz alaşıma hem Cr hem de Fe elementlerinin eş zamanlı olarak eklendiği durumlarda, amorf alaşımın sertlik değerinin en yüksek seviyede ölçülmesinin temel nedeni, Cr ve Fe elementlerinin diğer elementlerle güçlü bağlar oluşturması olarak değerlendirilmektedir. Özellikle Cr-B, Fe-B, Cr-W, Fe-W, Cr-Ta ve Fe-Ta atomları arasındaki yüksek kohezyon enerjisi, alaşımı oluşturan atomlar arasındaki toplam bağlanma enerjisini artırmakta ve dolayısıyla amorf yapının sertliğini yükseltmektedir. Bu durum, yapı içerisindeki atomlar arasındaki güçlü bağlar sayesinde yapının mekanik dayanımını artırmaktadır.

Yalnızca Cr veya Fe elementlerinin bulunduğu $Ni_{17,76}Co_{17,76}Cr_{17,76}B_{15}W_{23,7}Ta_8$ ve $Ni_{17,76}Co_{17,76}Fe_{17,76}B_{15}W_{23,7}Ta_8$ alaşımlarının karşılaştırılması sonucunda ise, Cr elementinin yapıdaki diğer atomlar ile bağlanma enerjisinin, Fe elementinin yapıdaki diğer atomlarla olan bağlanma enerjisinden daha yüksek olduğu düşünülmektedir. Bu durum, Cr içeren alaşımların sertlik değerlerinin, Fe içeren alaşımlara kıyasla bir miktar daha yüksek olmasına neden olmaktadır. Ayrıca Şekil 4b'de gösterilen amorf yapıdaki numunelerin mikrosertlik görüntülerine bakıldığında $Ni_{13,25}Co_{13,25}Cr_{13,25}Fe_{13,25}B_{15}W_{23,7}Ta_8$ kompozisyonunun sertlik değerinin çok yüksek olması 500 gram yük altındaki ölçümlerde dahi köşegenlerde uzun çatlakların oluşmasına neden olmaktadır. Bu durum amorf yapısından dolayı tokluk seviyesinin çok düşük olduğunun bir göstergesidir. $Ni_{21,50}Co_{21,50}Fe_{10,30}B_{15}W_{23,7}Ta_8$ kompozisyonu ise en düşük sertlik değerine sahip olduğu için amorf yapıda da olsa aynı yük altında oluşan iz köşegenlerinde herhangi bir çatlak görülmemektedir. Tokluğunun nispeten daha iyi olmasından kaynaklanmaktadır.

4. Sonuçlar (Conclusions)

Bu çalışmada, daha önce camlaşma kabiliyeti 1,5 mm olan Ni-Co-W-Ta-B metalik cam alaşım sistemi, baz alaşım olarak seçilmiş ve bu alaşıma Cr ve Fe elementleri belirli oranlarda eklenerek etkileri incelenmiştir. Yapılan analizler, Cr elementinin alaşımda kristallenmeyi artırarak camlaşma kabiliyeti üzerinde olumsuz bir etkiye sahip olduğunu göstermiştir. Buna karşılık, Fe elementi miktarının belirli oranlarda alaşıma katkısı ile camlaşma kabiliyetini artabileceği belirlenmiştir. Özellikle, %10 Fe ilaveli alaşımın, baz alaşımın 1,5 mm olan camlaşma kabiliyetine ulaşamasa da, 1 mm kalınlıkta camlaşmayı başarabildiği görülmüştür. Bu sonuçlar, Fe elementinin uygun oranlarda eklenmesiyle camlaşma kabiliyetinin artırılabileceğini, ancak Cr katkısının camlaşma eğilimini olumsuz etkilediğini ortaya koymaktadır. Ayrıca, Ni-Co-Fe-W-Ta-B sisteminde Fe içeriğinin optimize edilmesinin,

Tablo 2. Alaşımların ısıl özellikleri (T_g, T_x, T_l), GFA parametreleri, kritik döküm kalınlıkları ve mikrosertlik değerleri (Thermal properties of alloys (T_g, T_x, T_l), GFA parameters, critical casting thicknesses, and microhardness values).

Kompozisyon	Ni	Co	Fe	Cr	Ta	W			B
$Ni_{13,25}Co_{13,25}Cr_{13,25}Fe_{13,25}B_{15}W_{23,7}Ta_8$	-	565	1373	-	-	0.3	1375		15,00
$Ni_{17,76}Co_{17,76}Cr_{17,76}B_{15}W_{23,7}Ta_8$	-	751	1352	-	-	0.3	1310		15,00
$Ni_{17,76}Co_{17,76}Fe_{17,76}B_{15}W_{23,7}Ta_8$	-	644	1366	-	-	0.3	1267		15,00
$Ni_{21,50}Co_{21,50}Fe_{10,30}B_{15}W_{23,7}Ta_8$	629	747	1363	0.551	0.3554	1	1253		
$Ni_{21,50}Co_{21,50}Fe_{10,30}B_{15}$	681	759	1294	0.609	0.409	1.5	1271	[21]	15,00

metalik cam alaşımların camlaşma kabiliyeti ve termal kararlılığı üzerinde olumlu etkiler yaratabileceği anlaşılmıştır. Bu çalışma, yüksek oranda bor içeren ve ultra yüksek sertliğe sahip CoWB borür fazını içeren metalik cam alaşımlarının camlaşma kabiliyetinin bu tip çalışmalar doğrultusunda artırılabileceğini göstermektedir. Bu bulgu, yüksek dayanım ve tokluk özelliklerine sahip MMC malzemelerin üretiminde, bor içeriği yüksek metalik cam alaşımlarının öncül olarak kullanım potansiyelini artırmaktadır.

5. Teşekkür (Acknowledgements)

Bu çalışması 17. FEN. BİL. 67 numaralı Afyon Kocatepe Üniversitesi, Bilimsel Araştırma Projeleri (BAP) tarafından desteklenmiştir.

6. Yazar Katkısı Beyanı (Author Contribution Statement)

Hakan Şahin: Konsept geliştirme, metodoloji, araştırma, doğrulama, yazım-özgün taslak, görselleştirme.

Aytekin Hitit: Araştırma, doğrulama, yazım-gözden geçirme ve düzenleme, danışmanlık, proje yönetimi, fon sağlama.

Kaynakça (References)

[1] Klement Jun, W., Willens, R. H., & Duwez, P. (1960). Non-crystalline structure in solidified gold-silicon alloys. *Nature, 187*, 869-870. https://doi.org/10.1038/187869b0

[2] Inoue, A., & Takeuchi, A. (2011). Recent development and application products of bulk glassy alloys. *Acta Materialia*, *59*(6), 2243-2267. https://doi.org/10.1016/j.actamat.2010.11.027

[3] Hofmann, D. C., Andersen, L. M., Kolodziejska J., Roberts, S. N., Borgonia, J. P., Johnson, W. L., … & Kennett, A. (2016). Optimizing bulk metallic glasses for robust, highly wear-resistant gears. *Advanced Engineering Materials*, *19*(1), 1600541. https://doi.org/10.1002/adem.201600541

[4] Telford, M. (2004). The case for bulk metallic glass. *Materials Today*, *7*(3), 36-43. https://doi.org/10.1016/S1369-7021(04)00124-5

[5] Laghari, R. A., Jamil, M., Laghari, A. A., & Khan, A. M. (2025). Material characteristics and machinability of metal matrix composite materials: A critical review on recent advances and future perspectives. *Measurement*, *242*, Part B, 115839. https://doi.org/10.1016/j.measurement.2024.115839

[6] Biyik, S. (2019). Effect of cubic and hexagonal boron nitride additions on the synthesis of Ag-SnO2 electrical contact material. *Journal of Nanoelectronics and Optoelectronics*. *14*(7), 1010-1015. https://doi.org/10.1166/jno.2019.2592

[7] Subramanian, J., Seetharaman, S., & Gupta, M. (2015). Processing and properties of aluminum and magnesium based composites containing amorphous reinforcement: A review. *Metals*, *5*, 743-762. https://doi.10.3390/met5020743

[8] Hufenbach, W., Andrich, M., Langkamp, A., & Czulak, A. (2006). Fabrication technology and material characterization of carbon fibre reinforced magnesium. *Journal of Materials Processing Technology*, *175*, 218-224. https://doi.10.1016/j.jmatprotec.2005.04.023

[9] Hitit, A., Yazici, Z. O., Sahin, H., Ozturk, P., Asgin, A.M., & Hitit, B. (2019). A novel Ni-based bulk metallic glass containing high amount of tungsten and boron. *Journal of Alloys and Compounds*, *807*, 151661. https://doi.org/10.1016/j.jallcom.2019.151661

[10] Hitit, A., Yazici, Z. O., Ozturk, P., Sahin, H. Asgin, A. M. & Hitit, B. (2021). A Ni-CoWB composite developed by devitrification of Ni-Co-W-B bulk metallic glass. *Materials Science & Engineering*, *803*, 140479. https://doi.org/10.1016/j.msea.2020.140479

[11] Zakhariev, Z., Zlateva, R. & Petrov, K. (1986). Microhardness and high-temperature oxidation stability of CoWB. *Journal of the Less Common Metals*, *117*, 129-133. https://doi.org/10.1016/0022-5088(86)90021-4

[12] List, A., Gartner, F. Schmidt, T. & Klassen, T. (2012). Impact conditions for cold spraying of hard metallic glasses. *Journal of Thermal Spray Technology*, *21*, 531-540. https://doi.10.1007/s11666-012-9750-5

[13] Nayak, S. K., Kumar, A., & Laha, T. (2022). Developing an economical wear and corrosion resistant fe-based metallic glass composite coating by plasma and HVOF Spraying. *Journal of Thermal Spray Technology*, *31*, 1317-1329. https://doi.org/10.1007/s11666-021-01277-w

[14] Zhao, Z., Yang, G., & Zhao, K. (2022). 3D printing of Mg-based bulk metallic glasses with proper laser power and scanning speed. *Metals*, *12*, 1318. https://doi.org/10.3390/met12081318

[15] Badoniya, P., Srivastava, M., Jain, P. K., & Rathee, S. (2024). A state of the art review on metal additive manufacturing: Milestones, trends, challenges and perspectives. *Journal of the Brazilian Society of Mechanical Sciences and Engineering*, *46*, 339 https://doi.org/10.1007/s40430-024-04917-8

[16] Sohrabi, N., Jhabvala, J., & Loge, R. E. (2021). Additive manufacturing of bulk metallic glasses-Process, challenges and properties: A review. *Metals*, *11*(8), 1279. https://doi.org/10.3390/met11081279

[17] Madge, S. V., & Greer, A. L. (2021). Laser additive manufacturing of metallic glasses: Issues in vitrification and mechanical properties. *Oxford Open Materials Science*, *1*(1), itab015. https://doi.org/10.1093/oxfmat/itab015

[18] Hoff, A. (2018). *Understanding the origin of glass forming ability in metallic glasses*. [Doctoral dissertation, California Institute of Technology] Pasadena, California. https://doi.org/10.7907/Z7Y5-0B62

[19] Lu, Z. P, Li, Y., & Ng, S. C. (2000). Reduced glass transition temperature and glass forming ability of bulk glass forming alloys. *Journal of Non-Crystalline Solids*, *270*(1-3), 103-114. https://doi.org/10.1016/S0022-3093(00)00064-8

[20] Lu, Z. P., & Liu, C. T. (2002). A new glass-forming ability criterion for bulk metallic glasses. *Acta*

Materialia, *50*(13), 3501-3512. https://doi.org/10.1016/S1359-6454(02)00166-0

[21] Hitit, A., Yazici, Z. O., Öztürk, P., Eryesil, B., Barut, N., & Sahin H. (2021). The effects of tantalum addition on the glass forming ability, thermal stability, and mechanical properties of Ni-Co-W-B bulk metallic glasses. *Journal of Non-Crystalline Solids*, *572*, 121089. https://doi.org/10.1016/j.jnoncrysol.2021.121089

[22] Yazıcı, Z. O. (2020). Effect of vacuum conditions on stability and crystallization of cobalt based amorphous alloy. *Materials Science-Poland*, *38*(1), 181-188. https://doi.org/10.2478/msp-2020-0003

[23] Sun, Y., Wang, Y., Zhang, J., Li, R., Guo, L., Xu, H., & Wang, W. (2015). Effect of casting vacuum on thermodynamic and corrosion properties of Fe-based glassy alloy. *Transactions of Nonferrous Metals Society of China*, *25*(3), 844−849. https://doi.org/10.1016/S1003-6326(15)63672-X

[24] Igel, J., Kirk, D. W., Singh, C. V., & Thorpe, S.J. (2015). A practical investigation of the production of Zr-Cu-Al-Ni bulk metallic glasses by arc melting and suction casting. *Materials Transactions*, *56*(11), 1834-1841. https://doi.org/10.2320/matertrans.M2015235

BOR DERGİSİ
JOURNAL OF BORON
https://dergipark.org.tr/boron

Investigation of quorum sensing inhibition activity of some boron compounds

Özgür Ceylan [1,*], **Kutbettin Arslan** [1], **Aysel Uğur** [2]

[1]*Mugla Sitki Kocman University, Ula Ali Kocman Vocational School, Food Quality Control and Analysis Program, Mugla, 48000, Türkiye*
[2]*Gazi University, Department of Basic Sciences, Section of Medical Microbiology, Ankara, 06000, Türkiye*

ARTICLE INFO

Article History:
Received November 13, 2024
Accepted March 1, 2025
Available online March 31, 2025

Research Article

DOI: 10.30728/boron.1584819

Keywords:
Boron compounds
Quorum sensing inhibition
Violacein reduction

ABSTRACT

Boron is one of the important elements for organisms, especially for plants and animals. The importance of boron for humanity is increasing, and its uses are parallelly expanding. In this study, the quorum-sensing inhibition effects of five different boron compounds were investigated. The quorum-sensing inhibition assay was performed on CV026 and CV12472 using the broth dilution method. Considering the results of this study, it was determined that the highest violacein inhibition activity was provided by sodium tetraborate with 74.46%. Based on the quorum sensing activity, it was revealed that the minimum inhibitory concentration (MIC) value of boron oxide and sodium tetraborate provided the highest inhibition rate 95.15%. When the anti-quorum sensing activity data obtained from the study are examined, it was seen that these boron compounds showed high activity and should be supported by different tests such as animal experiments.

1. Introduction

Boron is an important element for organisms [1]. It is mostly acquired from plant-based boron compounds and boric acid in water. Studies show that boron is essential for certain animals, helping with cell growth and development [2]. Lack of boron can negatively affect bone health, brain function, cholesterol levels, and immune response. Animal studies have also shown that boron can protect against liver damage. Recently, research has focused more on boron's potential in cancer treatment, its antimicrobial properties, its use in drug delivery, and how it interacts with proteins and other molecules. When animals consume boron, it turns into boric acid in the small intestine and is quickly eliminated in urine, without much change. However, small amounts may build up in tissues like bones and the spleen [3]. Boron is often included in supplements and other nutrients like vitamin D, calcium, and magnesium. Some forms of boron, like boric acid and borax, raise concerns because they may accumulate in tissues over time. New forms, like boron esters, are not yet well understood, and current research is working to address this gap. Boron plays several roles in the body, including helping cell signaling, working as a co-factor for certain enzymes, aiding in electron transfer, and help maintaining cell structure. While boron's necessity in animal cells isn't fully proven, future studies may confirm this. It is also believed that boron could have contributed to evolution by forming complexes with certain organic molecules [4]. Boron can be used in pharmaceutical drug design as it has the potential to facilitate biological activities [5]. Although numerous products are produced from boron, the most common natural compounds of boron are various forms of borates. Boron compounds are also used individually across multiple chemical processes. Boron compounds have different uses in pharmaceuticals and other fields such as cosmetics, adhesives, insecticides, formicides, rodenticides, and plant nutritional compounds [6].

Quorum sensing (QS) is a connection system used especially by bacteria and fungi. Quorum-quenching (QQ) disrupts QS signaling and affects how different species interact. Bacteria use QQ to fight other species, while eukaryotes use it to defend against pathogens. QQ can happen in various ways: By stopping the production of signaling molecules, breaking them down, preventing them from binding to receptors, or blocking the expression of target genes. Inhibiting signal molecule production can act by disrupting key enzymes like acyl carrier protein or S-adenosylmethionine synthase, or by preclusion of the Lux system, a key QS system in Gram-negative bacteria [7].

Recently, research has focused more on the potential of boron in cancer treatment, wound healing effects, antimicrobial properties, use in drug delivery, and how it interacts with proteins and other molecules [10, 16]. Moreover, it is seen in the literature that there are studies investigating the cytotoxic [8], antimicrobial, antioxidant, antibiofilm, and neuroprotective [9-11], therapeutic effects [12], and enzyme inhibition [13] of boron compounds and boron derivatives.

*Corresponding author: ozgurceylan@mu.edu.tr

When the present studies in the literature were examined, it was determined that boron compounds have different activities, especially antimicrobial and antioxidant activity. Still, there is no data on anti-quorum sensing and violacein inhibition, especially considering the compounds examined in the study. From this point of view, this study, it was aimed to realize the quorum sensing performance of 5 different boron compounds (disodium octoborate, sodium pentaborate, boron oxide, sodium tetraborate, and boric acid).

2. Materials and Methods

2.1. Materials

2.1.1. Microbial strains

Three microorganisms were used for this study. These are *Pseudomonas aeruginosa* PA01, *Chromobacterium violaceum* CV12472, and *Chromobacterium violaceum* CV026. The density of the bacteria was adjusted to 0.5 McFarland and the test medium was Mueller-Hinton Broth (MHB).

2.2. Methods

2.2.1. Establishing of minimal inhibitory concentration (MIC)

200 µL of cell suspension was inoculated with different final concentrations of boron compounds (20, 10, 5, 2.5, 1.25, 0.625 mg/mL) in 96-well plates. The microplates were incubated at 37°C for 24 hours after inoculation.

2.2.2. Violacein inhibition test over C. violaceum CV12472

Firstly, the MIC values of the compounds were determined to establish the violacein inhibition. The MIC value was based on the broth dilution method and recorded as the lowest concentration at which no growth was observed [14]. Inhibition percentages against *C. violaceim* ATCC CV12472 at MIC and sub-MIC concentrations were then determined. Briefly, 10 µL of CV12472 was added to 180 µL of LB broth containing microplates, and 10 µL of compounds at MIC and sub-MIC concentrations were added. Then the plates were incubated at 30°C for 24 h. The reduction of violacein pigment was measured at 600 nm on a microplate reader. The study was carried out in triplicate. Violacein percentage inhibition was calculated by using Equation 1 [15].

$$\text{Violacein inhibition } (\%) = \frac{\text{OD 600 control} - \text{OD 600 sample}}{\text{OD 600 control}} \times 100 \quad \textbf{(1)}$$

2.2.3. Quorum sensing inhibition assay using C. violaceum CV026

The anti-quorum sensing test was carried out by using a method from a previous study [16]. First, 100 µL of an overnight culture of CV026 bacteria and 20 µL of C6HSL (a signaling molecule) were added to warm soft top agar (5 mL). The mixture was then spread on LB agar plates. After the agar solidified, small wells (5 mm) were made in the plates, and 50 µL of a filter-sterilized extract solution was added to each well at a concentration below the MIC. The plates were incubated at 30°C for 3 days. The experiment was conducted in three repetitions. Quorum sensing inhibition was calculated as a percentage using Equation 2.

$$\text{QS Inhibition } (\%) = \frac{\text{OD 600 control} - \text{OD 600 sample}}{\text{OD 600 control}} \times 100 \quad \textbf{(2)}$$

2.2.4. Statistical analysis

STATISTICA software (StatSoft Inc.,USA.) was used to calculate statistically significant differences between groups. One-way analysis of variance (ANOVA) followed by post-hoc Tukey's test was used to determine differences in measured parameters. All analyses were performed at a significance level of $p < 0.05$.

3. Results and Discussion

When the potential of boron compounds against test bacteria for anti-quorum sensing activity was examined, the MIC value was detected against CV026. The lowest MIC value was revealed by disodium octoborate with <0.625 mg/ml. Furthermore, sodium pentaborate, boron oxide, and boric acid also exhibited good activity against CV026 with a MIC value of 0.625 mg/ml (Table 1).

Table 1. MIC values of boron compounds

	Minimal Inhibitory Concentration (mg/mL)		
	C. violacaeum (CV026)	*C. violacaeum* (CV12472)	*P. aeruginosa* (PA01)
Disodium Octoborate	<0.625	2.5	1.25
Sodium Pentaborate	0.625	2.5	2.50
Boron Oxide	0.625	2.5	1.25
Sodium Tetraborate	1.250	5.0	2.50
Boric Acid	0.625	5.0	2.50

Numerous studies have been conducted on the antimicrobial activity of borons, which is highly effective against different microorganisms [17, 18]. Baygar et al. [19] investigated the biological activities of potassium metaborate in their study and revealed that it showed high activity in terms of antioxidative, antimicrobial, and anti-biofilm properties. In another study, the antimicrobial, antifibrinolytic, enzyme inhibitory, and wound-healing properties of zinc borate were examined, and it was declared that it could be used effectively in wound healing and can prevent wound infection [20]. However, there are limited or no studies on anti-quorum sensing and violacein inhibition of boron compounds. C. violaceum is a Gram (-) bacterium that is detected in different environments such as human skin, soil, and water. Bacteremia and abscesses are serious infections they cause. It is also

resistant to many antibiotics. The bacteria secrete a purple pigment called violacein, which has antibacterial effects. The expression of this pigment is controlled by quorum sensing, a bacterial communication process that regulates several functions, including antibiotic production and biofilm formation [21]. When the results of violacein inhibition were analyzed, it was found that all MIC and sub-MIC concentrations had activity. In addition, it was observed that all compounds inhibited violacein production even at the MIC/32 level (Figure 1).

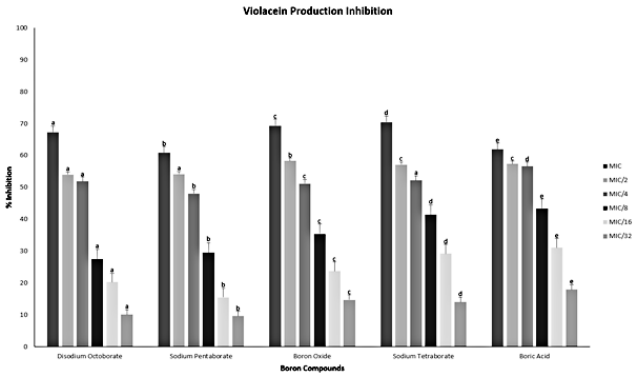

Figure 1. Violacein production inhibition of boron compounds. Data are presented as mean ± scanning electron microscope (SEM) of three replicates. Different letters above the error bars indicate significant differences between treatments ($p < 0.05$)

QS is a cellular signaling complex that lets bacteria adapt to the environment through cooperative and coordinated metabolic regulation. QS is particularly well characterized in Gram-negative bacteria and triggers the synthesis of various defense molecules (extracellular hydrolytic enzymes, virulence factors, and biofilms). This process involves synthesizing and releasing into the environment signaling molecules (such as AHLs) that affect transcription and translation [22-25]. According to the anti-quorum sensing activity results obtained from the study, boron compounds showed inhibition between 37-95% (Figure 2).

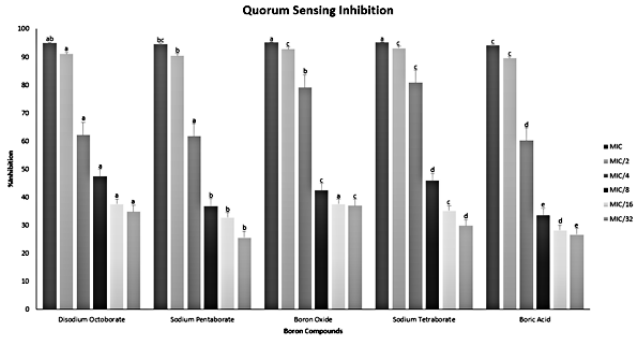

Figure 2. Quorum sensing inhibition of boron compounds. Data are presented as mean ± SEM of three replicates. Different letters above the error bars indicate significant differences between treatments ($p < 0.05$)

In the literature, it was reported that boron compounds showed high activity against antioxidants, enzyme inhibition, antibiofilm, and cancer cell lines [26, 27]. Therefore, the inhibitory potential of these compounds on the quorum sensing mechanism is parallel with our study results. This reveals that boron compounds can disrupt the quorum-sensing mechanism that provides cellular communication and reduces the cellular defense and virulence factor.

Our current knowledge has now revealed that boron compounds have a wide range of uses. Sevim et al. [28] investigated the anti-inflammation potential of boric acid and borax and reported that potential therapeutic effects were achieved in improving tissue damage even at low doses. Temel et al. [29] investigated the antimicrobial, antioxidant, cytotoxic and enzyme inhibition activities of boric acid and its derivatives. They emphasized that the new compounds showed a dominant potential in terms of antioxidants did not show cytotoxic effects, and showed antimicrobial activity of 6.50 mg/mL against E. coli. Another study revealed the wound-healing potential of boron [30]. Another study focused on the use of boron-containing compounds for triggering the immune system [31]. In another similar study, the antimicrobial, enzyme inhibition, and anti-cancer activity of quercetin-boronate esters were determined, and based on the antimicrobial activity, they showed superior glucosidase enzyme inhibition and exhibited significant anti-cancer activity with an MIC of 32.5 µg/mL against E. faecalis. These compounds demonstrated superior glucidase enzyme inhibition and exhibited significant anti-cancer activity, reducing pancreatic cell viability at 50 µM [32]. However, studies on anti-quorum sensing activity have been very limited, and this issue needs to be focused on. The inhibition of this mechanism, which is of great importance in bacterial communication and virulence, can be achieved using natural products, particularly boron compounds that are essential for organisms. This approach can not only prevent the activation of bacterial resistance development mechanisms but can also reduce the costs associated with synthetic product production. Moreover, the gap in the literature on this subject will be filled to some extent. According to the results, the quorum-sensing inhibition exhibited by the compounds is remarkable (Figure 3). Figure 3 shows that the compounds showed quorum-sensing inhibition even at the MIC/32.

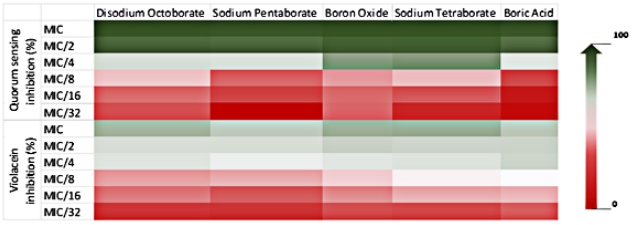

Figure 3. Heatmap of boron compounds of inhibition (%) quorum sensing and violacein production

4. Conclusions

This study reveals the potential of boron compounds to inhibit quorum-sensing mechanisms. Studies have shown that boron-containing molecules can interfere

with the quorum-sensing signaling mechanisms of gram-negative and gram-positive bacteria, thereby reducing pathogenic effects. In particular, boron compounds were found to disrupt bacterial communication and inhibit biofilm formation by interacting with quorum-sensing signaling molecules (e.g., AHL or AI-2). However, the specific effects of these compounds vary depending on bacterial species, concentrations used, and environmental factors. The findings indicate the potential of boron compounds to be evaluated as new anti-QS agents. However, extensive biochemical and pharmacological studies are required to develop these compounds as effective, safe, and specific antibacterial agents. Future research on the anti-QS activity of boron compounds may provide important contributions to developing new therapeutic strategies, especially against pathogens of clinical importance. Based on this study, further studies can be designed to understand the biological activities of boron-containing compounds.

5. Conflict of Interest

The authors declare no conflict of interest.

6. Author Contribution Statement

Özgür Ceylan: Sample and data collection, conceptualization, data curation, organization, analysis, methodology.

Aysel Uğur: Supervision, project administration.

Kutbettin Arslan: Data analysis, writing original draft, writing review, and editing.

References

[1] Jans, K., Lüersen, K., & Rimbach, G. (2021). Drosophila melanogaster as a model organism to study lithium and boron bioactivity. *International Journal of Molecular Sciences*, *22*(21), 11710. https://doi.org/10.3390/ijms222111710

[2] Tombuloglu, A., Copoglu, H., Aydin-Son, Y., & Guray, N. T. (2020). In vitro effects of boric acid on human liver hepatoma cell line (HepG2) at the half-maximal inhibitory concentration. *Journal of Trace Elements in Medicine and Biology*, *62*, 126573. https://doi.org/10.1016/j.jtemb.2020.126573

[3] Aydin, H. E., Koldemir Gündüz, M., Kizmazoğlu, C., Kandemir, T., & Arslantaş, A. (2021). Cytotoxic effect of boron application on glioblastoma cells. *Turkish Neurosurgery*, *31*(2), 206-210. https://doi.org/10.5137/1019-5149.JTN.30316-20.1

[4] Gündüz, M. K., Bolat, M., Kaymak, G., Berikten, D., & Köse, D. A. (2022). Therapeutic effects of newly synthesized boron compounds (BGM and BGD) on hepatocellular carcinoma. *Biological Trace Element Research*, *200*, 134-146. https://doi.org/10.1007/s12011-021-02647-9

[5] Ali, F., Hosmane, N. S., & Zhu, Y. (2020). Boron chemistry for medical applications. *Molecules*, *25*(4), 828. https://doi.org/10.3390/molecules25040828

[6] Yakin, A., Avar, B., Simsek, T., & Chattopadhyay, A. K. (2023). Synthesis of boron-based alloys and compounds by mechanical alloying: A review. *Materials Today Communications*, *37*, 106980. https://doi.org/10.1016/j.mtcomm.2023.106980

[7] Prazdnova, E. V., Gorovtsov, A. V., Vasilchenko, N. G., Kulikov, M. P., Statsenko, V. N., Bogdanova, A. A., … & Chikindas, M. L. (2022). Quorum-sensing inhibition by gram-positive bacteria. *Microorganisms*, *10*(2), 350. https://doi.org/10.3390/microorganisms10020350

[8] Aydin, H. E., Gunduz, M. K., Kizmazoglu, C., Kandemir, T., & Arslantas, A. (2021). Cytotoxic effect of boron application on glioblastoma cells. *Turkish Neurosurgery*, *31*(2), 206-210. https://doi.org/10.5137/1019-5149.JTN.30316-20.1

[9] Koldemir-Gündüz, M., Aydin, H. E., Berikten, D., Kaymak, G., Köse, D. A., & Arslantaş, A. (2021). Synthesis of new boron derived compounds; anticancer, antioxidant and antimicrobial effect in vitro glioblastoma tumor model. *Journal of Korean Neurosurgical Society*, *64*(6), 864-872. https://doi.org/10.3340/jkns.2021.0032

[10] Meiyanto, E., Susidarti, R. A., Jenie, R. I., Utomo, R. Y., Novitasari, D., Wulandari, F., & Kirihata, M. (2020). Synthesis of new boron containing compound (CCB-2) based on curcumin structure and its cytotoxic effect against cancer cells. *Journal of Applied Pharmaceutical Science*, *10*(2), 060-066. https://doi.org/10.7324/JAPS.2020.102010

[11] Barrón-González, M., Montes-Aparicio, A. V., Cuevas-Galindo, M. E., Orozco-Suárez, S., Barrientos, R., Alatorre, A., … & Soriano-Ursúa, M. A. (2023). Boron-containing compounds on neurons: Actions and potential applications for treating neurodegenerative diseases. *Journal of Inorganic Biochemistry*, *238*, 112027. https://doi.org/10.1016/j.jinorgbio.2022.112027

[12] Gündüz, M. K., Bolat, M., Kaymak, G., Berikten, D., & Köse, D. A. (2022). Therapeutic effects of newly synthesized boron compounds (BGM and BGD) on hepatocellular carcinoma. *Biological Trace Element Research*, *200*, 134-146. https://doi.org/10.1007/s12011-021-02647-9

[13] Kahriman, N., Haşimoğlu, Z., Serdaroğlu, V., Beriş, F. Ş., Barut, B., & Yaylı, N. (2017). Synthesis of novel pyrazolines, their boron-fluorine complexes, and investigation of antibacterial, antioxidant, and enzyme inhibition activities. *Archiv der Pharmazie*, *350*(2), 1600285. https://doi.org/10.1002/ardp.201600285

[14] Espinel-Ingroff, A., Fothergill, A., Ghannoum, M., Manavathu, E., Ostrosky-Zeichner, L., Pfaller, M., ... & Walsh, T. (2005). Quality control and reference guidelines for CLSI broth microdilution susceptibility method (M38-A document) for amphotericin B, itraconazole, posaconazole, and voriconazole. *Journal of Clinical Microbiology*, *45*(7). https://doi.org/10.1128/jcm.00399-07

[15] Tamfu, A. N., Ceylan, O., Fru, G. C., Ozturk, M., Duru, M. E., & Shaheen, F. (2020). Antibiofilm, antiquorum sensing and antioxidant activity of secondary metabolites from seeds of Annona senegalensis, Persoon. *Microbial Pathogenesis*, *144*, 104191. https://doi.org/10.1016/j.micpath.2020.104191

[16] Ceylan, O., Tamfu, A.N., Doğaç, Y.İ., & Teke, M. (2020). Antibiofilm and anti-quorum sensing activities of polyethylene imine coated magnetite and nickel ferrite nanoparticles. *3 Biotech*, *10*, 513. https://doi.org/10.1007/s13205-020-02509-6

[17] Fink, K., & Uchman, M. (2021). Boron cluster compounds as new chemical leads for antimicrobial therapy. *Coordination Chemistry Reviews*, *431*, 213684. https://doi.org/10.1016/j.ccr.2020.213684

[18] Celebi, O., Celebi, D., Baser, S., Aydın, E., Rakıcı, E., Uğraş, S., … & Abd El-Aty, A. M. (2024). Antibacterial activity of boron compounds against biofilm-forming pathogens. *Biological Trace Element Research*, *202*, 346-359. https://doi.org/10.1007/s12011-023-03768-z

[19] Baygar, T., Saraç, N., Ceylan, Ö., Uğur, A., Boran, R., & Balcı, U. (2022). In vitro biological activities of potassium metaborate; antioxidative, antimicrobial and antibiofilm properties. *Journal of Boron*, *7*(2), 475-481. https://doi.org/10.30728/boron.1076636

[20] Boran, R., Baygar, T., Saraç, N., Ayrıkçil, S., Yılmaz, D., & Uğur, A. (2023). Antimicrobial, antifibrinolytic, enzyme inhibitory and wound healing properties of zinc borate. *Journal of Boron*, *8*(3), 99-104. https://doi.org/10.30728/boron.1180847

[21] Bali, E. B., Türkmen, K. E., Erdönmez, D., & Sağlam, N. (2019). Comparative study of inhibitory potential of dietary phytochemicals against quorum sensing activity of and biofilm formation by Chromobacterium violaceum 12472, and swimming and swarming behaviour of Pseudomonas aeruginosa PAO1. *Food Technology and Biotechnology*, *57*(2), 212. https://doi.org/10.17113/ftb.57.02.19.5823

[22] Durán, N., Justo, G. Z., Durán, M., Brocchi, M., Cordi, L., Tasic, L., … & Nakazato, G. (2016). Advances in Chromobacterium violaceum and properties of violacein-Its main secondary metabolite: A review. *Biotechnology Advances*, *34*(5), 1030-1045. https://doi.org/10.1016/j.biotechadv.2016.06.003

[23] Kothari, V., Sharma, S., & Padia, D. (2017). Recent research advances on Chromobacterium violaceum. *Asian Pacific Journal of Tropical Medicine*, *10*(8), 744-752. https://doi.org/10.1016/j.apjtm.2017.07.022

[24] Krzyżek, P. (2019). Challenges and limitations of anti-quorum sensing therapies. *Frontiers in Microbiology*, *10*, 2473. https://doi.org/10.3389/fmicb.2019.02473

[25] Alisjahbana, B., Debora, J., Susandi, E., & Darmawan, G. (2021). Chromobacterium violaceum: A review of an unexpected scourge. *International Journal of General Medicine*, *14*, 3259-3270. https://doi.org/10.2147/IJGM.S272193

[26] Temel, H., Atlan, M., Türkmenoğlu, B., Ertaş, A., Erdönmez, D., & Çalışkan, U. K. (2023). In silico and biological activity evaluation of quercetin-boron hybrid compounds, anti-quorum sensing effect as alternative potential against microbial resistance. *Journal of Trace Elements in Medicine and Biology*, *77*, 127139. https://doi.org/10.1016/j.jtemb.2023.127139

[27] Çelebi, Ö., Başer, S., Balkan Bozlak, Ç. E., Taghizadehghalehjoughi, A., Mahmoudnezhad, A., & Celebi, D. (2023). Boron compounds with antibiofilm and synergistic effects on Escherichia coli infection. Kafkas *Journal of Medical Sciences*, *13*(3), 271-278. https://doi.org/10.5505/kjms.2023.22605

[28] Sevim, Ç., Ozkaraca, M., Kara, M., Taghizadehghalehjoughi, A., Genç, S., Yeni, Y., … & Tsatsakis, A. (2025). Exploring the anti-inflammatory activity of boron compounds through the miR-21/PTEN/AKT pathway in cecal ligation and puncture-induced sepsis. *Molecular Medicine Reports*, *31*(2), 52. https://doi.org/10.3892/mmr.2024.13417

[29] Temel, H., Atlan, M., Ertas, A., Yener, I., Akdeniz, M., Yazan, Z., … & Akyuz, E. (2022). Cream production and biological in vivo/in vitro activity assessment of a novel boron-based compound derived from quercetin and phenyl boronic acid. *Journal of Trace Elements in Medicine and Biology*, *74*, 127073. https://doi.org/10.1016/j.jtemb.2022.127073

[30] Sedighi-Pirsaraei, N., Tamimi, A., Sadeghi Khamaneh, F., Dadras-Jeddi, S., & Javaheri, N. (2024). Boron in wound healing: A comprehensive investigation of its diverse mechanisms. *Frontiers in Bioengineering and Biotechnology*, *12*, 1475584. https://doi.org/10.3389/fbioe.2024.1475584

[31] Romero-Aguilar, K. S., Arciniega-Martínez, I. M., Farfán-García, E. D., Campos-Rodríguez, R., Reséndiz-Albor, A. A., & Soriano-Ursúa, M. A. (2019). Effects of boron-containing compounds on immune responses: Review and patenting trends. *Expert Opinion on Therapeutic Patents*, *29*(5), 339-351. https://doi.org/10.1080/13543776.2019.1612368

[32] Yildirim, M., Kilic, A., Cimentepe, M., Necip, A., & Turedi, S. (2025). Synthesis of bioactive quercetin-boronate esters as a novel biological agent: Enzyme inhibition, anti-microbial properties, computational insights and anti-cancer activity. *Journal of Molecular Structure*, *1321*, 140216. https://doi.org/10.1016/j.molstruc.2024.140216

YAZAR KILAVUZU

GENEL BİLGİLER

• Makale başvurusu için Makale Metni Dosyası, Telif Hakkı Devir Dosyası ve Benzerlik Oran Dosyası olmak üzere üç ayrı formun doldurulması ve sisteme yüklenmesi gerekmektedir.
• Başvurularda iletişimde bulunulacak yazar ve diğer yazarların iletişim bilgileri bulunmalıdır.
• Makale metni içerisindeki makale kontrol listesi ve kapak sayfası eksiksiz olarak doldurulmalıdır.
• Makale metni dosyası içerisinde bulunan makale kontrol listesi ve kapak sayfası eksiksiz doldurulmalıdır.
• Derleme makalelerde başka yayınlara ait şekil ve tablolar kullanılacaksa, kaynak gösterilecek makalenin yayıncısından izin alınmalıdır. Yayıncıdan izin alındığı ve şekillerin uyarlanıp uyarlanmadığı veya doğrudan kullanılıp kullanılmadığı bilgisi şekil başlığında belirtilmelidir. İlgili izin yazısının journalofboron@tenmak.gov.tr adresine gönderilmesi gerekmektedir.
• Her makale, konusu ile ilgili en az iki hakeme gönderilerek şekil, içerik, özgün değer, uluslararası literatüre katkısı bakımından incelettirilir. Hakem görüşlerinde belirtilen eksikler tamamlandıktan sonra, son baskı formatına getirilir ve yazarlardan makalenin son halinin onayı alınır. Dergide basıldığı haliyle makale içinde bulunabilecek hataların sorumluluğu yazarlara aittir.

MAKALE METNİ DOSYASI

• Makale metninin yazımında yazım kurallarına uyulması gerekmektedir.
• Makale metninde kapsayıcı ve bilimsel bir dil kullanılmalıdır.
• Makale metni referanslar dahil araştırma makaleleri için 14.000 kelimeyi tarama makaleleri için ise 22.000 kelimeyi geçmemelidir.
• Makalenin metni, Times New Roman 12 punto ile Makale Metni Dosyası'nın sayfa düzeni değiştirilmeden yazılmalıdır.
• Makale metninin Microsoft Office Word 2010 ve üzeri bir kelime işlemci ile hazırlanması ve yazım hatalarının kontrol edilmesi ve düzeltilmesi gerekmektedir.
• Eğer makale Türkçe ise, Türkçe başlıklarla bire bir uyumlu olacak şekilde oluşturulmuş İngilizce başlıklar parantez içerisinde yazılmalıdır.
• Makale içerisinde kullanılan kısaltma ve sembollerin anlamları ilk kullanıldıklarında açıklanmalıdır.
• Makale metni içerisindeki alt başlıklar numaralandırılmalıdır. Numaralandırma işlemleri ana bölümler için 1.'den başlamalı ve tüm ana başlıklar (Özet, Teşekkür ve Kaynaklar ve Ekler bölümleri hariç) için devam etmelidir. İkincil başlıklar ana bölüm numaralandırmasına uygun olarak 1.1., 1.2., 1.3., ... şeklinde devam etmelidir. Üçüncü başlıklar ikinci başlıklara uygun olarak 1.1.1., 1.1.2., 1.1.3., ... şeklinde devam etmelidir.

TELİF HAKKI DEVİR DOSYASI

• İmzalı Telif Hakkı Devir Dosyası taranarak sisteme yüklenmelidir.
• İmzalı Telif Hakkı Devir Dosyası'nı göndermeyen yazarların başvuruları değerlendirmeye alınmaz.

BENZERLİK ORAN DOSYASI

• Makalenin referanslar bölümü hariç metni "iThenticate" veya "Turnitin" programları ile taranmalıdır.
• Benzerlik oranı raporunun PDF formatında sisteme yüklenmelidir.
• Benzerlik oranı %15'in üzerinde olmamalıdır.

GİZLİLİK POLİTİKASI

Journal of Boron gizliliğe saygı duymaktadır. Kişisel bilgiler, sadece derginin belirtilen amaçları doğrultusunda kullanılacak ve üçüncü kişilerle paylaşılmayacaktır.

YAZIM KURALLARI

MAKALE BAŞLIĞI
• Makale başlığı standart kısaltmalarla birlikte en çok 15 kelimeden oluşmalıdır.
• Eğer makale Türkçe ise, İngilizce başlıkla bire bir uyumlu olacak şekilde Türkçe makale başlığı da oluşturulmalıdır.

ÖZET
• Özet, 250 kelimeyi geçmemelidir.
• Standart olmayan kısaltmalar ilk kullanıldığında tam açıklamalarından sonra parantez içerisinde yazılmalıdır.
• Eğer makale Türkçe ise, İngilizce özetle bire bir uyumlu olacak şekilde Türkçe özet de oluşturulmalıdır.

ANAHTAR KELİMELER
• En fazla 5 anahtar kelime, alfabetik sıraya göre yazılmalıdır.
• Kısaltmalar anahtar kelime olarak kullanılmamalıdır.
• Eğer makale Türkçe ise, İngilizce anahtar kelimelerle bire bir uyumlu olacak şekilde Türkçe anahtar kelimelere de oluşturulmalıdır.

GİRİŞ
• İlgili literatürün özeti, çalışmanın amacı ve özgün değeri ve kurulmuş olan hipotezi içermelidir.
• Kaynaklar, toplu olarak ve aralıklı verilmemeli (örnek [1-5] veya [1, 2, 3, 5, 8]), her kaynağın çalışmaya katkısı irdelenmeli ve metin içerisinde belirtilmelidir.

MALZEMELER VE YÖNTEMLER
• Yürütülmüş olan çalışma deneysel bir çalışma ise deney prosedürü/metodu anlaşılır bir şekilde açıklanmalıdır.
• Teorik bir çalışma yürütülmüşse teorik metodu detaylı bir şekilde verilmelidir.
• Yapılan çalışmada kullanılan metot daha önce yayınlanmış bir metot ise diğer çalışmaya atıf yapılarak bu çalışmanın diğer çalışmadan farklı belirtilmelidir.

SONUÇLAR VE TARTIŞMA
• Elde edilen sonuçlar açık ve öz bir şekilde verilmelidir.
• Elde edilen tüm sonuçlar atıf yapılarak literatür ile karşılaştırılmalıdır.
• Tablolar numaralandırılmalıdır ve düzenlenebilir formatta olmalıdır. Eğer makale Türkçe ise, tablo üst yazılarının bire bir İngilizce çevirileri parantez içerisinde verilmelidir.
• Makale içerisindeki şekiller numaralandırılmalıdır ve en az 300 dpi çözünürlükte olmalıdır. Şekillerin üzerindeki yazılar okunabilir büyüklükte ve yazı tipinde olmalıdır. Kabul edilen şekil formatları TIFF, JPG ve JPEG'dir. Eğer makale Türkçe ise, şekil alt yazılarının bire bir İngilizce çevirileri parantez içerisinde verilmelidir.

SONUÇLAR
• Çalışmadan elde edilen ana sonuçlar ve çıkarımlar kısa ve öz bir şekilde verilmelidir.
• Çalışmaya ait gelecek perspektifleri bu bölümde verilir.

TEŞEKKÜRLER
• Çalışmanın gerçekleşmesi için sağlanan maddi kaynaklar ve kullanılan altyapı bu bölümde belirtilir.

ÇIKAR ÇATIŞMASI
• Yazarın veya yazarın kurumunun mali veya kişisel ilişkileri dahil olmak üzere her türlü çıkar çatışması beyan edilmelidir.

YAZAR KATKI BEYANI
• Her yazarın katkıları belirtilmelidir.
• Katkı rolleri şunlardır: kavramsallaştırma, veri analizi, veri toplama, fon edinimi, metodoloji, proje yönetimi, kaynak bulma, yazılım analizi, denetim, doğrulama, görselleştirme, orijinal taslak yazma, inceleme yazma ve düzenleme.

KAYNAKLAR
• Basılmış kaynakların DOI ve ISBN numarası belirtilmelidir.
• İnternet sitesi adresleri (URL) kaynak olarak verilmemelidir. Ancak metin içerisinde istatistiksel bir verinin geçtiği yerde veriden sonra belirtilebilir.
• Kaynaklar listesi metin içerisinden kullanılma sırasına uygun olarak numaralandırılmalıdır.
• Kaynaklar, "APA Publication Manual, Seventh Edition" kurallarına uygun olarak hazırlanmalıdır.
• Kaynaklar İngilizce olarak hazırlanmalıdır. Türkçe kaynakların İngilizce karşılıkları köşeli parantez içerisinde belirtilmelidir.
• APA formatı ve örneklere aşağıdaki bağlantıdan ulaşılabilir.
https://apastyle.apa.org/style-grammar-guidelines/references/examples

EKLER
• Makaledeki ekler EK A (Appendix A), EK B (Appendix B) ve EK C (Appendix C) vb. olarak adlandırılmalıdır.
• Ekler içerisindeki denklemler A1, A2, A3 vb. olarak adlandırılmalıdır, tablo ve şekiller Tablo A1, Tablo A2, Şekil A1, Şekil A2 vb. olarak adlandırılmalıdır.

AUTHOR'S GUIDE

GENERAL INFORMATION

• For article application, 3 individual files which are Manuscript File, Copyright Transfer File and Similarity Ratio File, must be filled in and uploaded to the system.
• Applications should include the contact information of the author and other authors to be contacted.
• The article checklist and cover page in the Manuscript File should be filled in completely.
• Each article is sent to at least two referees related to its subject and examined in terms of format, content, novelty, contribution to literature.
• If figures and tables from other publications are to be used in review articles, permission must be obtained from the publisher of the article to be cited. The information that permission has been granted from the publisher and whether the figures have been adapted or used directly should be mentioned in the figure caption. The relevant permission letter should be sent to journalofboron@tenmak.gov.tr.
• After the deficiencies stated in the referee's comments are completed, it is brought to the final print format and the approval of the final version of the article is obtained from the authors. The responsibility of errors that may be found in the article as it is published in the journal belongs to the authors.

MANUSCRIPT

• Writing rules must be followed, during writing of the manuscript.
• Inclusive and scientific language must be used in the manuscript.
• Manuscript should not exceed 14,000 words for research articles and 22,000 words for review articles, including references.
• The manuscript should be written in Times New Roman 12 points without changing the page layout of the Manuscript File.
• The manuscript should be prepared with a word processor of Microsoft Office Word 2010 and above, and spelling errors should be checked and corrected.
• Abbreviations and symbols used in the manuscript must be explained when used fort he first time.
• Subheadings in the article should be numbered. Numbering should start at 1 for the main section and continue for all main headings (except the Summary, Acknowledgments and References and Appendices sections). Secondary titles continue as 1.1., 1.2., 1.3., ... in accordance with the main chapter numbering. The third headings continue as 1.1.1., 1.1.2., 1.1.3., ... in accordance with the second headings.

COPYRIGHT TRANSFER FILE

• Signed Copyright Transfer File should be scanned and uploaded to the system.
• Applications of the authors who do not send the signed Copyright Transfer File will not be evaluated.

SIMILARITY RATIO FILE

• The manuscript should be scanned with "iThenticate" or "Turnitin" programs, except for the references section.
• The similarity ratio report should be uploaded to the system in PDF format.
• The similarity ratio should not exceed 15%.

PRIVACY POLICY

Journal of Boron respects privacy. Any personal information will only be used in line with the stated purposes of the journal and will not be shared with third parties.

WRITING RULES

TITLE
• The title of the manuscript should consist of a maximum of 15 words with standard abbreviations.

ABSTRACT
• The abstract should not exceed 250 words.
• Non-standard abbreviations should be written in parentheses after their full explanation, when they are used for the first time.

KEYWORDS
• A maximum of 5 keywords should be written in alphabetical order.
• Abbreviations should not be used as keywords.

INTRODUCTION
• The summary of the relevant literature, aim and novelty of the study, and the established hypothesis should be included.
• References should not be given in bulk and in intervals (example [1-5] or [1, 2, 3, 5, 8]), the contribution of each source to the study should be examined and stated in the text.

MATERIALS AND METHODS
• If the study carried out is an experimental study, the test procedure/method should be clearly explained.
• If a theoretical study has been carried out, the theoretical method should be given in detail.
• If the method used in the study is a previously published method, the other study should be mentioned by citing.

RESULTS AND DISCUSSION
• Obtained results should be given in a clear and concise manner.
• All of the results should be compared with the literature by citing.
• Tables should be numbered and in editable format.
• Figures in the manuscript should be numbered and have at least 300 dpi resolution. The texts on the figures should be in legible size and font. Accepted figure formats are TIFF, JPG, and JPEG.

CONCLUSIONS
• Main conclusions and inferences obtained from the study should be given concisely.
• Future perspectives of the study are given in this section.

ACKNOWLEDGEMENTS
• The financial resources provided and the infrastructure used during the study are specified in this section.

CONFLICT OF INTEREST
• Any type of conflict of interest of author or the author's institution including financial or personal relationships must be declared.

AUTHOR CONTRIBUTION STATEMENT
• Contributions of each author must be stated.
• Contribution roles are as follows: conceptualization, data analysis, data curation, funding acquisition, methodology, project administration, sourcing, software analysis, supervi¬sion, validation, visualization, writing original draft, writing review and editing.

REFERENCES
• DOI and ISBN numbers of printed sources should be specified.
• Website addresses (URLs) should not be given as a source. However, it can be specified after the data where a statistical data is mentioned in the text.
• The list of references should be numbered according to the order in which they are used in the text.
• References should be prepared in accordance with the rules of "APA Publication Manual, Seventh Edition".
• References should be prepared in English. English equivalents of sources should be indicated in square brackets.
• APA format and examples can be found at the link below.
https://apastyle.apa.org/style-grammar-guidelines/references/examples

APPENDICES
• Appendices in the manuscript must be named as Appendix A (Appendix A), Appendix B (Appendix B) and Appendix C (Appendix C) etc.
• Equations in the appendices must be named as A1, A2, A3, etc., and table and figures numberings must be named as Table A1, Table A2, Figure A1, Figure A2 etc.

TENMAK BOREN BOR ARAŞTIRMA ENSTİTÜSÜ

BOR DERGİSİ
JOURNAL OF BORON
https://dergipark.org.tr/boron

İÇİNDEKİLER/CONTENTS

Türkiye Enerji Nükleer Maden Araştırma Kurumu (TENMAK)

Mustafa Kemal Mahallesi, Dumlupınar Blv. No:192, Ankara, 06530, Türkiye
Tel: (0312) 212 62 30
e-mail: journalofboron@tenmak.gov.tr
web:https://dergipark.org.tr/tr/pub/boron